NUCLEAR MAGNETIC RELAXATION IN IONIC SINGLE CRYSTALS

Kenneth M. Swanson

A Thesis Submitted for the Degree of PhD
at the
University of St Andrews

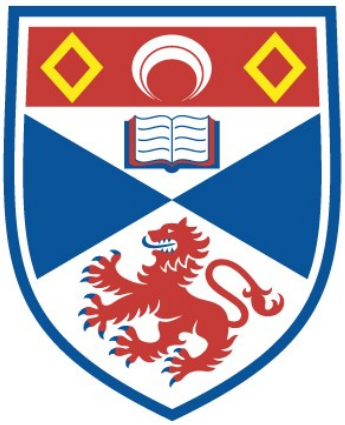

1958

NUCLEAR MAGNETIC RELAXATION IN IONIC SINGLE CRYSTALS.

being a Thesis presented by Kenneth M. Swanson, B.Sc., to the University of St. Andrews in application for the degree of Doctor of Philosophy.

[1958]

Conferred 7/11/59.

ProQuest LLC.
789 East Eisenhower Parkway
P.O. Box 1346
Ann Arbor, MI 48106 – 1346

ms 2088

Declaration.

I hereby declare that the following Thesis is based on the results of experiments carried out by me, that the Thesis is my own composition and that it has not previously been presented for a higher degree.

The research was carried out in the Physical Laboratory of the United College of the University of St. Andrews and at the Physics Laboratory of the University College of North Wales, Bangor, under the direction of Professor J. F. Allen, F.R.S., and Professor E. R. Andrew, F.R.S.E.

Certificate

We certify that Kenneth M. Swanson B.Sc. has spent nine terms at research work under our direction, four terms in the Physical Laboratory of the United College of the University of St. Andrews, and five terms externally in the Physics Laboratory of the University College of North Wales, Bangor, that he has fulfilled the conditions of ordinance No. 16 (St. Andrews) and that he is qualified to submit the accompanying Thesis in application for the Degree of Doctor of Philosophy.

Directors of Research.

Career.

I matriculated in the University of St. Andrews in October 1947 and followed a course leading to graduation in June 1951, obtaining the degree of Bachelor of Science with First Class Honours in Natural Philosophy. I recommenced my studies in January 1954 after serving in the Royal Air Force, starting then research on the work which is now being submitted as a Ph.D. Thesis. My director of research was Dr. E. R. Andrew, who was subsequently appointed Professor of Physics in the University College of North Wales, Bangor. In January 1955 I moved to Bangor to continue my research externally. In October 1955 I was appointed a Junior Lecturer at Bangor which post I have held until the completion of this research.

"Never quarrel with your Mother's milk"

Lord Rutherford

Acknowledgements.

It is a pleasure to acknowledge my debt to Professor E. R. Andrew and Professor J. F. Allen who have nurtured the growth of my education in Physics as an undergraduate and in post-graduate research. I have never failed to get from them the encouragement, practical help and direction needed in my research and I tender them my sincere thanks.

ACKNOWLEDGMENTS

I would like to thank my co-workers at Bangor, particularly Dr. R.G. Bates, Mr. N.D. Finch, and Mr. B.R. Williams for their friendly co-operation. My thanks go also to Mr. E.A. Welch who made the photographic prints for this thesis and to my wife who drew some of the figures.

Contents

Nuclear Magnetic Relaxation in Ionic Crystals

1. Introduction.

It has been known since 1946 that energy can be absorbed from a radiofrequency field by the nuclear spins in bulk material placed in a uniform magnetic field. For this absorption of energy to be a continuous process it is necessary for the spins to have some thermal contact with the surrounding lattice, so that they can pass on the absorbed energy and then take part in further absorption. In general a nucleus can exchange energy with the lattice by means of interaction between its magnetic dipole moment and fluctuating magnetic fields supplied by the lattice, or by interaction between the electric quadrupole moment of the nucleus and fluctuating electric fields supplied by the lattice. Either or both of these interactions can provide the relaxation mechanism which allows the nucleus to lose to the surrounding lattice the excess energy gained from the applied radiofrequency field in nuclear magnetic resonance absorption. This thesis describes a method of showing experimentally which of these interactions is dominant in providing the relaxation mechanism in cases where either mechanism can operate.

2. Introduction to Nuclear Magnetic Resonance.

Since its establishment as an experimental fact in 1945 by Purcell, Torrey and Pound at Harvard and Bloch, Hansen and Packard at Stanford the fundamental theory of Nuclear Magnetic Resonance Absorption has been reviewed by a number of authors, including Pake 1950, 1956, Andrew 1955, Grivet 1955, Wertz 1955 and Kopfermann 1958.

2.1. Nuclear Magnetism and the Spin-Lattice Relaxation Time T_1.

Nuclear Magnetic Resonance is observed in diamagnetic material and is due to the paramagnetism of nuclei possessing spin.

Nuclei of spin I and magnetic moment μ when placed in a magnetic field H_o will produce an equilibrium macroscopic magnetisation M_o given by the Langevin formula

$$M_o = n_o \mu \frac{I+1}{3I} \frac{\mu H_o}{kT} = \chi_o H_o \text{ e.m.u.} \qquad 2(1)$$

where T is the lattice temperature and n_o is the number of nuclear magnets per unit volume, and χ_o is the static susceptibility.

Before the field H_o is applied the $2I + 1$ energy levels of the nuclear magnet in an external field are degenerate. Thus when the field is suddenly applied to split these levels they will be equally populated and the magnetisation along the field M_z will be instantaneously zero. If we introduce the concept of the temperature T_S of the spin system then

$$M_z = n_o \mu \frac{I+1}{3I} \frac{\mu H_o}{kT_S} = \chi_o H_o \times \frac{T}{T_S} \qquad 2(2)$$

with $T_S = \infty$ when the field is initially applied. The equilibrium value of M_z given by 2(1) is established by thermal contact between the spin

system and the lattice, the excess energy of the spin system being shared with the vibrational degrees of freedom of the atoms. The exponential growth of M_Z to the equilibrium value M_o is described by means of the longitudinal or spin-lattice relaxation time T_1

$$M_z = M_o (1 - \exp(-t/T_1)) \qquad 2(3)$$

M_o is very small compared to the atomic diamagnetisation and is usually completely masked by it.

2.2. Transverse Magnetisation and the Transverse Relaxation Time T_2

Nuclear paramagnetism can be detected however by resonance methods. When a magnetic field H_1 oscillating with a radiofrequency ν is applied at right angles to H_o, a 'transverse' magnetisation' is produced when ν is near the Larmor frequency of the nuclear magnets in the magnetic field H_o. This transverse magnetisation rotates about the Z axis with the Larmor frequency and is capable of inducing a detectable r.f. voltage in a suitably placed coil. This macroscopic transverse magnetisation is the result of individual nuclear moments precessing at the Larmor frequency being pulled into phase by the applied field H_1. There are relaxation processes which tend to reduce this macroscopic transverse magnetisation by destroying the phase coherence of the individual precessing spins. In particular as the rotating field produced by one spin at the site of a neighbour is of the correct frequency to induce transition, there is the possibility of a spin-spin collision or energy exchange in which a mutual flipping in the field and exchange of energy takes place between two identical spins. This leads to phase jumps and loss of coherence. Similarly the local field due to neighbouring nuclear magnets varies from

nucleus to nucleus causing a variation in precession rates and a progressive loss of phase coherence. A second relaxation time T_2 is introduced to account for the observed decay of the transverse magnetization. It is given by

$$\frac{dM_x}{dt} = -\frac{M_x}{T_2} , \qquad \frac{dM_y}{dt} = -\frac{M_y}{T_2} \qquad 2(4)$$

where x and y are axes at right angles to Z, the field direction.

2.3. The Bloch Equations.

The nuclear magnetization vector is parallel to the spin vector and is related to it by the nuclear gyromagnetic ratio γ. This same ratio γ must hold between the macroscopic magnetization M and the vector sum of the nuclear angular momenta which we designate P.

$$M = \gamma P$$

Then we have an angular momentum P with associated magnetization vector M precessing in a magnetic field H. The classical equation of motion is then

$$\frac{dP}{dt} = M \times H$$

$$\frac{dM}{dt} = \gamma (M \times H) \qquad 2(5)$$

The components of H are H_o along the Z axis and an oscillating field $2H_1$ cos wt along the x axis. H_1 is equivalent to two fields rotating in opposite directions (H_1 cos wt, H_1 sin wt, 0) and (H_1 cos wt, $-H_1$ sin wt, 0). The field which rotates in the same direction as M precesses, exercises a tipping effect on M. The other rotating component does not

preserve a phase relationship with M and so can normally be neglected. The equation 1(5)written in full is then:

$$\frac{dM_x}{dt} = \gamma (M_y H_o \pm M_z H_1 \sin \omega t) - \frac{M_x}{T_2}$$

$$\frac{dM_y}{dt} = \gamma (M_z H_1 \cos \omega t - M_x H_o) - \frac{M_y}{T_2} \qquad 2(6)$$

$$\frac{dM_z}{dt} = \gamma (\mp M_x H_1 \sin \omega t - M_y H_1 \cos \omega t) - \frac{(M_z - M_o)}{T_1}$$

where the upper sign is used when γ is positive.

Equations 2.6 were first given by Bloch 1946.

Their steady state solution for the case of slow passage through resonance is:

$$M_x = \tfrac{1}{2} X_o \omega_o T_2 \frac{2H_1 \cos \omega t \, (\omega_o - \omega) T_2 + 2H_1 \sin \omega t}{1 + (\omega - \omega_o)^2 T_2^2 + \gamma^2 H_1^2 T_1 T_2} \qquad (a)$$

$$M_y = \tfrac{1}{2} X_o \omega_o T_2 \frac{2H_1 \cos \omega t - 2H_1 \sin \omega t \, (\omega_o - \omega) T_2}{1 + (\omega - \omega_o)^2 T_2^2 + \gamma^2 H_1^2 T_1 T_2} \qquad (b) \; 2(7)$$

$$M_z = X_o H_o \frac{1 + (\omega_o - \omega)^2 T_2^2}{1 + (\omega - \omega_o)^2 T_2^2 + \gamma^2 H_1^2 T_1 T_2} \qquad (c)$$

where $\omega_o = \gamma H_o$ is the Larmor frequency.

The absorption of energy by the nuclear magnets can be described in terms of a complex susceptibility $X = X' - i X''$. Representing the oscillating magnetic field as the real part of $H = 2H_1 \exp i\omega t$ we have

$$M_x = X' (2H_1 \cos \omega t) + X'' (2H_1 \sin \omega t) \qquad 2(8)$$

Comparison of 2(8)with 2(7) gives:

$$X'' = \tfrac{1}{2}X_o w_o T_2 \left(1 + T_2^2 (w_o - w)^2 + \gamma^2 H_1^2 T_1 T_2\right)^{-1} \qquad 2(8)$$

$$X' = \tfrac{1}{2}X_o w_o T_2 (w_o - w) T_2 \left(1 + T_2^2 (w_o - w)^2 + \gamma^2 H_1^2 T_1 T_2\right)^{-1} \qquad 2(9)$$

The energy absorbed by unit volume of the sample per second is

$$A = \frac{w}{2\pi} \int_{t=0}^{t=\frac{2\pi}{w}} H \, dM$$

Only the out of phase component contributes to A

$$A = 2w^2 X'' H_1^2 \int_0^{\frac{2\pi}{w}} \cos^2 wt \, dt$$

$$= 2wX'' H_1^2$$

$$= wH_1^2 X_o \frac{w_o T_2}{1 + T_2^2 (w_o - w)^2 + \gamma^2 H_1^2 T_1 T_2}$$

The absorption of energy is then proportional to X''. It thus has a resonant character, and maximum absorption occurs at $w = w_o$. Also when the saturation term $\gamma^2 H_1^2 T_1 T_2$ is small the line-width at half intensity is given by $T_2 (w_o - w_{\frac{1}{2}}) = 1$.

There fore the half-width of the line is $\frac{1}{T_2}$.

2.4. Saturation Effects.

When H_1 is increased until the term $\gamma^2 H_1^2 T_1 T_2$ is not small then the nuclear spin system is said to be partially saturated. This means that the spin lattice relaxation process can no longer maintain the spin system at the lattice temperature and the spin temperature rises.

Then the maximum value of M_Z is given by 2(7)(c)

$$M_Z = \chi_o H_o \left(\frac{1}{1 + \gamma^2 H_1^2 T_1 T_2} \right) \qquad 2(10)$$

Comparison with equation 2.2 gives an effective value of T_S

$$T_S \text{ eff.} = T (1 + \gamma^2 H_1^2 T_1 T_2) \qquad 2(11)$$

since if H_o only were applied at a lattice temperature equal to T_S effective, then the equilibrium value of M_Z would be given by 2.10.

In terms of spin energy level populations the rise in spin temperature means that the distribution of spins over the levels corresponds to a Boltzmann distribution at temperature T_S rather than T. The $2I + 1$ equally spaced energy levels are designated by the quantum numbers m where m takes values $-I, -I + 1, \ldots\ldots, +I$. For a Boltzmann distribution the excess population in a lower level over that in the next highest is $\frac{\mu H}{IkT_S}$ where $\frac{\mu H}{I}$ is the energy level separation. That is:

$$N_m - N_{m-1} = \frac{\mu H}{IkT_S} \qquad 2(12)$$

where N_m is the population of the level m

2.5. <u>Validity of assigning a Spin Temperature</u>.

The following question is now raised: if the distribution of spin population over the different energy levels corresponds to a Boltzmann distribution at one instant, so that a common spin temperature T_S^1 can be assigned to the assembly of spins, are the processes causing transfer of population between levels of such a nature that the distribution will still be Boltzmann at a later time so that a common spin temperature T_S

can always be assigned to the assembly ? This question which is important in the theory behind the experiments to be described in this thesis, will now be examined in detail.

2.5. (i) Single Line Spectrum.

When the energy level differences are all equal then the absorption spectrum consists of one line. In this case the spin-spin exchange of energy can take place between spins in any pair of levels where one spin has the possibility of moving to a higher level and the other spin has the possibility of simultaneously moving to a lower level. For instance a spin in level $m + 1$ can exchange energy with a spin in level $m - 1$, both spins moving to level m in the exchange. Also the frequency of such transitions is governed by T_2 which in solids is much shorter than T_1 in general, so that the T_2 process is the dominant one as far as level population changes are concerned.

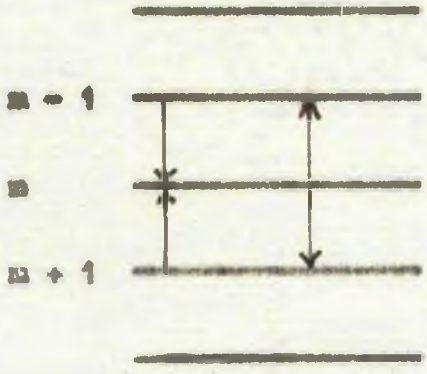

The probability for an exchange such as is outlined above is proportional to the number of spins in the levels concerned.

Probability for $(m + 1 \longrightarrow m,\ m - 1 \longrightarrow m) \propto N_{m+1} \times N_{m-1}$ *

Probability for $(m \longrightarrow m + 1,\ m \longrightarrow m - 1) \propto N_m^2$

Probability for a net change due to this particular exchange process is $\propto (N_{m+1} \times N_{m-1} - N_m^2)$. If we express the energy populations as

$$N_m = \frac{N}{2I + 1} + n_m$$ where N is the total number of spins present and n_m is the difference in population of the m level from the average population per level then all terms n_m will be small.

* In the Thesis $\propto$ normally signifies "is proportional to".

Then

$$(N_{m+1} \times N_{m-1} - N_m^2) = \frac{N}{2I+1}(n_{m+1} + n_{m-1} - 2n_m)$$

And this is proportional to the probability for the spin-spin transition being investigated. When a Boltzmann distribution holds for a set of equally spaced levels then

$$n_{m+1} - n_m = n_m - n_{m-1} = n_{m-1} - n_{m-2} = \ldots.$$

We see then that when a Boltzmann distribution has been established the probability for a net change of populations due to the spin-spin exchange is zero. Conversely if a Boltzmann distribution is not established the probability for the spin-spin exchange of population levels is not zero. A similar analysis of all possible spin-spin exchanges shows that the same argument holds. Also the spin-spin exchanges are such as to establish a Boltzmann distribution. Thus for the case of a single line spectrum the spin-spin exchange process which is a very rapid process will always ensure that the separate levels have a Boltzmann distribution of population and thus a single spin temperature T_s will always be applicable to the assembly.

2.5 (ii) Quadrupole Split Spectrum.

When a nucleus which has an electric quadrupole moment is in a crystal lattice where the electric field gradient at the nucleus is not zero then in a magnetic field the nuclear Zeemann energy levels are perturbed from their equally spaced values by the interaction of the nuclear quadrupole moment with the electric field gradient. (The interaction is assumed to be small. When it is large the change of energy levels is too great to be treated by perturbation theory).

The amount of perturbation of the energy levels changes with the relative orientation of the principal axis of the field gradient tensor and the applied magnetic field H_o. For our experiments we are interested in the case where the perturbation is just large enough to cause the transitions between the different energy levels to give rise to separate spectral lines. This is the case where the energy levels are nearly enough equally spaced to be related to each other by the same Boltzmann factor when thermal equilibrium with the lattice is reached. At the same time the lines are just separated so that the T_2 process, which is a resonant process, cannot act. In this case does the population of the energy levels still maintain a Boltzmann distribution ?

To find the answer we have to examine the equations governing the populations of the different levels taking into account only the spin-lattice relaxation transitions. Here we have to distinguish two cases. If the spin-lattice relaxation process is through a magnetic interaction then only transitions where m changes by $\pm$ 1 are allowed. The selection rule is $\Delta m = \pm 1$.

If on the other hand the relaxation process is through the electric quadrupole moment of the nucleus interacting with the time dependent electric field gradient the selection rule is $\Delta m = \pm 1, \pm 2$.

(a) Magnetic Relaxation Process $\Delta m = \pm 1$.

To prove that if a common spin temperature can be assigned at one instant during relaxation, then a common spin temperature can be assigned at all later times.

Let the nuclei have spin I and be suddenly subjected to a homogeneous magnetic field H_o which splits the energy terms into

2I + 1 not quite equally spaced levels designated by their magnetic quantum numbers m. Let the transition probabilities between adjacent levels due to the magnetic relaxation process be $W_{m \rightarrow m-1}$ etc. Then the change of population of each level with time is given by:

$$\dot{N}_{-I} = -N_{-I} W_{-I \rightarrow -I+1} + N_{-I+1} W_{-I+1 \rightarrow -I}$$

$$\dot{N}_{-I+1} = -N_{-I+1}(W_{-I+1 \rightarrow -I} + W_{-I+1 \rightarrow -I+2}) + N_{-I} W_{-I \rightarrow -I+1} + N_{-I+2} W_{-I+2 \rightarrow -I+1}$$

2(13)

$$\dot{N}_{-I+2} = -N_{-I+2}(W_{-I+2 \rightarrow -I+1} + W_{-I+2 \rightarrow -I+3}) + N_{-I+1} W_{-I+1 \rightarrow -I+2} + N_{-I+3} W_{-I+3 \rightarrow -I+2}$$

$$\vdots$$

$$\dot{N}_{I} = -N_{I} W_{I \rightarrow I-1} + N_{I-1} W_{I-1 \rightarrow I}$$

If the lattice temperature is T the probability for transitions downwards by interaction with the lattice exceeds that for transitions upwards by interaction with the lattice by the Boltzmann factor $\exp \frac{h\nu_0}{kT} = (1 + \Delta)$ where $\Delta = \frac{h\nu_0}{kT}$ and ν_0 is the unperturbed frequency of the absorption line.

Then
$$W_{-I \rightarrow -I+1} = W_{-I+1 \rightarrow -I}\,(1 + \Delta)$$

$$W_{-I+1 \rightarrow -I+2} = W_{-I+2 \rightarrow -I+1}\,(1 + \Delta) \qquad 2(14)$$

$$W_{+I-1 \rightarrow I} = W_{I \rightarrow I-1}\,(1 + \Delta)$$

Now initially the populations of all levels is equal to $\frac{N}{2I+1}$ and the spin temperature $T_s = \infty$. If a common spin temperature can be ascribed later then the differences in population of adjacent levels, which

are to a first order equally spaced, must be equal. (The perturbation of the levels in our experiments gives a line splitting of the order of a few Kc/s in 10 Mc/s).

Then we must have

$$\dot{N}_{-I+1} - \dot{N}_{-I} = \dot{N}_{-I+2} - \dot{N}_{-I+1} = \ldots\ldots = \dot{N}_{I} - \dot{N}_{I-1} \qquad 2(15)$$

Substituting for equations 2(14) in 2(13) and putting in the initial condition that $N_i = \frac{N}{2I+1}$ we find that the general form of equation 2(15) is

$$\ldots\ldots = n_o \left(2W_{m+1 \rightarrow m} - W_{m+2 \rightarrow m+1} - W_{m \rightarrow m+1} \right) = \ldots \qquad 2(16)$$

where $n_o = \frac{N\Delta}{2I+1}$

Now the transition probabilities for magnetically induced transitions are given by

$$W_{m \rightarrow m-1} = W(I+m)(I-m+1) \qquad 2(17)$$

where W is a constant.

Then equation 2(16) reduces to

$$\ldots\ldots = \left[2(I+m+1)(I-m)W - (I+m+2)(I-m-1)W - (I+m)(I-m+1) \times W \right] n_o$$

$$= \ldots\ldots$$

$$\therefore \quad \ldots\ldots = 2Wn_o = \ldots\ldots$$

:that is all the equations are identically equal. Therefore a single spin temperature is always applicable. Furthermore, the time constant of the relaxation process for each pair of levels is given by

$$\dot{N}_{m+1} - \dot{N}_m = 2Wn_o = \frac{n_o}{T_1}$$

$$\therefore T_1 = \frac{1}{2W}$$

and the same relaxation time T_1 is applicable to each pair of levels.

(b) Quadrupole Relaxation Case $\Delta m = \pm 1, \pm 2$.

We repeat the analysis of section (a) when transitions involving $\Delta m = \pm 2$ are also allowed.

On suddenly applying field H_o we have

$$\dot{N}_{-I} = -N_{-I}\left(W_{-I \to -I+2} + W_{-I \to -I+1}\right) + N_{-I+1} W_{-I+1 \to -I} + N_{-I+2} W_{-I+2 \to -I}$$

$$\dot{N}_{-I+1} = -N_{-I+1}\left(W_{-I+1 \to -I+2} + W_{-I+1 \to -I+3} W_{-I+1 \to -I}\right) + N_{-I} W_{-I \to -I+1} + N_{-I+2} W_{-I+2 \to -I+1} + N_{-I+3} W_{-I+3 \to -I+1} \qquad 2(16)$$

etc.

Because the W terms arise from thermal processes we have:

$$W_{-I \to -I+1} = W_{-I+1 \to -I}(1 + \Delta)$$
$$W_{-I \to -I+2} = W_{-I+2 \to -I}(1 + 2\Delta) \qquad 2(17)$$

We use the initial condition that all $N_i = \frac{N}{2I+1} = n_o/\Delta$

and get the general equation

$$\cdots\cdots = \dot{N}_m - \dot{N}_{m-1} = \dot{N}_{m+1} - \dot{N}_m = \dot{N}_{m+2} - \dot{N}_{m+1} = \cdots$$

which is true only if a common spin temperature is applicable. The form of this general equation is given by

$$\dot{N}_{m+1} - \dot{N}_m = n_o \left(2W_{m+1 \to m} + 2W_{m+1 \to m-1} - W_{m+2 \to m+1} - 2W_{m+3 \to m+1} - W_{m \to m-1} - 2W_{m \to m-2} + 2W_{m+2 \to m} \right)$$

2(18)

The transition probabilities are given by Pound 1950.

$$W_{m \to m-1} = \left[\frac{e^2}{2} \frac{eQ}{2I(2I-1)} \right]^2 (2m-1)^2 (I-m+1)(I+m) \frac{2}{\nabla E_{\pm 1}}$$

$$W_{m \to m-2} = \left[\frac{e^2}{2} \frac{eQ}{2I(2I-1)} \right]^2 (I+m)(I+m-1)(I-m+1)(I-m+2) \frac{2}{\nabla E_{\pm 2}}$$

where eQ is the electric quadrupole moment of the nucleus and $\nabla E_{\pm 1, \pm 2}$ are the components of the electric field gradient tensor responsible for the $\Delta m = \pm 1, \pm 2$ transitions. For the purposes of our analysis we assume that

$$\frac{2}{\nabla E_{\pm 1}} = \frac{2}{\nabla E_{\pm 2}} = \frac{2}{\nabla E}$$

Evaluating the W terms in 2(18) we find that

$$\ldots\ldots = \dot{N}_{m+1} - \dot{N}_m = n_o (8I^2 + 8I - 6) \left(\frac{e^2}{2} \frac{eQ}{2I(I-1)} \right)^2 \frac{2}{\nabla E}$$

2(19)

This is independent of m so that we can say that a spin temperature can be assigned to the spin population at all times during the recovery. Also the relaxation time T_1 is the same for the spins responsible for each line in the narrow-split spectrum and is given by

$$\dot{N}_m - \dot{N}_{m-1} = \frac{n_o}{T_1} = n_o (8I^2 + 8I - 6) \left(\frac{e^2}{2} \frac{eQ}{2I(I-1)} \right)^2 \frac{2}{\nabla E}$$

2(20)

When in later analysis we require a relation between $\frac{1}{T_1}$ and W, a common factor of the transition probabilities, we always chose $\overset{\circ}{W} = \frac{1}{2T_1}$ by analogy with the magnetic relaxation case.

Then W is given by

$$W = \frac{1}{8}(8I^2 + 8I - 6)\left(\frac{6^{\frac{1}{2}}}{2}\frac{eQ}{2I(I-1)}\right)^2 \overline{\nabla E}^2 \qquad 2(21)$$

We can take it then that under the conditions of narrow splitting the relaxation time T_1 measured with reference to any line of the narrow-split spectrum should be the same.

3. Spin-Lattice Relaxation in Ionic Crystals

3.1. Magnetic dipole relaxation

Spin-lattice relaxation times in liquids, gases, and solids with thermal motions other than simple lattice vibrations are explained on the basis of the relaxation theory of Bloembergen, Purcell and Pound 1948. The magnetic dipole-dipole interaction between the nuclei in combination with the thermal variation of the space coordinates of the nuclei provides a thermal contact between the spins and the other degrees of freedom which leads to theoretical spin-lattice relaxation times in agreement with experiment.

When we apply this theory to ionic insulating crystals which do not contain rotating or oscillating groups of atoms the predicted spin-lattice relaxation times are much longer than those found experimentally. The interaction of the magnetic dipoles in such a lattice due to the thermal vibrations in the lattice leads to spin-lattice relaxation times T_1 of the order of 10^{11} seconds at room temperature. This is the prediction from the theory of Waller 1932 for paramagnetic relaxation, adapted to the nuclear problem. As the values of T_1 found for such crystals are of the order of 1 second the discrepancy is too large to hope for agreement by modifications of the Waller theory. Instead two theories depending on different spin-lattice relaxation mechanisms have been proposed. The first of these, due principally to Bloembergen 1949, applies to all nuclei of spin $I \geq \frac{1}{2}$ while the second, due to Pount 1950 and Van Kranendonk 1954 applies to the nuclei of $I > \frac{1}{2}$.

The theory of Bloembergen explains the short relaxation times by considering the action of paramagnetic impurities present in minute amounts in the purest ionic crystals. As electron spin magnetic moments μ^1 are $\sim 10^3$ times as large as nuclear magnetic moments μ, they have a coupling $\mu\mu^1/r^3$ with neighbouring nuclear moments 10^3 times as large as the direct dipole-dipole coupling between nuclei. Thus on Waller's theory they would provide a T_1 smaller by a factor proportional to the square of the reaction energy, that is 10^6, for those nuclei in the field of the paramagnetic impurity. Bloembergen has shown however that the paramagnetic impurities are even more effective than is shown by this estimate, for as well as their enhanced direct coupling with neighbouring nuclear spins, the fluctuating field provided by their magnetic moments moving through spin-orbit coupling with the lattice, gives a thermal link more effective than the nuclear dipole fluctuating field by an extra factor of 10^3. Thus for nuclear spins near a paramagnetic impurity a T_1 less than one second is predicted at room temperature. This only applies to a small proportion of the nuclear spins present, as the paramagnetic impurity may well be in concentrations of a few parts per million. In this case the major proportion of the nuclei are many lattice spacings removed from an impurity and their interaction with it is weak enough to give $T_1 \sim 10^4$ sec.

Bloembergen overcomes this difficulty by showing that the process of nuclear spin-spin collisions in which there is a mutual exchange of energy causes the excess energy of an excited spin to diffuse in a

random walk from spin to spin. As the time for a random step is related to the lifetime of a spin state T_2 which is of the order of 10^{-4} secs, and it takes on average n^2 steps to remove the energy to the neighbourhood of a paramagnetic impurity n lattice spacings away, it is shown that the spin energy is carried distances of $\sim$ 20 lattice spacings in times $\sim 10^{-1}$ secs. This time rapidly rises for greater distances (10^{12} sec. for 1 cm), but gives the correct times for the impurity concentrations found in the crystals used. Once the excess spin energy is transferred to the paramagnetic spin it is very rapidly lost to the other degrees of freedom of the lattice due to the strong paramagnetic relaxation.

3.2. Quadrupole Relaxation.

Pound has proposed a spin-lattice relaxation mechanism for nuclei with $I > \frac{1}{2}$ which makes use of the electric quadrupole moment possessed by such nuclei. Because in its vibrations in the lattice a nucleus varies its distance to a nearby charge in the same way as it varies its distance to a nearby dipole moment, the ratio of the resultant relaxation times will be as the square of the reaction energies.

$$\frac{T_{1\mu}}{T_{1Q}} = \left(\frac{e^2Q}{r^3}\right)^2 \Big/ \left(\frac{\mu^2}{r^3}\right)^2 = \left(\frac{e^2Q}{\mu^4}\right)^2$$

where Q is the quadrupole moment, T_{1Q} is the value of T_1 predicted using the quadrupole relaxation process, and $T_{1\mu}$ is the value of T_1 predicted using the nuclear dipole-dipole process. Values of

$T_{1\mu}/T_{1Q}$ for some nuclei are given in table 3.1.

Nucleus	$T_{1\mu}/T_{1Q}$
Li^7	4×10^4
B^{11}	3×10^5
Al^{27}	5×10^4
Na^{23}	10^6

Table 3.1.

It is seen that the electron quadrupole interaction is much stronger than the nuclear dipole-dipole interaction and is comparable to the direct nuclear dipole-paramagnetic dipole interaction in Bloembergen's theory. Thus to give T_1 of the same order as Bloembergen's theory, a fluctuating electric field is required which bears the same relation to the fluctuating field of one electron charge at a lattice point as the fluctuating magnetic field of the paramagnetic ion does to the fluctuating field of the nuclear dipole at a lattice point. Thus in a model which treats the electric field in the lattice as being due to point charges at the lattice points, these charges have to be of the order of 10^3 electron charges to predict T_1 values due to quadrupole relaxation in agreement with experiment.

Kranendonk 1954 in a detailed analysis shows that this is indeed the case and he looks for the actual mechanism which gives a coupling equivalent to 10^3 electrons on the point charge model in two effects. Firstly the nuclear quadrupole moment of the nucleus polarises the surrounding charge cloud in such a way as to induce quadrupole and higher moments, and these also react with the crystalline field to give

an effective quadrupole moment which may be as much as 10^2 times larger than the nuclear quadrupole moment. This is the antishielding effect. Secondly the crystalline field at the nucleus is not simply the field due to the charges on neighbouring lattice points. The surrounding ion is polarised by this field to give a shielding effect at the nucleus. This reduces the local field, an effect opposite to that for which we seek. The enhancement of the local fluctuating field, Kramandank proposes, is caused by the covalent effect. If the lattice is deformed by the lattice vibrations some p- or d- like orbitals are mixed with the original s-like wave functions of the ions, and the electrons in these non spherically symmetric orbitals produce an electric field gradient at the nucleus which can react with the nuclear quadrupole moment. The resultant quadrupole spin-lattice coupling can be much larger than that arising from the direct field alone, and the dependence of the interaction energy on the lattice vibrations will be much stronger than for the direct interaction. It can be seen that in this rather arbitrary model of what constitutes the quadrupole spin-lattice interaction we can easily find the last factor of ten required to bring the interaction to the strength of the Bloembergen interaction, or indeed a factor large enough to completely dominate the Bloembergen relaxation mechanism if experimentally this is found to be the case.

Pound has in fact shown conclusively that the quadrupole relaxation mechanism does dominate the relaxation process in a pure crystal of sodium nitrate. The bonding in sodium nitrate is

expected to be purely ionic and if in fact there is no covalent bonding the result, in view of the Kranendank theory, is surprising.

On the other hand alternative theories of the origin of the large fluctuating electric field necessary to give the coupling to the nuclear quadrupole moment are difficult to uphold. For instance, suppose that the necessary fluctuating electric field was supplied by crystal imperfections which give a good thermal contact with the lattice as far as neighbouring spins are concerned, and relax the spins as a whole through the spin diffusion process. Unfortunately it is not easy to see how dislocations can provide such a field and anyway the experimental results support a relaxation which is directly through the quadrupole process and not through the intermediary of spin diffusion. Neither can it be held that the quadrupole-quadrupole interaction provides a spin-spin interaction which can shorten the spin diffusion time and so make what paramagnetic impurities there are present more effective, for the quadrupole-quadrupole interaction e^2Q^2/r^5, even when multiplied by an antishielding factor, is of the order of 10^{-2} times the dipole-dipole coupling. It is possible however that the distortion of the charge cloud of the ion due to the polarization effect of the nuclear quadrupole moment in purely ionic crystals, gives rise to fluctuating fields at the ion centre of magnitude comparable to the fields expected from a degree of covalent binding.

In any case it seems likely that the relative strengths of the magnetic and electric processes will vary widely from crystal to crystal and it is desirable to have some experimental evidence of the nature of the relaxation mechanism in different ionic crystals.

4. Theory of the Experiments.

4.1. Quadrupole split spectra

(neglecting magnetic interaction)

For nuclei with $I > \frac{1}{2}$ arranged in a crystal lattice we have / two terms in the Hamiltonian. One represents the Zeeman energy of the nuclear magnetic moment in the external magnetic field H and would give rise to a set of $2I + 1$ uniformly spaced energy levels. The second term represents the energy of the quadrupole electric moment of the nucleus in the electric field gradient at the nucleus and depends on the angular relation between the electric internal field and the applied magnetic field. For an isolated nucleus of spin greater than $\frac{1}{2}$ the energy levels are given by (Pound 1950)

$$E_m = \frac{-m\mu H_z}{I} + \frac{eQ\left(3m^2 - I(I+1)\right)}{4I(2I-1)} \frac{d^2V}{d_z^2} \qquad 4(1)$$

where m takes values from + I to - I and V is the electrostatic potential at the nucleus due to all charges outside it, account being taken of the fact that quadrupole and higher moments are induced in the surrounding charge cloud by the quadrupole moment of the nucleus. We have the possibility then of nuclei of suitable quadrupole moment in sufficiently high external electric field gradients giving rise to a nuclear magnetic resonance spectrum where the spectral lines corresponding to different transitions are not superposed. The second term of equation 4(1) leads in general to a different energy gap between $E_m \rightarrow E_{m-1}$ and $E_{m-1} \rightarrow E_{m-2}$ so a spectrum of 2I lines is

predicted. When we have suitable conditions, namely nuclei in identical positions in a crystal lattice of lower than cubic symmetry (so that $\frac{d^2\nu}{dz^2} \neq 0$) we find such spectra (Pound 1948, Petch 1951 etc.). Where the second term of equation 4(1) is small enough to be treated as a perturbation of the energy level due to the first term only, then the theory of the frequency shifts of the spectral lines with angle is well founded, (Volkoff 1953) and experimental results for some crystals are available (e.g. Eades 1955).

4.2. Detection of Quadrupole Relaxation.

Pound (1950) showed that when one line of the spectrum of 2I lines of the nuclear magnetic resonance in such a crystal is saturated with a strong radiofrequency power applied to a coil wound round the crystal, the populations of the energy levels giving rise to the other lines of the spectrum are affected when the relaxation mechanism is quadrupolar but not affected when the dominant relaxation mechanism is magnetic. The difference in behaviour stems from transitions for which the magnetic quantum number m changes by 2, which are allowed for quadrupolar interactions but not for magnetic interactions. The energy level populations are thus much more inter-related in the quadrupole case and Pound was able to show such interdependence by examining the strengths of the other lines of the spectrum measured at low power in a second coil wound orthogonally on the crystal. As the strength of these lines did depend markedly on the power applied to the first line he concluded that, in the crystal of sodium nitrate he was examining, nuclear magnetic relaxation was due to a quadrupole process.

Pound's two coil method is not always convenient as it entails a duplication of radiofrequency power sources to feed the two coils, and some difficulty in design of sample head to allow for the winding of two orthogonal coils maintaining the high filling factor and high 'Q' required because of the inherently weak signals from most of the crystals of interest. We were able to show that the same distinction could be drawn from a study of the saturation behaviour of the lines using one radiofrequency and one coil wound round the sample crystal. The distinction between the mechanisms is brought out particularly well when the crystal is so oriented that two lines are superposed.

4.3. Analysis of Steady State Energy Level Populations under Saturation Conditions

The strength of the absorption signal for any absorption line is proportional to the product of the transition probability P_m for the transition in question, times the population difference in the two energy levels involved.

$$\text{Signal} \propto (N_m - N_{m-1})\, P_m$$

To see how the line intensities will vary with varying applied power we now give an analysis of the behaviour of the population differences between the energy states of the nucleus under the action of the applied R.F. field.

It is possible in the case of single crystal specimens to arrange that the line splitting be small by suitably orienting the crystal in the magnetic field. We are then able to use the

approximation of narrow splitting in our analysis, as even in cases where the maximum energy splitting is an appreciable fraction of the total energy of the line we are able to study the lines at an orientation where the splitting is small.

The equation governing the change of population of the sublevel m is:

$$\frac{dN_m}{dt} = \dot{N}_m = -N_m(W_{m\to m+1} + W_{m\to m-1} + W_{m\to m+2} + W_{m\to m-2} + P_{m\to m-1} + P_{m+1\to m}) + N_{m-1}(W_{m-1\to m} + P_{m\to m-1}) + N_{m+1}(W_{m+1\to m} + P_{m+1\to m}) + N_{m-2}W_{m-2\to m} + N_{m+2}W_{m+2\to m} \qquad 4(1)$$

m - 1 _____

m _____

m + 1 _____

m + 2 _____

The W terms are the probabilities of transitions per unit time brought about by the relaxation process. The p terms are the probabilities of transitions brought about by the radiofrequency field.

4.3.a. Magnetic Relaxation - Lines Resolved.

If the relaxation is predominantly magnetic in origin we can neglect quadrupole relaxation transitions. All terms $W_{m\to m\pm 2}$ can then be omitted from equation 4(1). The upward transition probabilities $W_{m\to m-1}$ are proportional to $(I+m)(I-m+1)$ so we can write

$$\begin{aligned} W_{m\to m-1} &= W(I+m)(I-m+1) \\ W_{m-1\to m-2} &= W(I+m-1)(I-m+2) \\ W_{m+1\to m} &= W(I+m+1)(I-m) \end{aligned} \qquad 4(2)$$

where the spin-lattice relaxation time of the system $T_1 = \frac{1}{2W}$. In order that the relaxation transitions should produce a Boltzmann distribution in the steady state the downward transitions must be related to the upward transitions by the Boltzmann factor

$$W_{m-1 \to m} = W_{m \to m-1} e^{\frac{\mu H_z}{IkT}} = W_{m \to m-1}(1 + \Delta)$$

where $\Delta = \frac{\mu H_z}{IkT} = \frac{h\nu_0}{kT} \ll 1.$

In order that we may relate all the transition probabilities by the same Δ we treat the case of narrow splitting for which the frequencies ν_0 of the lines are sufficiently near each other to make the Δ terms appropriate to the different energy gaps all equal

Then
$$W_{m-1 \to m} = W_{m \to m-1}(1 + \Delta)$$
$$W_{m-2 \to m-1} = W_{m-1 \to m-2}(1 + \Delta) \quad 4(3)$$
$$W_{m \to m+1} = W_{m+1 \to m}(1 + \Delta)$$

The p terms of equation 4(1) are such that $p_{m \to m-1} = p_{m-1 \to m}$ for by the theory of the Einstein coefficients the probability of transition upwards by absorption is equal to the probability of transition downwards by stimulated emission. The p terms are given by (Bloembergen, Purcell and Pound 1948)

$$p_{m \to m-1} = p_{m-1 \to m} = \frac{1}{4}\gamma^2 H_1^2 g(\nu)(I + m)(I - m + 1)$$
$$= (I + m)(I - m + 1) P_m W \quad 4(4)$$

where γ is the nuclear gyromagnetic ratio, $2H_1$ is the amplitude of the radiofrequency magnetic field, and $g(\nu)$ is the normalized line-shape

function. $P_m = \frac{1}{2}\gamma^2 T_1 \left[H_1^2 g(\nu)\right]_m$. At the centre of each line $g(\nu) = 2T_2$ and $P = \gamma^2 H_1^2 T_1 T_2$.

When the nuclear spin system is in a steady state $\dot{N}_m = 0$ and substituting the values from equations 4(2), 4(3), 4(4) in 4(1) we have

$$\dot{N}_m = 0 = W\left\{-N_m\left[2(I^2 - m^2 + I) + (I + m + 1)(I - m)\Delta + (I - m + 1)(I + m)P_m + (I + m + 1)(I - m)P_{m+1}\right] + N_{m-1}(I + m)(I - m + 1)(1 + \Delta + P_m) + N_{m+1}(I + m + 1)(1 + P_{m+1})(I - m)\right\} \quad 4(5)$$

When $m = -I$ we have from 4(5):

$$0 = -N_{-I}\,2I(1 + \Delta + P_{-I+1}) + N_{-I+1}\,2I(1 + P_{-I+1}) \quad (a)$$

$$\therefore N_{-I+1} - N_{-I} = \frac{N_{-I}\Delta}{1 + P_{-I+1}} = \frac{n_o}{1 + P_{-I+1}} \quad (x)$$

where $n_o = N_m \Delta$ is the excess population $N_m - N_{m-1}$ in the lower level of a Boltzmann distribution.

When $m = -I + 1$ we have:

$$0 = N_{-I}\,2I(1 + \Delta + P_{-I+1}) - N_{-I+1}\left[2(3I - 1) + 2(2I - 1)\Delta + 2IP_{-I+1} + 2(2I - 1)P_{-I+2}\right] + N_{-I+2}(2)(2I - 1)(1 + P_{-I+2}) \quad (b)$$

Adding (a) + (b)

$$0 = -N_{-I+1}\left[4I - 2 + 2(2I - 1)\Delta + 2(2I - 1)P_{-I+2}\right] + N_{-I+2}\,2(2I - 1)(1 + P_{-I+2}) \quad (c)$$

$$\therefore N_{-I+2} - N_{-I+1} = \frac{N_{-I+1}\Delta}{1 + P_{-I+2}} = \frac{n_o}{1 + P_{-I+2}} \quad (y)$$

when $m = -I + 2$ we have:

$$0 = N_{-I+1}\ 2(2I-1)(1+\Delta+P_{-I+2}) - N_{-I+2}\left[2(5I-4)\right.$$

$$\left.+3(2I-1)\Delta\ +2(2I-1)P_{-I+2}+3(2I-2)P_{-I+3}\right]$$

$$+N_{-I+3}\ 3(2I-2)(1+P_{-I+3}) \qquad (d)$$

Adding (c) + (d) we have:

$$0 = -N_{-I+2}\left[2(3I-3)+3(2I-2)\Delta+3(2I-2)P_{-I+3}\right]$$

$$+N_{-I+3}\ 3(2I-2)(1+P_{-I+3}) \qquad (e)$$

$$\therefore\quad N_{-I+3} - N_{-I+2} = \frac{n_o}{1+P_{-I+3}} \qquad (s)$$

and so on. In general:

$$\therefore\quad N_m - N_{m-1} = \frac{n_o}{1+P_m} \qquad 4(6)$$

and if all the lines have the same shape function $g(\nu)$ and the radiofrequency power applied to each is the same we have all the P_m terms equal so that putting $P_{-I} = P_{-I+1} = \ldots\ldots = P$

$$N_m - N_{m-1} = \frac{n_o}{1+P} \qquad 4(7)$$

Thus for magnetic relaxation the population difference between any two adjacent energy levels depends only on the transition probability for transitions between these levels induced by the applied radiation and is independant of the probability of transitions between next neighbouring levels. Also the intensity of one line is not affected by the simultaneous saturation of an adjacent line. The saturation factor for each of the lines is $(1+P_m)^{-1}$ and the normalized saturation

curve found by plotting relative signal intensity against applied R.F. power will be the same for any line irrespective of what power, if any, is applied to the other lines.

4.3.b. Quadrupolar Relaxation - Lines Resolved. $I = \frac{3}{2}$

If on the other hand the relaxation process is predominantly quadrupolar in origin we can neglect the magnetic transitions brought about by the lattice. In this case we find that the population difference between any two levels is changed not only by the application of power to the line appropriate to those levels, but also by applying power to the other lines. The saturation functions differ from line to line and the equations are very involved for the general case. The experiments which have been done have involved only nuclei with $I = \frac{3}{2}$ and $I = \frac{5}{2}$, and only the cases $I = 1$, $I = \frac{3}{2}$, and $I = \frac{5}{2}$ are treated for quadrupole relaxation.

For $I = \frac{3}{2}$ we write down the set of four equations corresponding to equation 4(1) substituting for the p terms those given by equation 4(4)

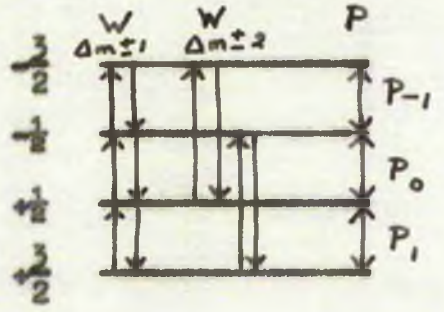

$$
\begin{aligned}
P_{-\frac{3}{2}\rightarrow-\frac{1}{2}} &= P_{-\frac{1}{2}\rightarrow-\frac{3}{2}} = 3P_{-1}W \\
P_{\frac{1}{2}\rightarrow-\frac{1}{2}} &= P_{-\frac{1}{2}\rightarrow\frac{1}{2}} = 4P_{o}W \qquad 4(8) \\
P_{\frac{1}{2}\rightarrow\frac{3}{2}} &= P_{\frac{3}{2}\rightarrow\frac{1}{2}} = 3P_{1}W
\end{aligned}
$$

The transition probabilities for the quadrupole relaxation are given by the squares of the matrix elements of the electric quadrupole tensor given by Pound 1950 equation (16)

$$W_{m \to m-1} \propto (2m-1)^2 (I-m+1)(I+m)$$
$$W_{m \to m-2} \propto (I+m)(I+m-1)(I-m+1)(I-m+2) \qquad 4(9)$$

leading for $I = \frac{3}{2}$ to

$$W_{\frac{3}{2} \to \frac{1}{2}} = W_{-\frac{1}{2} \to -\frac{3}{2}} = W_{\frac{3}{2} \to -\frac{1}{2}} = W_{\frac{1}{2} \to -\frac{3}{2}} = W$$
$$W_{\frac{1}{2} \to -\frac{1}{2}} = W_{-\frac{1}{2} \to \frac{1}{2}} = 0 \qquad 4(10)$$
$$W_{\frac{1}{2} \to \frac{3}{2}} = W_{-\frac{3}{2} \to -\frac{1}{2}} = W(1+\Delta)$$
$$W_{-\frac{1}{2} \to \frac{3}{2}} = W_{-\frac{3}{2} \to \frac{1}{2}} = W(1+2\Delta)$$

These values are also substituted in equation 4(1) to give the equations for the steady state

$$\frac{1}{W}\dot{N}_{-\frac{3}{2}} = 0 = -N_{-\frac{3}{2}}(2+3\Delta+3P_{-1}) + N_{-\frac{1}{2}}(1+3P_{-1}) + N_{\frac{1}{2}}$$

$$\frac{1}{W}\dot{N}_{-\frac{1}{2}} = 0 = N_{-\frac{3}{2}}(1+\Delta+3P_{-1}) - N_{-\frac{1}{2}}(2+2\Delta+3P_{-1}+4P_0) + N_{\frac{1}{2}}4P_0 + N_{\frac{3}{2}}$$

$$\frac{1}{W}\dot{N}_{\frac{1}{2}} = 0 = N_{-\frac{3}{2}}(1+2\Delta) + N_{-\frac{1}{2}}4P_0 - N_{\frac{1}{2}}(2+\Delta+4P_0+3P_1) + N_{\frac{3}{2}}(3P_1+1)$$

$$\frac{1}{W}\dot{N}_{\frac{3}{2}} = 0 = N_{-\frac{1}{2}}(1+2\Delta) + N_{\frac{1}{2}}(1+\Delta+3P_1) - N_{\frac{3}{2}}(2+3P_1) \qquad 4(11)$$

We have four equations for four unknown populations but we can get any one of the equations by adding the other three. Thus we only have three independent equations and can only hope to find explicitly the three population differences

$$N_{-\frac{1}{2}} - N_{-\frac{3}{2}} = N_{-1} \,.$$

$$N_{\frac{1}{2}} - N_{-\frac{1}{2}} = N_{0}$$

$$N_{\frac{3}{2}} - N_{\frac{1}{2}} = N_{1}$$

We put the equations in terms of N_{-1}, N_{0}, and N_{1} and put all terms

$$N_i \Delta = n_0$$

$$\begin{aligned}
0 &= (2 + 3P_{-1})\, N_{-1} + N_0 - 3n_0 && \text{(a)} \\
0 &= -(1 + 3P_{-1})\, N_{-1} + (1 + 4P_0)\, N_0 + N_1 - n_0 && \text{(b)} \\
0 &= -N_{-1} - (1 + 4P_0)\, N_0 + (1 + 3P_1)\, N_1 + n_0 && \text{(c)} \\
0 &= -N_0 - (2 + 3P_1)\, N_1 + 3n_0 && \text{(d)}
\end{aligned} \qquad 4(12)$$

We notice that these equations are symmetrical in N_{-1} P_{-1}, N_{+1} P_{+1}

(i) Let the radiofrequency power be first applied to the centre line only. Then $P_1 = P_{-1} = 0$. In this case obviously $N_1 = N_{-1}$ from the symmetry of the equations and equation 4(12) a becomes

$$N_0 = \frac{n_0}{1 + 4P_0} \qquad 4(13)$$

The saturation factor for the centre line is then $(1 + 4P)^{-1}$

(ii) To find the saturation factor for a satellite line let $P_1 = P_0 = 0$ and the power be applied only to the P_{-1} transition. Then from 4(12) d

$$N_1 = \frac{-N_o + 3n_o}{2}$$

which gives for 4(12) b

$$-(1 + 3P_{-1})N_{-1} + \tfrac{1}{2}N_o + \tfrac{1}{2}n_o = 0$$

Eliminating N_o with 4(12) a we get

$$N_{-1} = \frac{n_o}{1 + \frac{2}{4}P_{-1}} \qquad 4(14)$$

An exactly analogous calculation gives for the other satellite

$$N_1 = \frac{n_o}{1 + \frac{2}{4}P_1} \qquad 4(15)$$

The saturation factor for a satellite line is then $(1 + \frac{2}{4}P)^{-1}$

Comparing the saturation factors of the centre and satellite lines we see that if the lines have the same shape and the relaxation is quadrupolar a given degree of saturation of the centre line requires only $\frac{2}{16}$ of the power required to produce the same percentage saturation in the satellite. This distinguishes clearly between the magnetic and quadrupolar relaxation processes, for in the magnetic relaxation case equal applied powers produced equal degrees of saturation of centre line and satellites.

We can see qualitatively where the difference arises by drawing in the energy level diagram the relaxation transitions allowed in each case when power is applied to the centre line and satellite in turn. For the centre line, in the magnetic case the excess population in the $+\frac{1}{2}$ level is maintained by relaxation transitions directly from $-\frac{1}{2}$ to $+\frac{1}{2}$. In the quadrupolar case an excess spin in the $-\frac{1}{2}$ level has to find

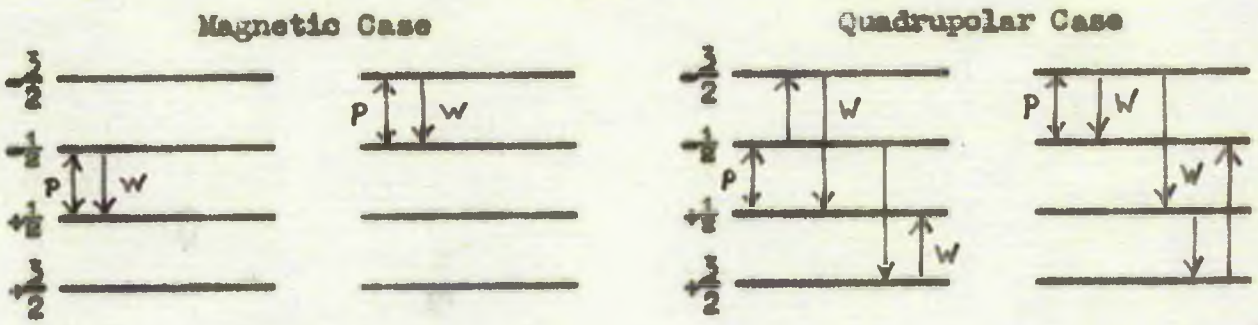

its way to the $+\frac{1}{2}$ level by making two transitions, one involving a $\Delta m = \pm 2$ and another involving $\Delta m = \mp 1$.

If we now apply the power to the upper satellite lines, in the magnetic case relaxation is again by a direct $-\frac{3}{2} \rightarrow -\frac{1}{2}$ transition analogous to the magnetic relaxation of the centre line. In the quadrupolar case the relaxation can take place by a $-\frac{3}{2} \rightarrow -\frac{1}{2}$ transition or by a $-\frac{3}{2} \rightarrow +\frac{1}{2}$, $+\frac{1}{2} \rightarrow +\frac{3}{2}$, $+\frac{3}{2} \rightarrow -\frac{1}{2}$ combination of transitions which is not analogous to the quadrupole relaxation of the centre line

Superposition of Spectral Lines

4.3.c. Magnetic Relaxation - Lines Superposed. $I = \frac{3}{2}$

So far in our equations we have assumed that the only processes which alter energy level populations are transitions induced by the applied power and spin-lattice relaxation transitions. However when we come to study the case where two or more lines occur at the same frequency, we have to take into account the fact that where equal energy quanta are concerned spin-spin collisions occur in which there is a direct interchange of energy between spins, one spin gaining a quantum and the other losing an equal quantum. In terms of energy level populations this spin-spin interaction means that we have a process whereby a transition upwards between two levels occurs simultaneously

with a downward transition between another two levels equally spaced. This process is governed by the time constant T_2 of equation 2 (4) which is generally much smaller than the time constant T_1 in solids. For the case $I = \frac{3}{2}$ the possible transitions of the spin-spin relaxation process are as shown in fig. 4.1.

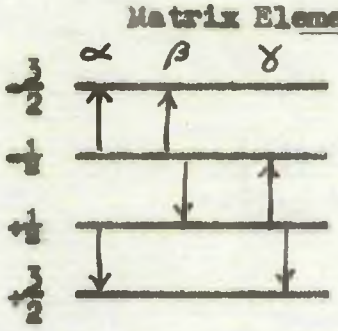

Fig. 4.1.

The probabilities governing such transitions are proportional to the appropriate matrix element for each transition and the number of spins in the level. Thus for the α process the probability is proportional to

$$3\,(N_{-\frac{1}{2}}\,N_{+\frac{1}{2}} - N_{-\frac{3}{2}}\,N_{\frac{3}{2}})$$

the second term being the probability for the reverse process.

Similarly for the β process we have the probability proportional to $\sqrt{12}\,(N_{-\frac{1}{2}}^{\,2} - N_{-\frac{3}{2}}\,N_{\frac{1}{2}})$

and for the γ process $\sqrt{12}\,(N_{\frac{1}{2}}^{\,2} - N_{+\frac{3}{2}}\,N_{-\frac{1}{2}})$

If we put

$$N_{-\frac{3}{2}} = \frac{N}{4} + n_{-\frac{3}{2}}$$

$$N_{-\frac{1}{2}} = \frac{N}{4} + n_{-\frac{1}{2}}$$

$$N_{\frac{1}{2}} = \frac{N}{4} + n_{\frac{1}{2}}$$

$$N_{\frac{3}{2}} = \frac{N}{4} + n_{\frac{3}{2}}$$

where N is the total number of spins, then all quantities n_i are small and neglecting second order terms we get for the probabilities

$$\begin{aligned} &\alpha \text{ process} && 3\,(n_{-\frac{1}{2}} + n_{\frac{1}{2}} - n_{-\frac{3}{2}} - n_{\frac{3}{2}}) \\ &\beta \text{ process} && \sqrt{12}\,(2n_{-\frac{1}{2}} - n_{-\frac{3}{2}} - n_{\frac{1}{2}}) \\ &\gamma \text{ process} && \sqrt{12}\,(2n_{\frac{1}{2}} - n_{\frac{3}{2}} - n_{-\frac{1}{2}}) \end{aligned} \qquad 4(16)$$

The α process adds one to the populations of each of the $\frac{3}{2}$ and $-\frac{3}{2}$ levels and subtracts one from the $\frac{1}{2}$ and $-\frac{1}{2}$ levels. The β process adds one to the $-\frac{3}{2}$ and $+\frac{1}{2}$ levels and subtracts two from the $-\frac{1}{2}$ level. The γ process adds one to the $-\frac{1}{2}$ and $\frac{3}{2}$ levels and subtracts two from the $+\frac{1}{2}$ level.

We now consider the effect of these transitions in the case of magnetic relaxation. They are only operative when two or more of the lines are superposed, in which case the appropriate terms of 4(16) appear in equations 4(1). The equation 4(1) without such terms leads to the solution

$$\begin{aligned} n_{-\frac{1}{2}} &= n_{-\frac{3}{2}} + \frac{n_o}{1+P} \\ n_{\frac{1}{2}} &= n_{-\frac{1}{2}} + \frac{n_o}{1+P} \\ n_{+\frac{3}{2}} &= n_{\frac{1}{2}} + \frac{n_o}{1+P} \end{aligned}$$

for the case of magnetic relaxation. Substituting this solution in the extra terms 4(16) introduced by the spin-spin process we see that they are all identically zero: e.g. when the β process is active and the centre

line is superposed with the $-\frac{1}{2} \rightarrow -\frac{3}{2}$ satellite, terms appear proportional to $(2n_{-\frac{1}{2}} - n_{-\frac{3}{2}} - n_{+\frac{1}{2}})$

$$= (n_{-\frac{1}{2}} + n_{-\frac{3}{2}} + \frac{n_o}{1+P} - n_{-\frac{3}{2}} - n_{-\frac{1}{2}} - \frac{n_o}{1+P}) = 0$$

Thus the solution

$$N_m - N_{m-1} = \frac{n_o}{1+P} \qquad 4(7)$$

holds good in the magnetic case even when lines are superposed and the spin-spin relaxation mechanism is taken into account. Thus the saturation factor for any number of superposed lines is a linear combination of terms $(1+P)^{-1}$. Then the saturation factor in the magnetic spin-lattice relaxation case is the same for all lines and all combinations of superposed lines and equal to $(1+P)^{-1}$

4.3.d. Quadrupole Relaxation - Lines Superposed. $I = \frac{3}{2}$

Now we consider the quadrupole spin-lattice relaxation case when lines are superposed.

(i) First let us consider an orientation of the crystal at which all the lines are superposed. In this case all three spin-spin relaxation processes would be active. We first solve the equations neglecting the spin-spin terms.

Putting $P_{-1} = P_o = P_{+1} = P$ in 4(12) we have from the symmetry of the equations that $N_{-1} = N_1$

$$\text{so} \qquad \begin{aligned} 0 &= (2+3P)\,N_{-1} + N_o - 3n_o \\ 0 &= -3P\,N_{-1} + (1+4P)\,N_o - n_o \end{aligned} \qquad 4(17)$$

which leads to

$$N_{-1} = N_0 = N_1 = \frac{n_0}{1+P} \qquad 4(18)$$

In fact when all lines are superposed the quadrupole relaxation case is indistinguishable from the magnetic dipole relaxation case and the spin-spin terms are identically zero. This case is not commonly found in practice as second order perturbations usually prevent all three lines coalescing at any crystal orientation.

(ii) The case where the two satellite lines are superposed gives us $P_1 = P_{-1} = P$, $P_0 = 0$. We have from the symmetry of equations 4(12) with these substitutions that $N_1 = N_{-1}$ and neglecting for the moment the spin-spin terms the equations reduce to:

$$(2+3P)N_{-1} + N_0 - 3n_0 = 0$$

$$-3P\,N_{-1} + N_0 - n_0 = 0$$

$$\therefore N_1 = N_{-1} = \frac{n_0}{1+3P} \qquad 4(19)$$

In this case only the a process would be active which would introduce terms proportional to

$$(n_{-\frac{1}{2}} + n_{\frac{1}{2}} - n_{-\frac{3}{2}} - n_{\frac{3}{2}})$$

$$= (N_{-1} - N_1)$$

$$= 0$$

So the solution 4(19) holds good when the spin-spin relaxation is taken into account and the power absorbed when the satellite lines are superposed is proportional to:

$$N_1P_1 + N_{-1}P_{-1} \propto \frac{3n_o}{1+3P} + \frac{3n_o}{1+3P} = \frac{6n_o}{1+3P}$$

The normalised saturation factor is then $(1+3P)^{-1}$ for the case of superposed satellites which is again distinct from the other quadrupole cases.

(iii) The case where a satellite line is superposed on the centre line gives us $P_{+1} = P_o = P$. $P_{-1} = o$. If we start again by finding a solution neglecting the spin-spin terms, and then substitute this solution in the spin-spin terms we find that they are not zero. We then have to solve the equations including the spin-spin terms. In this case only the β process is active as only the levels appropriate to the γ process have equal energy gaps.

The probability for the β process is proportional to

$$\sqrt{12}\,\frac{N}{4}\,(2n_{\frac{1}{2}} - n_{\frac{3}{2}} - n_{-\frac{1}{2}})$$

$$= aW\,(2n_{\frac{1}{2}} - n_{\frac{3}{2}} - n_{-\frac{1}{2}})$$

$$= aW\,(N_o - N_{+1})$$

where a is a constant of proportionality of the order of

$$\frac{T_1}{T_2} \qquad a \sim \frac{1}{T_2W} \sim \frac{T_1}{T_2}$$

The γ process adds one spin to $N_{\frac{3}{2}}$ and $N_{-\frac{1}{2}}$ and takes two spins from $N_{\frac{1}{2}}$ so modifying equation 4(12) we have

$$\frac{1}{W}\dot{N}_{-\frac{3}{2}} = 0 = 2N_{-1} + N_0 - 3n_0$$

$$\frac{1}{W}\dot{N}_{-\frac{1}{2}} = 0 = -N_{-1} + (1 + 4P)N_0 + N_1 - n_0 + a(N_0 - N_1)$$

$$\frac{1}{W}\dot{N}_{\frac{1}{2}} = 0 = -N_{-1} - (1 + 4P)N_0 + (1 + 3P)N_1 + n_0 - 2a(N_0 - N_1)$$

$$\frac{1}{W}\dot{N}_{\frac{3}{2}} = 0 = -N_0 - (2 + 3P)N_1 + 3n_0 + a(N_0 - N_1)$$

We can neglect one of these equations as it is the sum of the others, so collecting terms we get

$$2N_{-1} + N_0 - 3n_0 = 0 \qquad (a)$$

$$-N_{-1} + (1 + 4P + a)N_0 + (1 - a)N_1 - n_0 = 0 \qquad (b)\ 4(20)$$

$$(-1 + a)N_0 - (2 + 3P + a)N_1 + 3n_0 = 0 \qquad (c)$$

Substituting for N_{-1} from equation (a) in equations (b) and (c) we have:

$$(\tfrac{3}{2} + 4P + a)N_0 + (1 - a)N_1 - \tfrac{5}{2}n_0 = 0$$

$$-(1 - a)N_0 - (2 + 3P + a)N_1 + 3n_0 = 0$$

Eliminating N_0 we get

$$N_1 = \frac{4 + 11a + 24P}{4 + 11a + 25P + 14aP + 24P^2}$$

and hence $N_0 = \dfrac{4 + 11a + 15P}{4 + 11a + 25P + 14aP + 24P^2}$

The signal for the combined line is proportional to :

$$\alpha \; P_1 N_1 + P_0 N_0$$

$$\alpha \; 3N_1 + 4N_0$$

$$\alpha \; \frac{1 + \frac{11}{4}a + \frac{33}{7}P}{1 + \frac{11}{4}a + \frac{25}{4}P + \frac{7}{2}aP + 6P^2} \qquad 4(21)$$

If we combine the centre line and the P_{-1} satellite we get the same result. In the crystals examined the line-width is of the order of a few kilocycles per second $\therefore T_2 \sim 10^{-4}$ sec and $T_1 \sim 1$ sec so that a $\frac{T_1}{T_2} \sim 10^4 \gg 1$. In practice the signal is saturated with $P \sim 10$ so that we can neglect terms other than those containing 'a' in 4(21). Then we get the signal for the combined line

$$\alpha \; \frac{\frac{11}{4}a}{\frac{11}{4}a + \frac{7}{2}aP}$$

$$\alpha \; \frac{1}{1 + \frac{14}{11}P}$$

Thus the saturation factor for the superposed centre line and satellite is $(1 + \frac{14}{11}P)^{-1}$

Actually it turns out that the value of 'a' is not critical as far as the saturation is concerned. Plotting (table 4.1) from equation 4(21) the relative signal strength at half saturation is seen to vary only two percent when 'a' varies from 0 to ∞ . Thus little error results from neglect of the spin collision processes since this is given by the case a = o. In fact however the case a = ∞ is appropriate to the experiments*

*These spin-spin collision processes were in fact neglected in our paper on this work (Andrew and Swanson 1957). We are grateful to Dr. W.G. Proctor for giving us details of an application of these processes to relaxation by ultrasonic vibrations which helped us in considering their effect in our problem

Relative Signal Strength

P	a = 0	a = 1	a = ∞
0.01	0.984	0.987	0.987
0.03	0.956	0.962	0.963
0.1	0.873	0.882	0.886
0.3	0.707	0.716	0.724
1	0.431	0.434	0.440
3	0.206	0.206	0.208
10	0.073	0.073	0.073
30	0.025	0.026	0.026

Table 4.1.

The results of the analysis are given in table 4.2. and plotted in fig. 4.1.

$I = \frac{3}{2}$

N.M.R. Absorption Line	m m - 1	Saturation Factor: Magnetic Dipole Relaxation	Saturation Factor: Electric Quadrupole Relaxation
Satellite	$(-\frac{1}{2} \rightarrow -\frac{3}{2})$	$(1 + P)^{-1}$	$(1 + \frac{9}{4}P)^{-1}$
Satellite	$(\frac{3}{2} \rightarrow +\frac{1}{2})$	$(1 + P)^{-1}$	$(1 + \frac{9}{4}P)^{-1}$
Centre line	$(\frac{1}{2} \rightarrow -\frac{1}{2})$	$(1 + P)^{-1}$	$(1 + 4P)^{-1}$
Superposed satellites	$(-\frac{1}{2} \rightarrow -\frac{3}{2}) + (\frac{3}{2} \rightarrow \frac{1}{2})$	$(1 + P)^{-1}$	$(1 + 3P)^{-1}$
Superposed satellite and Centre Line	$(-\frac{1}{2} \rightarrow -\frac{3}{2}) + (\frac{1}{2} \rightarrow -\frac{1}{2})$	$(1 + P)^{-1}$	$(1 + \frac{14}{11}P)^{-1}$
Superposed satellite and Centre Line	$(\frac{3}{2} \rightarrow \frac{1}{2}) + (\frac{1}{2} \rightarrow -\frac{1}{2})$	$(1 + P)^{-1}$	$(1 + \frac{14}{11}P)^{-1}$
Three lines superposed	$(\frac{3}{2} \rightarrow -\frac{1}{2}) + (\frac{1}{2} \rightarrow -\frac{1}{2}) + (\frac{3}{2} \rightarrow \frac{1}{2})$	$(1 + P)^{-1}$	$(1 + P)^{-1}$

Table 4.2.

4.3.e. Case of Wide Splitting.

The analysis for $I = \frac{3}{2}$ for the case of wide splitting has also been covered. In this case we cannot make the approximation that the Boltzmann factors Δ are equal and we have $\Delta_{-1} = \frac{h\nu_{-1}}{kT}$, $\Delta_0 = \frac{h\nu_0}{kT}$ $\Delta_1 = \frac{h\nu_1}{kT}$ (c.f. equation 4(3)) where ν_{-1}, ν_1 are the satellite frequencies.

Putting $\Delta_{-1} = a_{-1}\Delta_o$ and $\Delta_1 = a_1\Delta_o$ we see that a_{-1} and a_1 vary linearly with the frequency excursion of the satellite lines from the centre line. The saturation factors found for the case of wide splitting are the same as those tabulated in table 4.2. multiplied in some cases by a_{-1} or a_1. So the normalized saturation factors are identical with those in table 4.2. and in fact this table is not restricted to the case of narrow splitting.

This does not mean that the saturation behaviour of a line does not in general change with splitting when that splitting is induced by change of orientation in the field. It is well established experimentally by Watkins and recently by B.R. Williams at Bangor that T_1 (i.e. W) does change with orientation in some crystals, and P $\alpha \frac{1}{W}$. However if the transition probability W remains constant with angle in the crystal then the saturation function does not change with change of splitting. If W does change with angle it is of course necessary to measure all saturation factors to be compared on the scheme of table 4.2. at the same orientation of the crystal in the field, when the saturation functions of table 4.2. should apply no matter how large the splitting should be at the angle chosen.

4.3.f. Quadrupole Relaxation. $I = \frac{5}{2}$

For the case $I = \frac{5}{2}$ we write down the set of six equations corresponding to equation 4(1) and substituting for the p terms those given by 4(4) and for the W terms from 4(9) we reduce those to a set corresponding to equation 4(12):

$$(15 + 20\,P_{-2})\,N_{-2} + 5N_{-1} - 20\,n_o = 0 \qquad (1)$$

$$-(10 + 20\,P_{-2})\,N_{-2} + (13 + 32\,P_{-1})\,N_{-1} + 9N_o - 12\,n_o = 0 \qquad (2)$$

$$-5\,N_{-2} - (9 + 32\,P_{-1})\,N_{-1} + (9 + 36\,P_o)\,N_o + 9N_1 - 4n_o = 0 \qquad (3)$$

$$-9N_o - (13 + 32\,P_1)\,N_1 + (10 + 20\,P_2)\,N_2 + 12n_o = 0 \qquad (4)$$

$$-5N_{+1} - (15 + 20\,P_2)\,N_2 + 20n_o = 0 \qquad (5)$$

4(22)

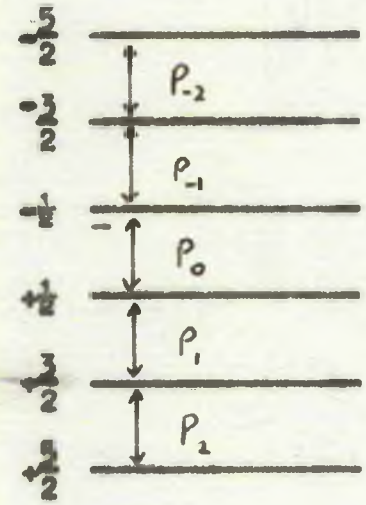

The sixth equation is a linear combination of the others, so that we have a set of five simultaneous equations for five unknowns. The analysis is tedious especially for unsymmetrical cases as for example when power is applied to one satellite only. The equations have been solved and the saturation factors found for all cases where the T_2 process is not operative.

The saturation factors are given in table 4.4. In the case in which satellites are superposed the T_2 process is active but ineffective due to the symmetry of the population distribution.

$I = \frac{5}{2}$

N.M.R. Absorption Line $m \to m-1$		Saturation Factor	
		Magnetic Dipole Relaxation	Electric Quadrupole Relaxation
Outer Satellite	$(-\frac{3}{2} \to -\frac{5}{2})$	$(1+P)^{-1}$	$(1+\frac{837}{539}P)^{-1}$
Outer Satellite	$(\frac{5}{2} \to \frac{3}{2})$	$(1+P)^{-1}$	$(1+\frac{837}{539}P)^{-1}$
Inner Satellite	$(-\frac{1}{2} \to -\frac{3}{2})$	$(1+P)^{-1}$	$(1+\frac{1704}{539}P)^{-1}$
Inner Satellite	$(\frac{3}{2} \to \frac{1}{2})$	$(1+P)^{-1}$	$(1+\frac{1704}{539}P)^{-1}$
Centre Line	$(\frac{1}{2} \to -\frac{1}{2})$	$(1+P)^{-1}$	$(1+\frac{49}{11}P)^{-1}$
Outer Satellites Superposed	$(-\frac{3}{2} \to -\frac{5}{2}) + (\frac{5}{2} \to \frac{3}{2})$	$(1+P)^{-1}$	$(1+\frac{18}{11}P)^{-1}$
Inner Satellites Superposed	$(-\frac{1}{2} \to -\frac{3}{2}) + (\frac{3}{2} \to \frac{1}{2})$	$(1+P)^{-1}$	$(1+\frac{48}{11}P)^{-1}$
All lines superposed		$(1+P)^{-1}$	$(1+P)^{-1}$

Table 4.4

4.3.g. <u>I = 1</u>

The relatively easy case of I = 1 is given here for completeness although no experiments were done on nuclei with I = 1. There are no suitable nuclei with I = 2 so this case is omitted. Cases with $I > \frac{5}{2}$ get progressively more tedious to solve, although it is relatively easy to write down the matrix corresponding to the set of equations equivalent to equation 4(12) for each case and such matrices

can then be diagonalized by electronic computer.

For I = 1 the set of equations corresponding to equation 4(12) is

$$(6 + 10\,P_{-1})\,N_{-\frac{1}{2}} + 4\,N_{\frac{1}{2}} - 10n_0 = 0$$

$$4\,N_{-\frac{1}{2}} + (6 + 10P_1)\,N_{\frac{1}{2}} - 10n_0 = 0$$

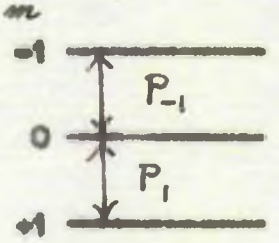

The resulting saturation curves are given in table 4.5

N.M.R. Absorption line $m \rightarrow m-1$		Saturation Factor	
		Magnetic Dipole Relaxation	Electric Quadrupole Relaxation
Upper line	$(0 \rightarrow -1)$	$(1 + P)^{-1}$	$(1 + 3P)^{-1}$
Lower line	$(+1 \rightarrow 0)$	$(1 + P)^{-1}$	$(1 + 3P)^{-1}$
Superposed lines	$(0 \rightarrow -1)$ $+(+1 \rightarrow 0)$	$(1 + P)^{-1}$	$(1 + P)^{-1}$

Table 4.5

It is seen that in this case the upper and lower lines have equal saturation factors in both magnetic and quadrupole cases, and the superposition of the lines would be necessary to make a distinction.

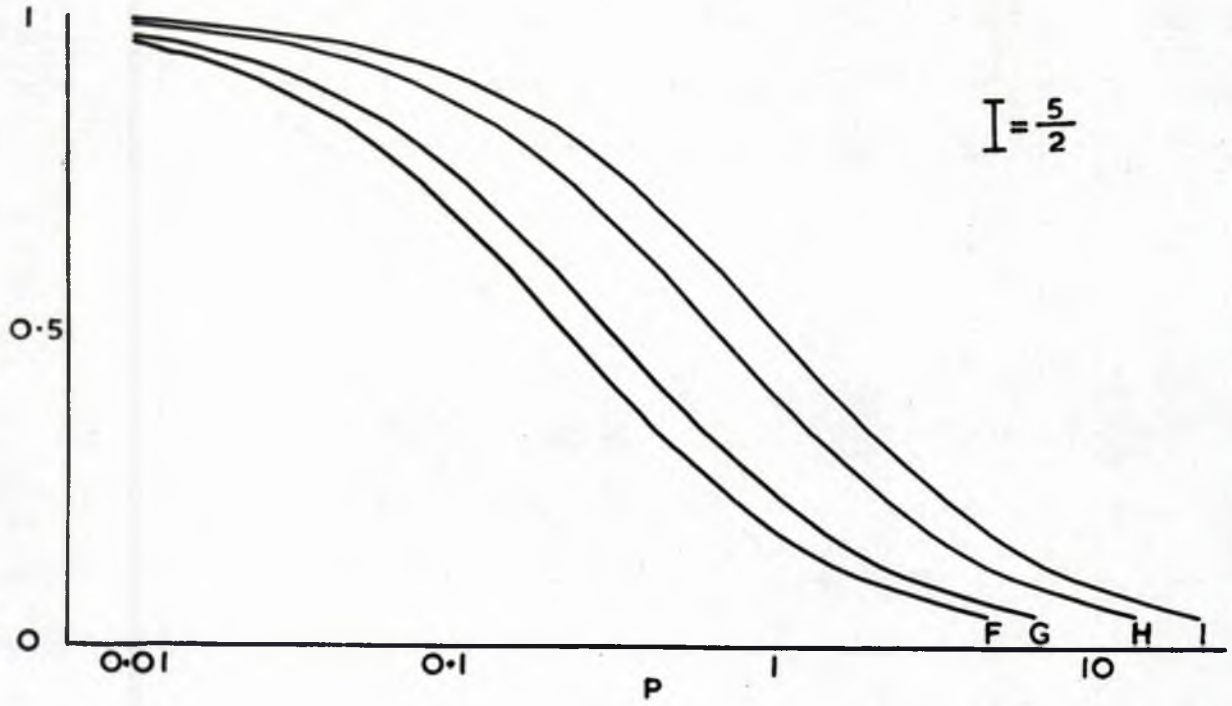

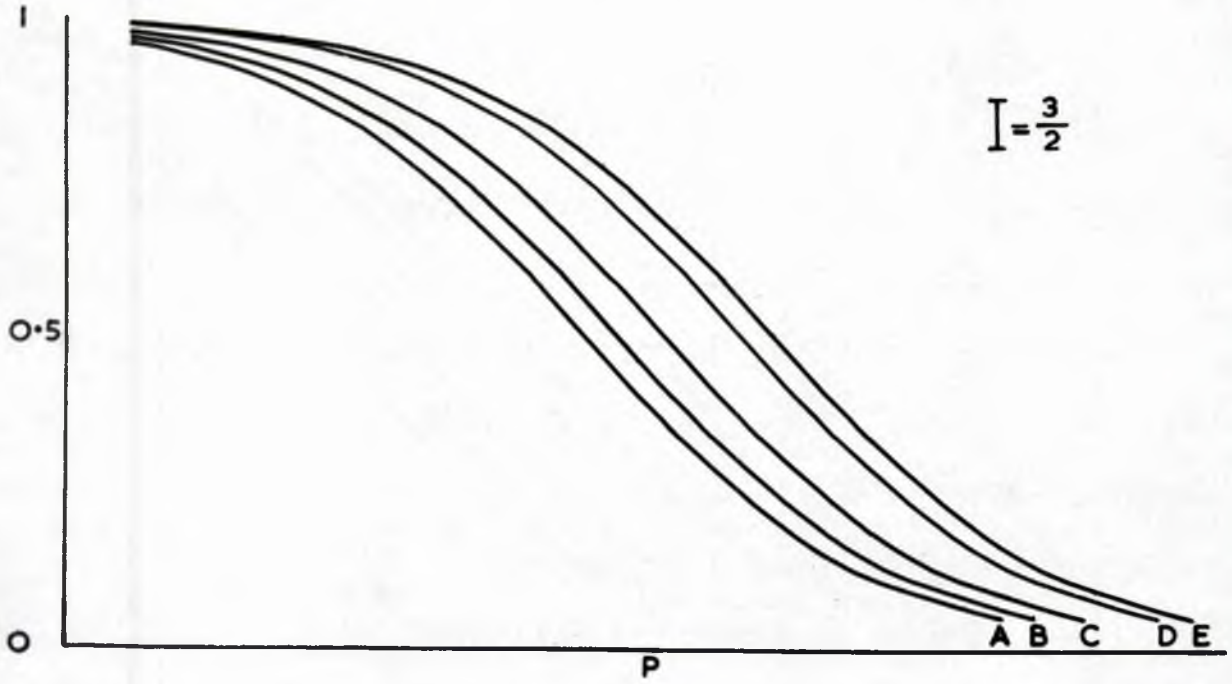

Figure 4.1.

Fig. 4.1. For $I = \frac{3}{2}$ and quadrupole relaxation, curve A is for the centre line, B is for superposed satellites, C is for a satellite line, D is for a satellite superposed on a centre line, and E is for the case of the three lines superposed.

For $I = 1$ curve B is for the single lines and curve E is for the two lines superposed.

For $I = \frac{5}{2}$ curve F is for the centre line. The curve for the inner satellites superposed is very near curve F and is not plotted. Curve G is for an inner satellite; H is an outer satellite. The curve for outer satellites superposed is very near H and is not plotted. Curve I is for the case of all lines superposed.

4.3.h. The Experimental Procedure.

(see also Appendix II)

From the plot of these saturation curves in fig. 4.1./it is seen that in the quadrupole case the curves are quite widely separated for different lines and combinations of lines. In the magnetic dipole case all the saturation curves are of course identical. The experimental procedure is then to find the absorption spectrum for identical nuclei at equivalent sites in a particular crystal. The various lines are identified by observing their splitting with different crystal orientations. The lines are then progressively saturated by increasing the applied R.F. power, and by comparing the plotted saturation curves with those of fig. 4.1 the relaxation mechanism predominating can be deduced .

Because of the wide range of applied R.F. power needed to saturate different nuclei in different crystals, a bridge method of observing the

nuclear magnetic resonance was judged most suitable for the experiments. Because of the inherently low signal to noise ratio of the absorption signal, phase sensitive amplification was necessary to give a bandwidth narrow enough to make the signal observable above the noise. In the phase sensitive amplifier to be described in section 5 the output is proportional to the first differential of the absorption spectrum and so the derivative maximum of the absorption is the peak signal recorded. Under the conditions of these experiments this maximum recorded signal behaves with saturation in the same way as the absorption signal for which the previous analysis has been made. The absorption signal is proportional to X^{11} the loss component of the susceptibility.

$$X^{11} = \frac{\pi}{2} X_o \nu_o Z g(\nu)$$

$$\alpha Z g(\nu)$$

Meter reading $\theta \alpha \frac{dX^{11}}{d\nu} \alpha \frac{d}{d\nu} (Z g(\nu))$ where $Z = \frac{T}{T_s} = Z(\nu, H_1)$ and $g(\nu)$ is the normalized line-shape function.

If the angular frequency of modulation W_m is high enough so that $W_m T_1 \gg 1$ (case 2, Bloembergen, Purcell and Pound 1948) then the saturation does not have time to vary during a modulation cycle and can be averaged at the centre ν_1 of the cycle.

Case 2 applies to most of our experiments as $W_m T_1 \quad 10$

Then Meter Reading $\theta \alpha Z(\nu_1, H_1) \quad \frac{d}{d\nu} g(\nu)$.

$g(\nu)$ is a function describing the way the energy levels are broadened and does not change with saturation. Only the relative populations of the levels changes with saturation. Thus if we fix a value of

frequency ν_1 at which to take the meter readings the term $\frac{d}{d\nu} g(\nu)_{\nu = \nu_1}$ is a constant and the meter readings $\theta_{\nu_1} \propto Z(\nu_1, H_1)$. In this case the meter readings are proportional to the absorption signal and would have the saturation factor of the theory. The experimental procedure for this condition is to find the frequency ν_1 corresponding to maximum meter deflection for the unsaturated case. Then keeping this frequency constant the input power is increased and the output meter reading taken at various power levels to give the saturation curve.

Another way of proceeding is to sweep through the line at different power levels recording the maximum meter deflection at each level. This maximum meter deflection does not occur at the same frequency (or field if the frequency is held constant and the field is swept) for different degrees of saturation, for

$$\theta_{max} \propto \left[Z(\nu_1, H_1) \frac{d}{d\nu} g(\nu) \right]_{max}$$

a condition which is found by equating $\frac{d\theta}{d\nu}$ to zero. At higher saturation the line is broadened and θ_{max} occurs at a frequency further from ν_o. The saturation curve plotting θ_{max} against input H_1 is not then identical with that found plotting maximum absorption against H_1. A detailed analysis of this difference, assuming the unsaturated line-shape $g(\nu)$ to be either Gaussian or Lorentzian, has been done by Professor E.R. Andrew. He finds that the departure of the θ_{max} saturation curve from the absorption saturation curve at half saturation is (in terms of the H_1 ordinate) 0.3 db. for the Gaussian shape and 0.7 db. for the Lorentzian. However these differences are constant when the

saturation factor is that for centre or satellite lines, or for combinations of lines. Thus the relative changes of H_1 for half saturation are the same when either the Θ_{max} or the true absorption saturation curves are plotted. The Θ_{max} curves are merely displaced along the H_1 ordinate by a small factor which depends on the actual unsaturated line shape, but their relative displacement is of second order.

Both the above procedures were used in the experiments to be described, but complete sets of saturation curves for comparison were always taken using the same procedure throughout.

5. The Apparatus.

5.1. The Function of the Apparatus.

In Chapter 2 it was shown that when nuclei of spin $I > 0$ are placed in a magnetic field resonant absorption of energy from a radiofrequency field takes place near specific frequencies. If the absorption of energy is strong enough one can detect it by measuring the fall in the voltage across the r.f. coil supplying the power to the sample. At resonance there is extra loss in the r.f. coil due to the absorption of energy by the spin system, so that the effective quality factor Q of the coil is reduced, and under constant current conditions there is a loss of voltage across the coil.

For nuclei in a solid state lattice the relaxation time is too long and the lines are too broad for the absorption to be strong enough to be detected in this way. The change in r.f. level due to resonant absorption in a solid is very small and comparable to, or less than, the random noise fluctuations in level which exist on the output of the radiofrequency generator, and are added to be any amplifier through which the signal is passed. The problem then is to design practical apparatus which will detect this loss of power to the spin system even when it is masked completely by random noise.

The solution, first found by Purcell, Torrey and Pound 1946, lies in applying a.c. methods to the detection of the absorption. The noise power is scattered, more or less evenly, over a wide range of frequencies although the 'flicker effect' enhances the low audio frequency noise power. Any system of detection which responds to a wide band of frequencies

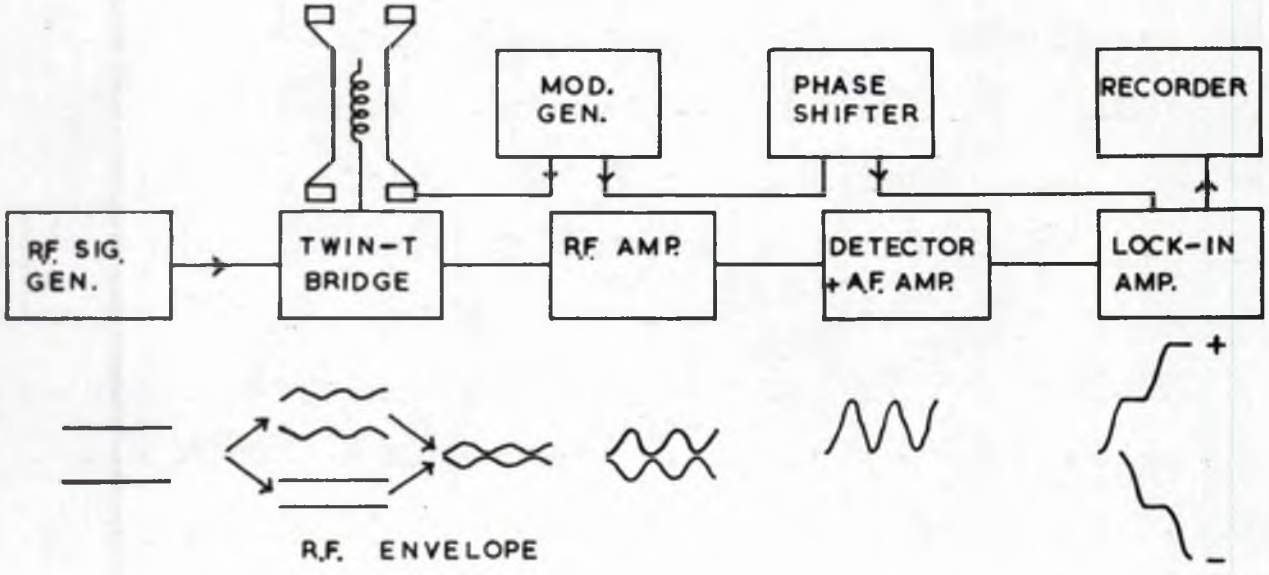

Figure 5.1.

Block Diagram of Apparatus. The signal waveform is also shown at different stages.

responds to all the noise signals and so will never pick out the absorption signal by amplification. Instead it is arranged that the absorption signal should appear cyclically on the radiofrequency carrier with a periodicity corresponding to a selected fixed frequency and that it should then be amplified by an amplifier which responds to this frequency but has a bandwidth of a small fraction of one cycle/sec. A block diagram of the apparatus used is given in fig. 5.1. along with a diagramatic representation of the signal waveform at different stages.

Such an amplifier cannot pass undistorted a signal as complicated as a complete absorption curve, the fourier spectrum of which contains a wide range of frequencies. Instead of sweeping through the whole absorption line the magnetic field is modulated at a low audio frequency, with an amplitude small compared to the width of the absorption line. When the steady magnetic field is such that N.M.R. absorption is taking place at (say) the point of maximum slope of the absorption curve then the greater absorption of power at one end of the small modulation excursion of the field causes the radiofrequency voltage to drop at that point in time, and to rise as the modulation carries the field to a point where the absorption is less. The result is that the radiofrequency carrier is modulated with a near simusoidal waveform, the periodicity of the sine wave being that of the magnet modulation, and the maximum slope of the sine wave being proportional to the slope of the absorption curve over the small range covered by the magnet modulation amplitude. As the main magnetic field is slowly scanned over the absorption line the maximum slope of the sine wave, and hence the depth of modulation of the r.f. carrier, varies with the slope of the absorption curve.

The depth of sinusoidal modulation at its greatest is very small. It is enhanced by adding to the r.f. carrier another r.f. signal from the same generator arranged to be out of phase with the modulated carrier. The modulation then preserves the same amplitude while the carrier is greatly reduced.

The reduced carrier with its modulation are then amplified by a carefully designed low noise radiofrequency amplifier. After radio-frequency amplification the carrier amplitude is monitored and its value shown on a signal strength meter, the 'S meter'.

The carrier is then passed through a detector stage after which the modulation waveform is given audio amplification and presented to the lock-in amplifier.

The lock-in amplifier receives also a looking signal from the same source which provides the magnetic field modulation. This looking signal is thus at the exact frequency of the signal modulation waveform. It is used to chop up the signal waveform so that the positive slope half-cycles can be used to apply positive pulses through a resistor to the positive side of a condenser, while the negative slope half-cycles are used to apply negative pulses through a resistor to the negative side of the condenser. To chop the signal waveform at the correct points the lock-in signal must be correctly phased.

The condenser has a leakage resistor across it so that when steady conditions are reached and the leakage current balances the current pulses coming in to the condenser, the D.C. voltage across the condenser is proportional to the size of the incoming pulses. They in turn are proportional to the slope of the signal waveform which is again

proportional to the slope of the absorption curve at the point where the magnet sweep rests. The D.C. voltage across the condenser is then directly proportional to the slope of the absorption curve. By slowly scanning the absorption curve a recording meter which measures the D.C. voltage across the condenser is made to trace out the differential curve corresponding to the absorption curve. This then is the final recorded signal.

The lock-in or phase sensitive amplifier chops the incoming waveform so that pulses corresponding to the signal modulation add at the condenser. Random pulses due to noise on the incoming waveform will cancel if averaged over a sufficiently long time. The time over which they are averaged is the time constant R.C. of the condenser C being fed through resistance R. The effective bandwidth of the lock-in amplifier is then $\frac{1}{RC}$. For the present experiments it was generally necessary to make the time constant 40 seconds giving a bandwidth of $\frac{1}{40}$ cycle/second. The rate of sweeping the absorption line must be long with respect to the time constant of the apparatus. A poor signal to noise ratio, which entails a long time constant to make the line visible, also entails a slow rate of gathering information.

The apparatus will now be described in detail. The refinements in power supplies were necessary because of the high degree of stability required over long periods. With a recording time constant of 40 seconds it requires over fifteen minutes to sweep through a line without distortion and of the order of three hours to do a set of ten runs at progressive saturation. During this time the frequency of the signal generator and the gain of the amplifiers must remain stable.

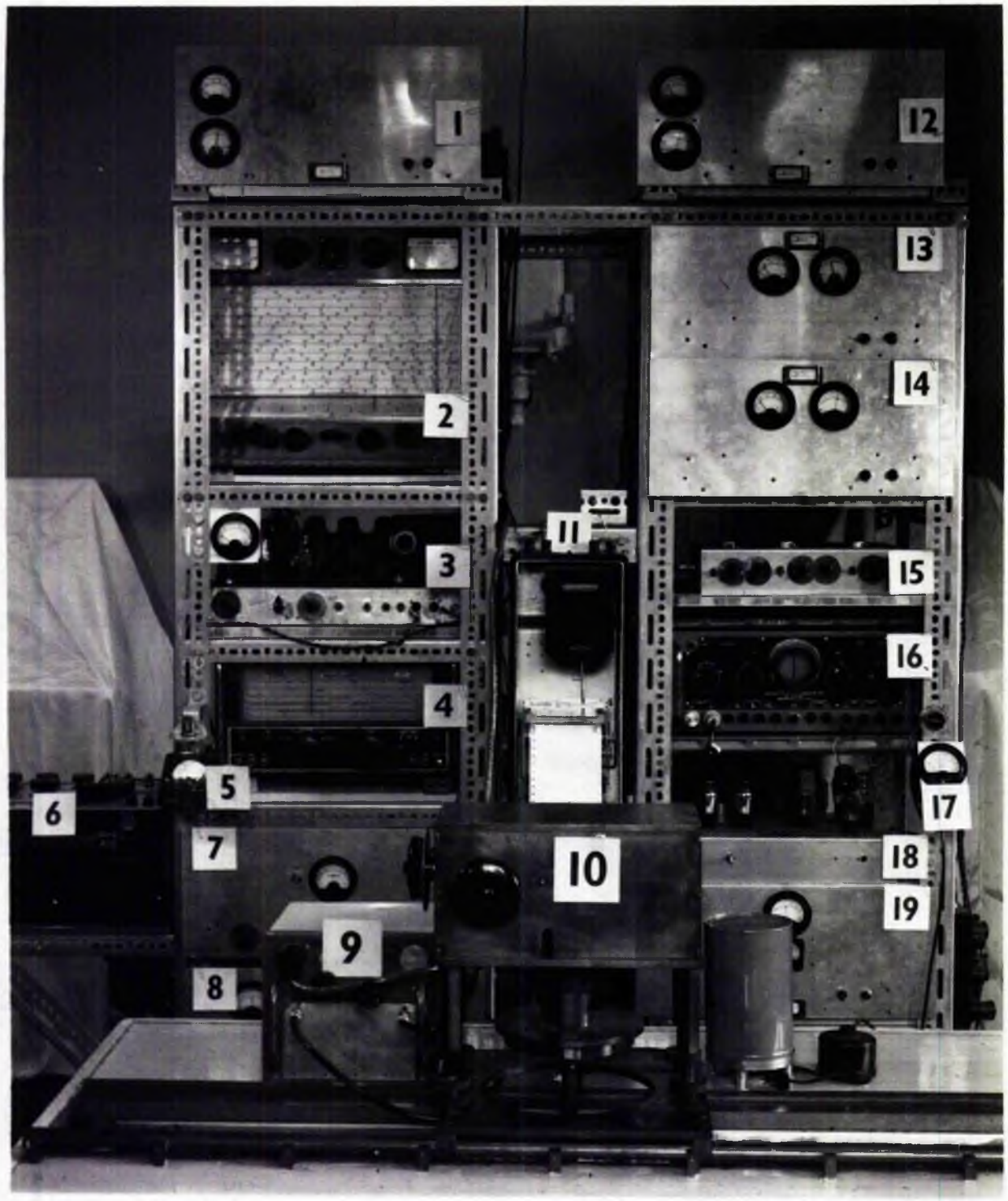

Figure 5.2.

5.2. Layout of the Apparatus.

A working set of apparatus was constructed in St. Andrews and on moving to Bangor much of this apparatus was taken along. On reassembly many improvements were made, and continued to be made over the course of the experiments. The descriptions which follow refer to the final form of the apparatus.

The apparatus is shown in fugure 5.2. Items 1, 12, 13, 14 and 19 are stabilized high tension power supplies. Item 8 and the corresponding unit in the bottom of the right hand rack are trickle chargers which supply the low tension current to all units except power supplies. Item 2 is a Marconi Radiofrequency Signal Generator which feeds into item 10 the Twin-T Bridge. The down-tube from the bridge ends between the poles of a permanent magnet. The field of the magnet is biased by current from the Field Sweep Unit (3) measured by means of a Tinsley Potentiometer (6). The magnet field is modulated sinusoidally by current from the 25 c/s Generator (18) measured by meter 17.

The output from the bridge (10) goes through the Cascode Preamplifier (9) to the Eddystone Receiver (4) and the audio output of the receiver is fed to the Lock-in Amplifier (7). The locking signal to the lock-in amplifier comes from the 25 c/s generator (18) through the Phase Changing Unit (15). The output of the lock-in amplifier is displayed on the Recording Milliammeter (11). The oscilloscope (16) was used to monitor power supply and modulation equipment performance.

5.3. The Magnet.

The permanent magnet was supplied by Mullards Ltd. As originally supplied, its magnetic field was found to be insufficiently homogeneous to meet our requirements. The field was plotted by using the proton resonance in a liquid paraffin sample placed in a twin-T bridge constructed to operate at proton frequency (23 Mc/s). A preamplifier using a single E.F. 54 valve with tuned input and output was also constructed for this frequency to facilitate the test. The inherent line-width of the proton resonance in the liquid paraffin is very small and the line obtained had line-width determined by the inhomogeneity of the field over the sample. The signal was very strong and was displayed directly on an oscilloscope, the field modulation being turned up to sweep right through the line, and the time-base of the oscilloscope being synchronised with the modulation. The line-width, and hence the field inhomogeneity was plotted at different points in the field.

The inhomogeneity was traced to badly machined pole caps. These were removed from the magnet and ground to a smooth finish in so far as the ring shim on the pole caps, which restricted the grinding, would allow. In this way the inhomogeneity was reduced from 3 gauss to 1 gauss over a 2 cc sample. This improvement being inadequate new pole caps were designed, which were machined to a higher standard. They were fitted with a small piece of copper foil in the centre of the polecap next to the backing plate. By tightening the retaining screws slightly the caps could then be tilted using the piece of copper as fulcrum, so that they could be adjusted for parallelism. Each time the polecaps were removed the magnet had to be demagnetised and remagnetised with the new polecaps in position.

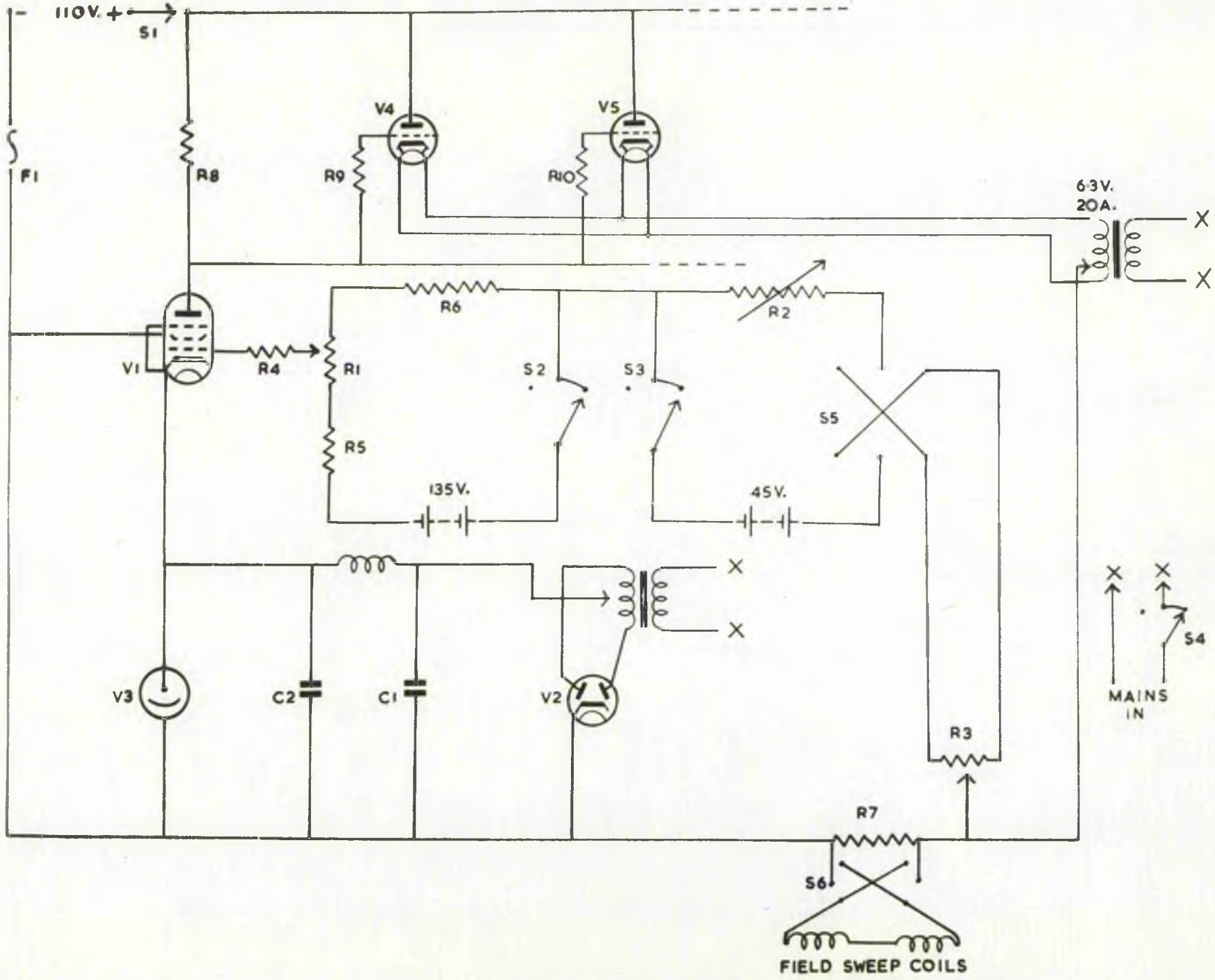

Figure 5.3.

The Field-Sweep Unit.

This required a current of 300 amps from the laboratory battery through the magnetising coils on the magnet, which presented some switching difficulties. The final homogeneity attained on this magnet by adjusting for parallelism and monitoring progress with the liquid proton signal was 0.1 gauss over a 1 cc. sample in a field of 6,036 gauss.

The field of the magnet varied with temperature in a reversible manner, the variation being -2 gauss per °C rise in temperature. For this reason a constant temperature enclosure was constructed around the magnet by Dr. Eades and Mr. D.G. Hughes, by means of which they attained magnet temperatures constant to ±0.03°C.

5.4. The Magnet Field Sweep Unit.

The circuit of the field sweep unit is given in fig. 5.3. It is based on a circuit given by Gutowsky, Meyer and McClure, 1953. The field sweep coils on the magnet are supplied with current passed through valves V_4, V_5, ... which are twenty 6B4. triodes in parallel. In a later modification of this circuit by R.G. Eades and N.D. Finch, 6 higher current capacity 6080 valves were used. The grids of these valves are controlled by the 6AC7 sharp cut off pentode V.1. The action of V1 is to compare the voltage across the field sweep coils with a reference voltage across the tapping on variable resistance R3. Any difference between these voltages is amplified by V1 and applied to the grids of V_4, V_5,.... in such a manner as to make the voltage across the field sweep coils equal to that of the reference.

The resistance R3 is a helical potentiometer which can be driven by an electric motor through a clutch, or manually with the clutch open.

When the motor is driving R3 the reference voltage varies linearly with time, and the high gain of V1 ensures that the voltage across the coils varies in sympathy so that the field is biased linearly.

R2 is a variable resistance which determines the total voltage across the helical potentiometer and hence the maximum excursion of the voltage across the sweep coils. With one particular gear between the motor and the helical potentiometer R3 is always traversed in the same time. Thus R2 gives a variation in the total sweep during that time and provides a sweep rate control. The sweep rate can also be altered over even wider limits by changing the gears between the motor and the helical potentiometer. Gear sets from the Evershed Vignoles recording milliammeter are used, so a range of ratios are available.

The variable potentiometer R1 enables any section of the total sweep range to be swept at the rate determined by the setting of R2. Switch S5 reverses the direction of sweeping and S6 determines whether the magnet is biased up or down on its permanent field. The ganged switches S1, S2, S3, and S4 have three positions, off, warm-up, and on.

The field sweep coils are such that the maximum field shift available is 70 gauss. The field shift is measured by passing the current to the field sweep coils through a standard resistor of 0.0517 ohms and measuring the voltage across the resistor by means of a Tinsley Potentiometer. The rate of sweeping is found to be linear with time over the wide range of sweep rates available. The sweep coils were calibrated by using a proton signal displayed on an oscilloscope screen, and finding the resonance frequency at different sweep settings. The frequency shifts were measured on a BC.221 wavemeter. It was found that the field

shift was 122.0 gauss per amp.

The circuit constants of the sweep unit are given in table 5.1.

Table 5.1.

V1	6AC7	R1	100K pot.
V2	5U4	R2	50K pot.
V3	V.R.105	R3	20K 10 turn helical pot.
V4, V5,.....	6B4's	R4	1M
F1	1.5A fuse	R5	47K
C1	16 μF	R6	470K
C2	32 μF	R7	10K
		R8	47K
		R9, R10,....	200Ω

5.5. The Magnet Field Modulation Equipment.

For most of the experiments this consisted of a 25 c/s generator held on frequency by a synchronising signal from an Airmec Frequency Standard. The generator consisted of a multivibrator followed by selective audio amplification using twin-T feedback networks to select a 25 c/s sinusoidal wave from the 25 c/s synchronised multivibrator output. The final output is through a power amplifier. This unit feeds the modulation coils, which are to a Helmholtz pair wound round the polecaps, and it also feeds into the phase shifting unit.

At a later stage high impedance modulation coils were fitted. They were designed to be fed directly from the output of a commercial audio frequency generator so that the modulation frequency can be easily changed.

The total number of turns on the coils is 7,650 tapped at 3,400. When fed in series they give 1.9 gauss peak to peak modulation per milliamp input, with a maximum of 10 gauss available at 0.1 watt input. To give finer control of small modulation settings the coils are switched so that the field from the first 3,400 turns can be made to oppose the field from the rest of the coils. The input impedance is thus kept near the same high value but the modulation with the coils in antiphase is 0.3 gauss peak to peak per milliamp input with 1.5 gauss maximum modulation available at 0.1 watt input. The modulation amplitude was calibrated using a proton signal and the previously calibrated field sweep.

5.6. The Radio Frequency Signal Generator.

This was a Marconi type. It was found necessary to replace the internal power supplies by an external D.C. L.T. supply and stabilised H.T. supply. This eliminates a small spurious modulation of the output at mains frequency, and increases the frequency stability. The twin-T bridge cancels out to a high degree any spurious modulation on the r.f. supply but its balance is sensitive to frequency variation. To attain maximum frequency stability the signal generator was never switched off during the period of a series of runs, that is over periods of months. To attain maximum stability all amplifiers were also kept running over long periods.

5.7. The Twin-T Bridge.

This bridge was modelled on one first used by Anderson 1949. The circuit is shown in figure 5.4. The conditions of balance are

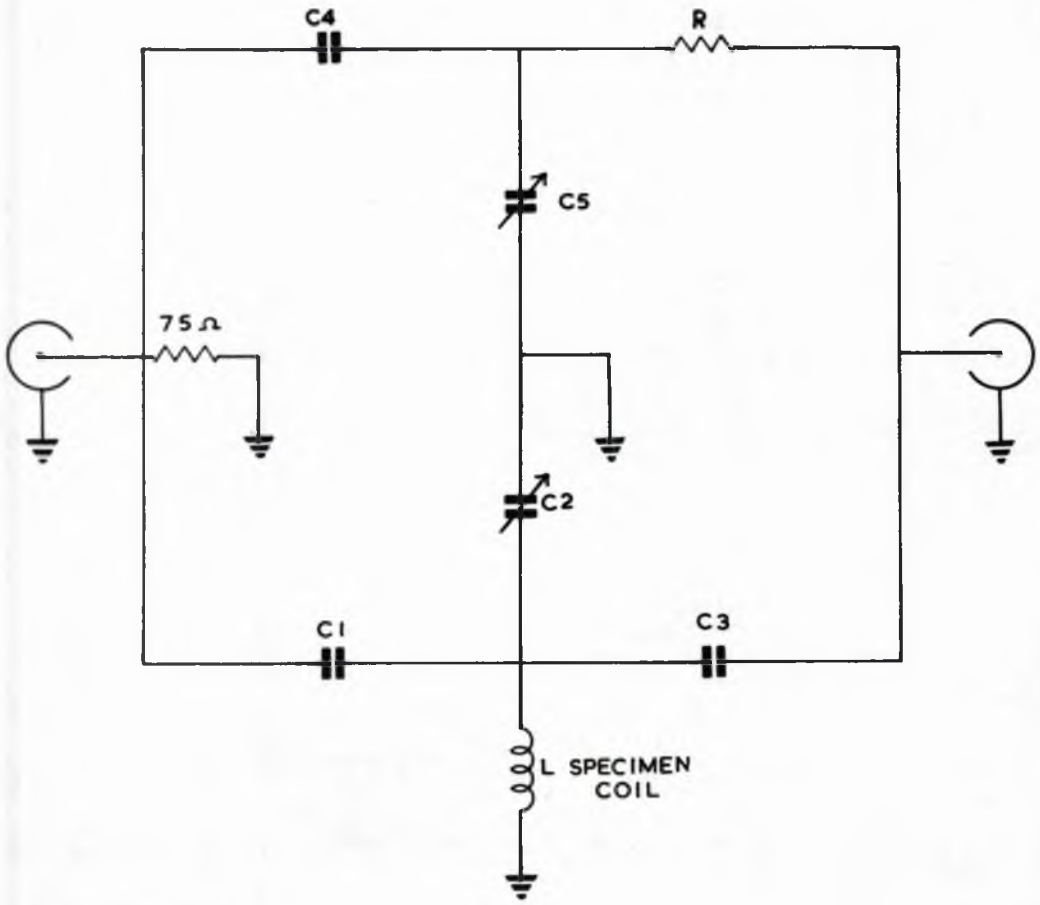

Figure 5.4.

The Twin-T Bridge.

$$\frac{1}{w^2 L} = c_1 + c_3 + c_2 + \frac{c_1 c_3}{c_4} \qquad \text{(Phase balance)}$$

$$\frac{1}{RL} = w^2 c_1 c_3 \left(1 + \frac{c_5}{c_4}\right) R \qquad \text{(Amplitude balance).}$$

R_L is the parallel loss resistance of the specimen coil and $w = 2\pi f$ where f is the R.F. frequency.

It is to be noted that c_5 does not appear in the condition for phase balance and c_2 does not appear in the condition for amplitude or resistive balance. By using the variable controls c2 and c5 the degree of balance of phase and amplitude can be controlled independently.

When the magnetic field at the specimen coil L is changed to the value at which resonance occurs it can be shown that the parallel impedance of the tuned circuit L, c_2 is reduced by a small fraction proportional to χ'' and the phase is changed by a small angle proportional to χ' where $\chi' - i\chi''$ is the complex nuclear magnetic susceptibility.

If the bridge is balanced perfectly in phase, with a residual unbalance in amplitude the change in the parallel impedance of L at resonance will give a change in the amplitude of the bridge output proportional to χ''. As the field is swept the modulation signal appearing on the bridge output will then be proportional to χ'' and the absorption signal will be recorded.

Similarly with perfect amplitude balance and a residual unbalance in phase a signal proportional to χ', i.e. to the dispersion accompanying the absorption, will be recorded.

In our experiments the bridge was always balanced perfectly in phase, and the amplitude unbalance was held at a position where the bridge output was 36 db down on the output before balance. Thus the absorption signal or rather the differential of the absorption signal was always recorded.

The bridge was built on a solid brass base with a plain brass bearing supporting a rotating head marked with a vernier scale measuring tenths of degrees. The down-tube containing the sample coil is a coaxial conductor with a brass outer envelope which plugs into the rotating head. The specimen in the sample coil can thus be turned in the magnet gap and its angle set to 0.1 degrees.

c_1, c_3, c_4, are high quality variable air trimmer condensers with values from 2 pf to 9 pf. R is 100 ohm. c_2 and c5 are 0 - 200 pf. variable air condensers with 0 - 10 pf trimming condensers on slow motion drives in parallel. Due to the solid construction, high quality components, and careful design of the down-tube containing the specimen coil, a perfect phase balance with -36 db residual amplitude unbalance can be maintained without resetting the phase or amplitude controls for periods of over fifteen minutes. The bridge was developed to this degree so that it can be left undisturbed while a weak line is traced out using a long time constant on the phase-sensitive amplifier.

5.8. The Cascode Preamplifier.

The Cascode preamplifier circuit is shown in figure 5.5. It follows recent design (see for example Valley and Wallman, Vacuum Tube Amplifiers) and it is designed specifically to have a low noise factor.

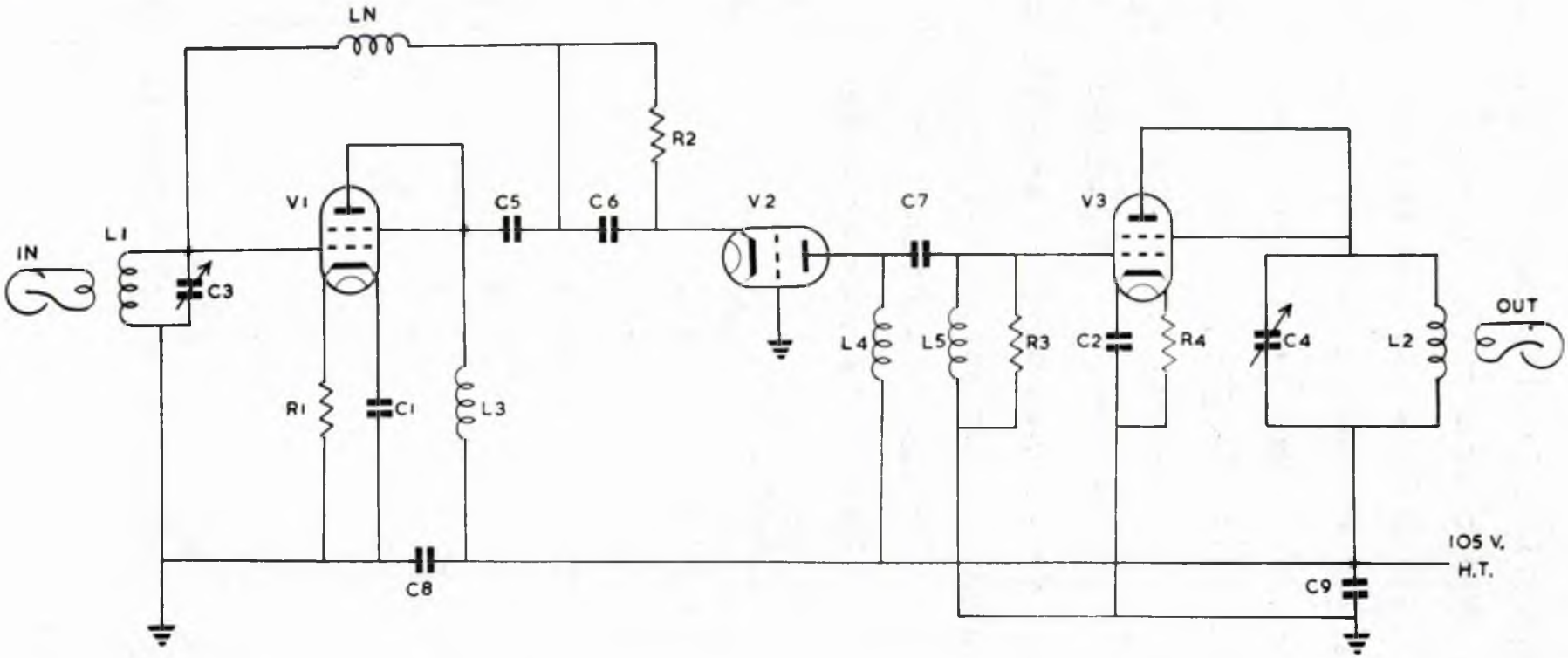

Figure 5.5.

The Cascode Preamplifier.

The noise factor obtainable is 1.06 at 6 Mc/s which approaches the theoretical optimum noise factor of 1.0. Ideally the preamplifier should amplify the output of the bridge to an extent where it is large compared to the noise voltage generated by the first stages of the r.f. amplifier in the receiver, so that any addition of noise to the signal after the preamplifier stage is negligible. The voltage gain through the cascode preamplifier in the form shown in figure 5.5., is 40 db. The circuit constants are given in table 5.2. The inductance Ln is designed to neutralise the grid-plate capacitance of 1.2 pf of V.1. but it is only important for high radiofrequencies and for use near 7 Mc/s it was omitted. L3 tunes the interstage capacitance of ~ 10 pf. L1 and L2 were coils of Q > 300 suitable for the frequency in use.

Table 5.2.

V1	6AK5	C1	0.001 µF	R1	70 ohms
V2	6J6	C2	0.001 µF	R2	100 "
V3	6AK5	C3	0-100 pf	R3	1500 "
		C4	0-100 pf	R4	150 "
L1	See text	C5	50 pf		
L2	"	C6	.005 µF		
L3	"	C7	0.001 µF		
Ln	"	C8	0.005 µF		
L4	R.F. choke	C9	0.005 µF		
L5	R.F. choke				

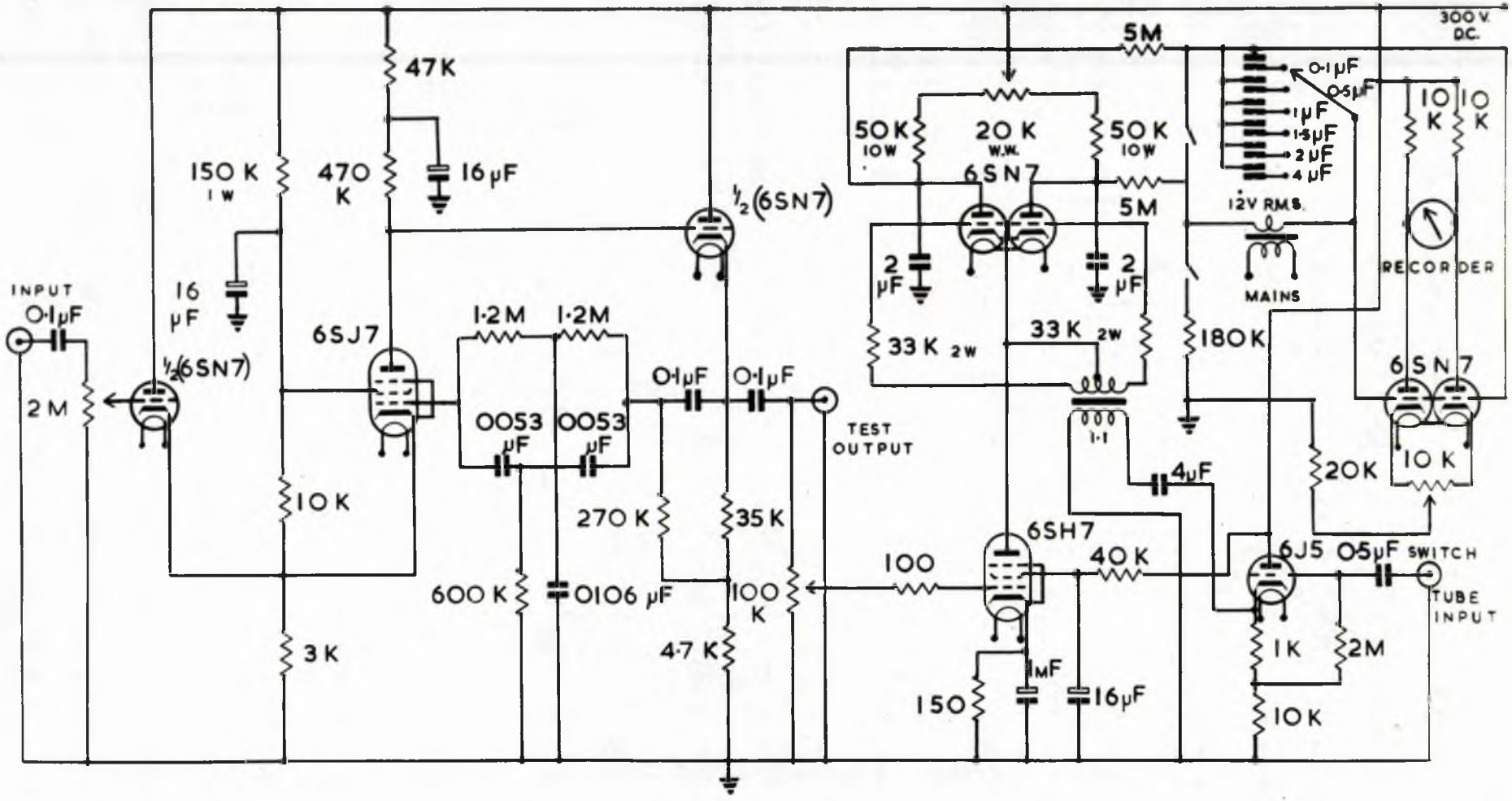

Figure 5.6.

Schuster Narrow-band Amplifier

With a preamplifier of noise factor as low as that of the cascode at low radiofrequencies further improvement in signal to noise ratio can only be reasonably sought by improving the Signal Generator. Further efforts to improve on a noise factor less than 1.1 can only lead to diminishing returns.

5.9. The Receiver.

The signal from the bridge is amplified by the preamplifier and fed into the receiver which is a modified Eddystone model 680 X. The receiver is fitted with an external stabilised power supply and its valve heaters are supplied with D.C. which improves its stability and cuts out spurious interference from mains supplies. The current from the second detector is brought out and passed through a microammeter which thus monitors the radiofrequency signal level being fed into the receiver.

5.10. The Audio Unit.

The audio output of the receiver is fed through a matching transformer to the audio unit. Its circuit is shown in figure 5.6. The first three stages comprise a narrow band amplifier which amplifies selectively an audio frequency picked out by the twin-T network which feeds back to the grid of the 6SJ7 valve. This twin-T network is mounted so that it plugs into a valve base and can be easily changed. The values shown are for 25 c/s which coincides with the modulation frequency principally used in our experiments. The maximum gain of this amplifier is 110 at 25 c/s with a band-width of 1 c/s. The purpose of this amplifier preceding the phase sensitive amplifier is to eliminate noise

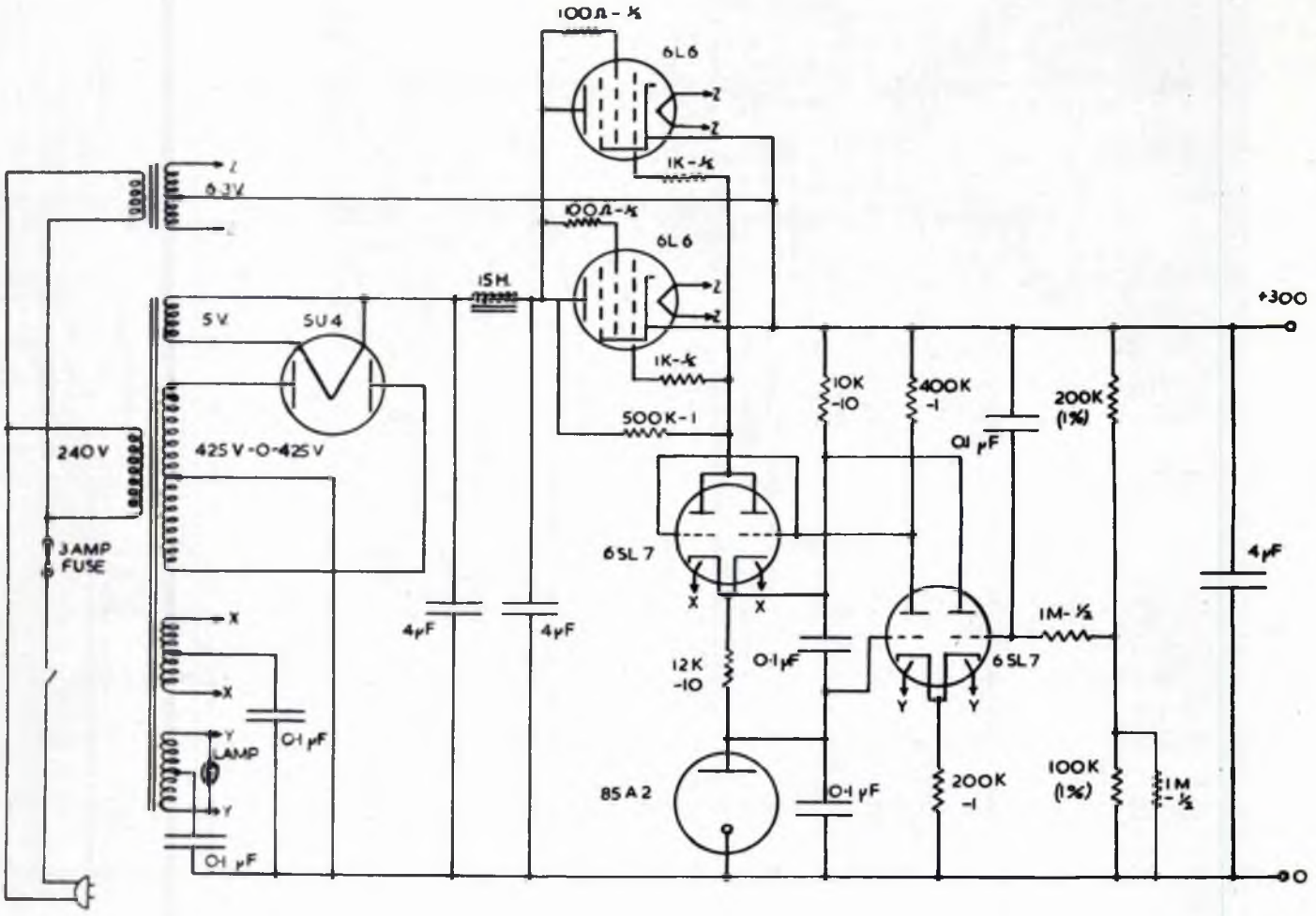

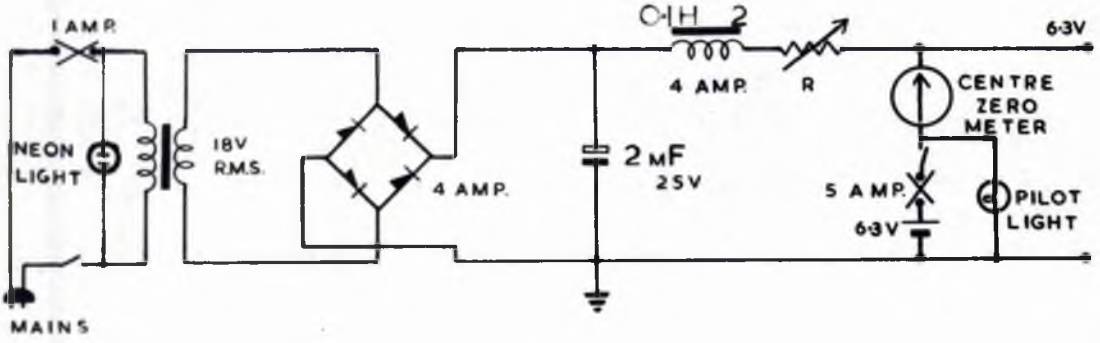

Figure 5.7.

Power Supplies

signals at harmonics of the modulation frequency to which the phase-sensitive amplifier can respond.

The phase-sensitive amplifier is due to Schuster 1951. The incoming signal is injected into the cathode of the twin triode 6SN7 valve by the 6SH7. The grids of the 6SN7 are simultaneously biased by a switching voltage derived from the modulation generator so that the incoming signal is fed alternately to each side of a condenser. This tends to average noise signals to zero while signals in phase with the switching voltage cause a build up of D.C. potential on the condenser. The time-constant of the averaging process is selected by switching in different condensers. The D.C. potential across the condenser is amplified and fed to the recording meter. A small 50 c/s a.c. voltage is superposed to shake the pen of the recording meter and prevent it dragging. A micro switch which can earth one side of the amplifier to the recording meter and so put marker lines on the chart is brought out to a position near the field sweep measuring potentiometer. Line-widths were then measured from field markers on the same chart as the recorded line.

5.11. Power Supplies.

The mains power is supplied to all units through a Servomex A.C. 7 mains stabiliser. This corrects for slow drifts in the mains supply.

The H.T. supplied to every unit is derived from stabilised power supplies of the type shown in fig. 5.7. They deliver up to 150 m.a. at 300 volts D.C. with a residual ripple of less than 1.5 m.v. on the output. The regulation factor defined as % change of a.c. input volts divided by % change of output D.C. volts is $\sim$ 1,500. Power supplies of comparable

performance can now be bought commercially from the Solartron Company.

Also shown in figure 5.7. is the trickle charger circuit which uses the very low impedance of lead-acid accumulators across the output to give a relatively smooth D.C. source of low tension current. Units of this type provided over 12 amps of D.C. current to the heaters of the Signal Generator and all amplifiers. In this way mains frequency pick up was virtually eliminated.

5.12. Comment.

The elaborate care which has to go into the design of the electronic apparatus is dictated by the inherently weak nature of the signals looked for, so that no opportunity of eliminating extraneous noise has to be neglected. Further worthwhile improvement to the apparatus as described might be sought by replacing the commercial signal generator by a r.f. generator using the more recent modifications to the oscillator circuit in the Pound-Watkins Spectrometer (Watkins' thesis, Harvard, 1951). Such oscillators, designed with the problem of noise and stability in mind, have been used as marginal oscillator r.f. spectrometers in the Bangor laboratory. They have been found to be very stable and when worked at their optimum level their performance is superior to that of any commercial r.f. signal generator at present available. A signal generator using this oscillator should significantly reduce the back-ground noise of the bridge spectrometer, while retaining the advantage of a wider range of input power than is available with the marginal oscillator spectrometer. This wide range of input power is essential when measuring a range of T_1 values by progressive saturation.

5.13. Measurement of T_1 by Progressive Saturation.

The principle behind the measurement of T_1 with the apparatus is now given. When T_1 is long enough it can be measured by saturating the absorption line, and then observing its growth under conditions of negligible saturation. The time constant of the growth is T_1.

When T_1 is too short to be measured directly i.e. when T_1 is less than the time constant of the recording apparatus required to observe the line, relative values of T_1 can be measured by progressive saturation.

The maximum deflection of the output meter of the lock-in amplifier is given for the absorption curve by

$$D_{max} = CGH_1 a \left(\frac{dX''}{dx}\right)_{max}$$

where C is a constant.

G is the receiver gain, a is the ratio of modulation amplitude to line-width, and $x = (W_o - W)T_2$. We substitute for

$$\left(\frac{dX''}{dx}\right)_{max}$$

from equation 2.9. In the case that T_1 is much longer than a modulation period (Case 1 Bloembergen, Purcell and Pound, 1948) the value of the denominator of 2.9. is constant over a modulation cycle and can be replaced by its value at the centre of the cycle. In this case we have

$$D_{max} = CGH_1 a \quad \tfrac{1}{2} X_o W_o T_2 (1 + \gamma^2 H_1^2 T_1 T_2)^{-\frac{3}{2}}$$

This result is explicitly for the damped oscillator line shape which is given by the Bloch theory.

If as H_1 is increased G is reduced so that GH_1 remains constant then a plot of D_{max} against H_1 gives the saturation curve. In order to compare

saturation behaviour D_{max} is plotted against log H_1, GH_1 being kept constant as H_1 is increased. For lines of similar line shape the value of D_{max} which is (say) 0.5 times the unsaturated value, will be reached when the parameters $\gamma^2 H_1^2 T_1 T_2$ have the same value for both lines. In this way relative values of T_1 may be found by comparing the values of H_1 at which the lines are half saturated, the values of T_2 being calculated from the observed line-widths. In cases where T_1 is short compared to a modulation period (Case 2, Bloembergen, Purcell and Pound 1948) the analysis leads to a different saturation curve. Fortunately the difference is small and is such as to give errors in T_1 of the order of 10% when comparing curves belonging to different cases. When comparing saturation curves where T_1 ratios are often > 10 a possible error of 10% through the conditions being that of case 1 for one curve and case 2 for another may be thought permissible, especially if the uncertainty of the measured saturation curve is also of this order due to the weakness of the line observed.

6. The Experiments and their Results

6.1. Choice of Sample Material

The choice of crystals was governed by three factors.

(a) The crystal must contain nuclei of $I \geqslant 1$ capable of giving observable signals. If the crystal has too many non-identical sites for the nucleus in question the absorption may be split over so many lines that the signal to noise/ratio may drop below the level which makes measurements possible. For instance a nucleus with $I = \frac{5}{2}$ in a crystal with four non-identical lattice sites for that nucleus gives rise to twenty lines at most crystal orientations and the signal to noise ratio of an unsaturated outer satellite line is 1/28 the value of the signal to noise ratio of the signal if the line were not split. As the nuclei of interest often form only a minor proportion of the total nuclei present in the crystal sample, it is essential to start with a nucleus which gives a high relative sensitivity.

(b) It is preferable that the crystal spectrum should have been examined previously using a variable frequency spectrometer for, to balance its advantage in range of power inputs, the bridge method, using a permanent magnet has the disadvantage that it can only conveniently be swept over a small range in field. The task of locating and plotting lines which may move through the complete range of the field sweep for a rotation of the order of a degree is formidable if one starts without any information as to the spectrum to be expected at a given orientation of the crystal. For instance with the signal to noise ratio available on most of the crystals of interest a recording time constant of 40 seconds

is necessary. To see a line $\sim$ 1 gauss in breadth it is necessary to take $>$ 40 minutes to sweep 100 gauss. As some of the lines of interest make excursions $\sim$ 1000 gauss with varying angle it is obviously desirable that they be plotted with a spectrometer which does not require constant attention and resetting. In fact one crystal, Borax, for which the spectrum was not known was examined, and the slower moving lines were found for a range of angles, but this work was continued only long enough to identify one centre line-satellite system on which the saturation experiment could be performed. A list of the ionic crystals for which spectra have been plotted is given in Appendix I.

(c) The crystal should be available or else be fairly readily grown without the use of elaborate crystal growing apparatus. Respect for the difficulties of the crystal growing art caused all the early crystals examined in the present experiments to be commercial samples artificially or naturally grown. The number of suitable artificially grown, and hence purer crystals available commercially is very limited, and single crystals of three different salts were finally grown from solution.

These were crystals of photographers' hypo, borax, and sodium chlorate. They were grown at constant temperature by slow evaporation of seeded saturated solution. The constant temperature enclosure used was designed to provide the constant temperature for the cold junctions of thermocouples. It was a block of metal with a suitable thermostatically controlled heater wound on it, and it kept a temperature near 40°C constant to better than $\frac{1}{10}$°C. 'Analar' chemicals twice recrystallised were used to grow the hypo and borax crystals.

Sodium chlorate is not available at high purity, and the commercial sample of it was recrystallised nine times. The final technique evolved consisted of placing a test tube of the appropriate solution in a hole in the metal block at 40°C. Some of the dry recrystallised chemical in a filter paper was then put in contact with the top of the solution which was then left for a few hours to become saturated at 40°C. Then the filter paper containing undissolved salt was removed and a carefully selected seed from the last recrystallisation was dropped into the solution. The top of the test tube was partially closed with a stopper containing a large capillary tube. This cut down the evaporation rate so that the tendency for secondary crystals to grow on nuclei other than the seed was lessened. In this way crystals of volumes of greater than 1 c.c. were grown in times of the order of a fortnight. They were tested for singularity by examination in a polarising microscope. They were tested for paramagnetic iron impurity by Mr. F. Holmes and Mr. D.R. Williams of the Chemistry Department, Bangor. They used a spectrophotometric method accurate to 0.1 parts per million. The relevant values are quoted when each crystal is discussed.

6.2. Sodium Nitrate.

6.2.a. Crystal Structure

Sodium nitrate crystals were obtained from two sources. A sawn section measuring 3 x 1 x 1 cm^3 of a reputedly single crystal was purchased from the Harshaw Chemical Company, Cleveland, U.S.A., but it

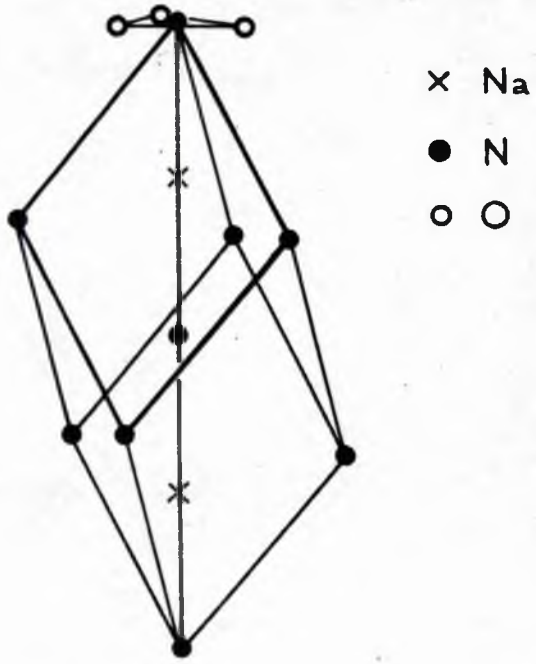

UNIT CELL OF $NaNO_3$

was found to contain at least three single crystals at differing orientations and this made the Na^{23} spectrum needlessly complicated. A large crystal obtained from Hilger and Watts Ltd. was found to be truly single and this crystal was cleaved to give a specimen crystal of ~ 1 cc. in volume.

The crystal has a rhombohedral cleavage. It also has a rhombohedral unit cell (Wyckoff, Crystal Structures Vol. I Chap. VII a). The faces of the cleavage rhomb are not parallel to those of the unit cell but the long body diagonal is in each case the same trigonal axis of symmetry of the crystal. The sodium sites are on this trigonal axis at $\frac{1}{4}$ and $\frac{3}{4}$ way along the long diagonal of the unit cell. As it appears from the results of Pound 1950 that the principal axis of the static electric field gradient tensor is also along this threefold axis, it is seen that the two different sodium sites in the unit cell are identical as far as field gradient is concerned, and they will give rise to the same spectrum.

6.2.b. <u>The Crystal Mount</u>.

It is desirable to mount the crystal so that the trigonal axis can make all angles with the magnetic field direction in one rotation. This was accomplished by mounting the cleaved crystal face on a plane inclined to the axis of rotation of the specimen tube at an angle θ calculated to make the trigonal axis $\perp^{r}$ to the axis of rotation. The three equal angles on the sides of the cleavage rhombohedron where they meet the trigonal axis are $102° 40'$. It follows that the trigonal axis makes an angle of $46° 12'$ with each side. The crystal

was mounted in the specimen tube on a perspex holder cut at this angle so that when a side of the crystal was cemented to it the trigonal axis was perpendicular to the specimen tube. A thin perspex tube with the radiofrequency coil wound on the outside was then slipped over the crystal and held with its axis parallel to the specimen tube by the perspex crystal mount. As the long diagonal of the cleavage rhomb was at right angles to the cylindrical radiofrequency coil the crystal occupied rather a small proportion of the total volume contained in the coil. The filling factor was $< \frac{1}{3}$ so that the signal to noise voltage available was only $\frac{1}{3}$ of that which would have been available if it had been possible to cut the crystal so that it filled the radiofrequency coil. One end of the radiofrequency coil was soldered to the central coaxial lead in the specimen tube. The other end was soldered to the outer brass shielding of the specimen tube. The specimen tube was made to plug into the rotating head on the bridge box and was then arranged at right angles to the field in the magnet gap.

6.2.c. <u>Na^{23} Spectrum in Sodium Nitrate</u>.

The spectrum of three lines was found for sodium (for which $I = \frac{3}{2}$) at 6.78 Mc/s in the magnet field of 6,000 gauss suitable biased by the field sweep unit. The crystal was then oriented to an angle where the splitting in the spectrum was small.

The frequency spectrum to be expected where the magnetic energy is much larger than the quadrupole energy, and where the electric fields at the nucleus are axially symmetric has been given by Pound 1950. For the case $I = \frac{3}{2}$ the freqqencies of the three lines are given by:

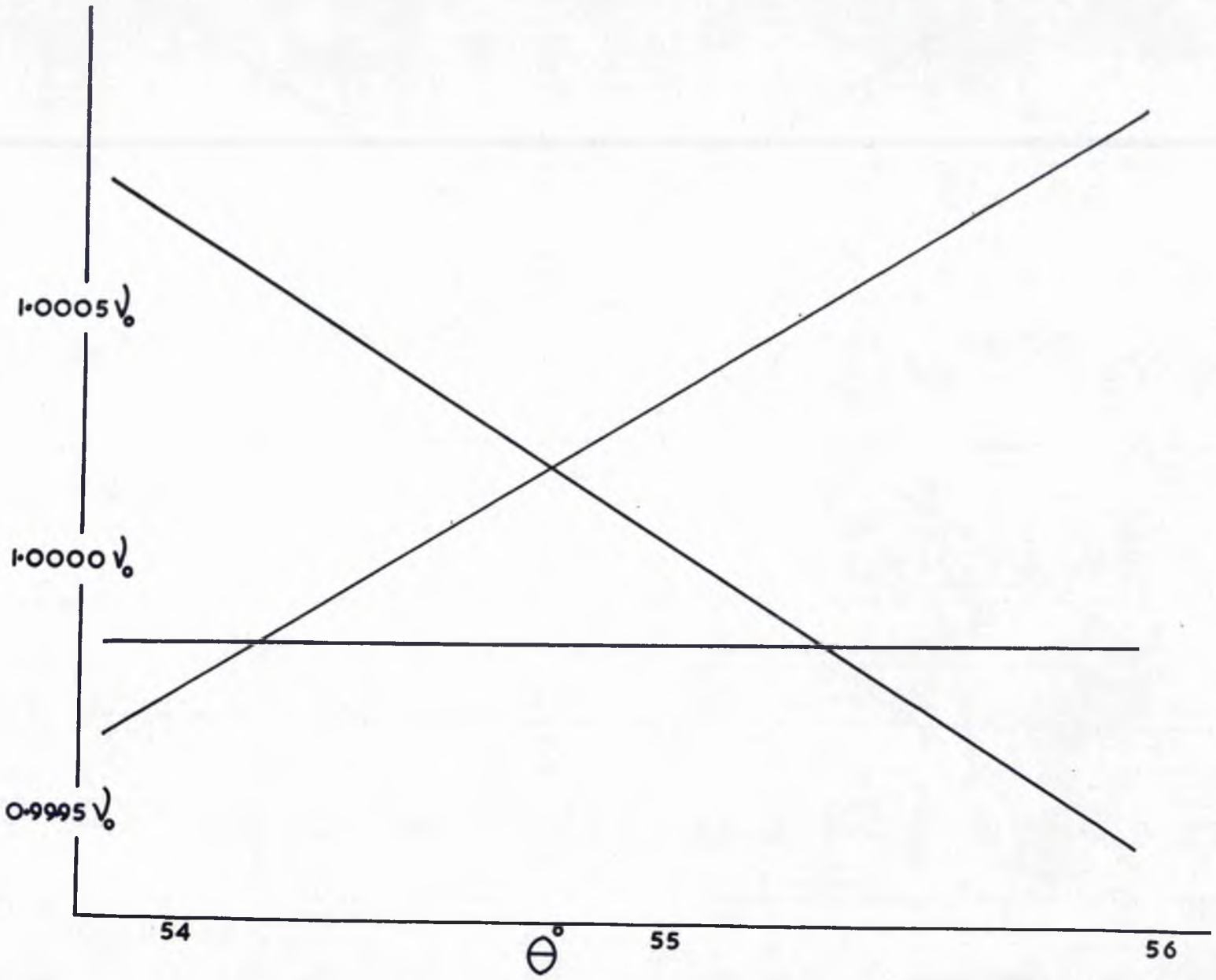

Figure 6.1.

$$\frac{1}{h}(E_{\frac{1}{2}} - E_{-\frac{3}{2}}) = \nu_o \left[1 - \frac{1}{4}\varsigma(3Z^2 - 1) + \frac{3}{8}\varsigma^2 Z^2(1 - Z^2)\right]$$

$$\frac{1}{h}(E_{\frac{1}{2}} - E_{-\frac{1}{2}}) = \nu_o \left[1 + \frac{3}{8}\varsigma^2\left(\frac{9}{8}Z^4 - \frac{5}{4}Z^2 + \frac{1}{8}\right)\right] \qquad 6(1)$$

$$\frac{1}{h}(E_{\frac{3}{2}} - E_{\frac{1}{2}}) = \nu_o \left[1 + \frac{1}{4}\varsigma(3Z^2 - 1) + \frac{3}{8}\varsigma^2 Z^2(1 - Z^2)\right]$$

where ν_o is the unperturbed larmor frequency of an isolated nucleus, $\varsigma = \frac{\Delta\nu_{max}}{\nu_o}$ where $\Delta\nu_{max}$ is the maximum splitting of the satellites and $Z = \cos\theta$ where θ is the angle between the applied magnetic field and the direction of the electric field gradient at the nucleus. ς is the ratio of the quadrupole to magnetic energies. $\varsigma = \frac{e^2qQ}{h\nu_o}$ where eq is the electric field gradient and eQ is the nuclear electric quadrupole moment. The perturbation calculation has been taken as far as the second order in equation 6(1) which predicts a cyclic and nearly symmetrical variation of the satellite lines about a nearly constant centre line as θ is varied.

Assuming a value of $\varsigma = 0.049383$ given by the measurements of Eades, Hughes and Andrew 1958 the frequencies of the three lines are plotted from equation 6(1) in fig. 6.1 for angles θ near $\cos^{-1}\theta = \frac{1}{\sqrt{3}}$. It is seen that the three lines do not coalesce at any orientation. For the frequency $\nu_o = 6.78$ Mc/s it is seen that when the centre line is superposed on a satellite at $\theta = 54.15^0$ and $\theta = 55.31°$, then the other satellite is separated from the superposed lines by 4.8 Kc/s. As the peak to peak linewidth of the first derivative of the lines was found to

be $\sim$1.5 Kc/s the satellite is clearly resolved from the superposed lines. In the case of $\theta = 54.74°$ where the satellites are superposed, the centre line is only 2.4 Kc/s away from them and the lines are resolved but not without considerable overlap, so that their independent saturation behaviour could not be studied at this angle.

The location of the crystal axis relative to the rotation head when the crystal is first mounted is only known to within a few degrees. The correlation of the angle of rotation with θ of equation 6(1) is found by studying the spectrum over a range of rotation angles. In this way the angles of rotation at which the satellites were separately superposed on the centre line were found and a series of progressive saturation runs were performed at these angles.

6.2.d. <u>The Saturation Runs</u>.

The method used was to sweep through the satellite and superposed line in turn at a given radiofrequency power. This power is progressively reduced while keeping constant the radiofrequency signal strength shown by the S meter of the receiver by altering the r.f. gain of the receiver whenever the input power is altered. It becomes apparent that the input power is no longer saturating the signal, when the recorded signal amplitude ceases to increase with decreasing input power. This steady value of the recorded signal amplitude is then used to normalise a set of runs at progressively increasing input power, and the saturation curves of the satellite and superposed lines are found.

The crystal was then turned through a few degrees until the centre line was clearly resolved separate from the satellite lines, and

saturation runs were done on the centre line only. The mean results of these runs are given in table 6.1 and they are plotted in figure 6.2.

R.f. level	Mean relative signal strength		
100 db ≡ 100 mv	Satellite	Centre Line	Superposed Centre Line and Satellite
92 db		0.90	0
94	0.90	0.91	0.93
96	0.87	0.83	0.95
98		0.75	
100	0.70	0.61	0.91
102	0.675	0.47	0.81
104	0.575	0.36	0.68
106	0.42	0.24	0.655
108	0.34	0.19	0.475
110	0.15		0.415
112	0.13		0.35
114			0.25
116			0.14

Line	Mean Unsaturated Linewidth	Shift along db scale
Satellite	1.46 gauss	0 db
Centre	1.80 gauss	-1.26 db
Superposed	1.70 gauss	-0.58 db

Table 6.1.

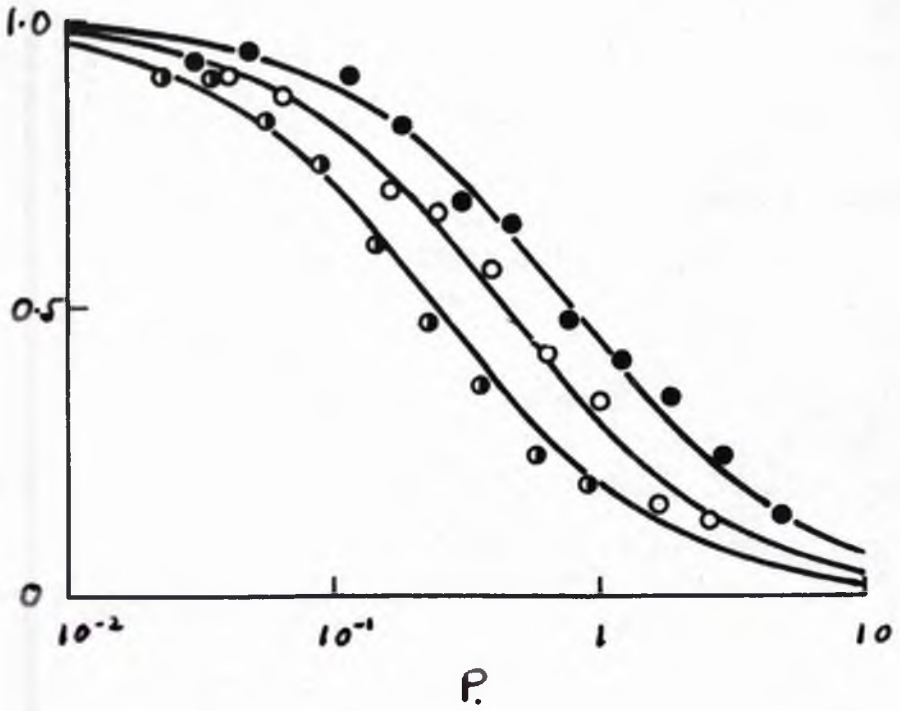

Figure 6.1.

The saturation parameter $P = \gamma^2 H_1^2 T_1 T_2$ takes account not only of the input power which is proportional to H_1 but also the inverse linewidth T_2. Correction was made for the T_2 term by displacing the curves of normalised signal amplitude plotted against 20 log H_1 by an amount equal to 10 log $\frac{T_2'}{T_2}$ where T_2' refers to the line being plotted and T_2 refers to the lone satellite line chosen as reference. T_2 was measured in each case as the inverse of the peak to peak value of the linewidth of the recorded first differential of the unsaturated absorption line. In figure 6.2 the experimental points for the lone centre line are given as half filled circles while the open circles refer to the lone satellite and filled circles to the superposed satellite and centre line. The curves a, b, and c are the theoretical curves for $I = \frac{3}{2}$ from fig 4.1 for the cases of centre line, satellite, and superposed centre line and satellite. It is seen that the agreement between experimental points and theoretical quadrupole relaxation curves is good enough to make it obvious that the relaxation mechanism is in fact quadrupolar in origin. If it had been magnetic all the relaxation curves would be superposed.

The quantitative fit of theory and experiment is seen to be far from established by those curves, but this can be attributed to the fairly poor signal to noise obtained from this crystal. A weak signal entails a long time constant in the phase sensitive amplifier, and a consequent slow gathering of information. Consequently each saturation run extends over periods of hours during which time conditions must be so controlled that the gain of the various amplifiers and the balance of the bridge remains constant to within a small fraction of 1 db. Also

a weak signal means that saturation runs to be compared may have to be taken on different days or over a period of weeks, and the faithful reproduction of all the conditions under which they are taken is difficult. Under these conditions a certain spread of experimental points is to be expected, and it is only the fact that the differences in saturation curves to be looked for are of the order of 2.5 db which makes the experiments practicable where weak signals are involved.

6.2.e. Anisotropy of T_1

It has been suggested by Van Kranendonk 1954, specifically for cubic crystals, that in the case of a quadrupolar relaxation mechanism there might be some anisotropy of the relaxation time T_1. A variation of T_1 with angle θ was looked for in the sodium nitrate crystal by doing a series of progressive saturation runs on the centre line at different angles θ. No variation of T_1 greater than could be encompassed by the experimental error was found. The results are tabulated in Table 6.2. The greatest change in saturation curve with angle corresponds to a shift of 1.4 db or 25% in T_1. As this is also the order of the maximum possible error on these runs the only significant result which can be claimed is that the variation of T_1 with angle if any is not as great as 50%.

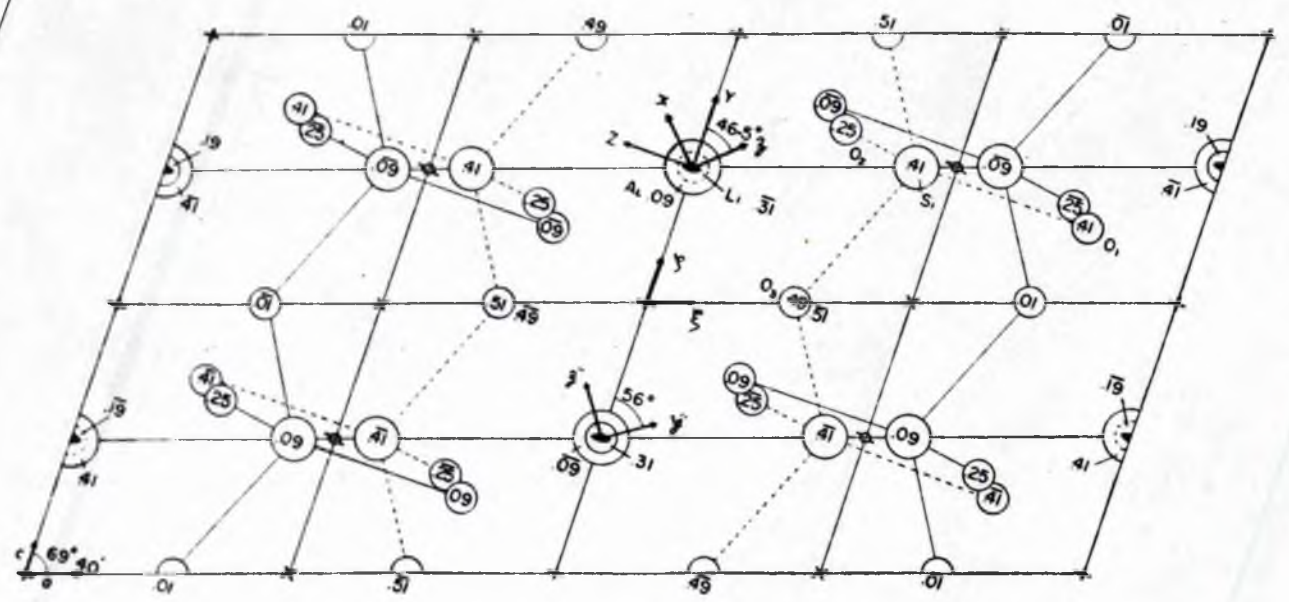

Figure 6.3.

Projection of unit cell of Spodumene on (010) plane.

Table 6.2.

θ	db. for half saturation	Uncertainty in db.	Unsaturated Line Width
0°	103.2	0.4	1.75 gauss
20°	102.8	1.0	1.75
40°	102.2	0.7	1.9
50°	102.8	0.7	1.85
90°	102.3	0.6	1.85
110°	103.0	0.8	1.80
130°	103.6	0.7	1.80
180°	102.6	0.4	1.85

6.3. Spodumene

Crystals of spodumene were chosen for study because naturally occurring single crystals were available, and the crystal contains $Li^7 (I = \frac{3}{2})$ and Al^{27} $(I = \frac{5}{2})$ nuclei in electric fields of lower than cubic symmetry.

6.3.a. Crystal Structure.

Spodumene is monoclinic and its structure is given by Warren and Biscoe 1931. Fig. 6.3. gives a projection of the unit cell on the (010) plane. The molecule Li Al $(SiO_3)_2$ occurs four times in the unit cell. The crystal consists of - O - SiO_2 - O - SiO_2 - O chains indicated by broken lines in fig. 6.3 running parallel to the c direction and bound together by Li and Al atoms. Both the Li and Al nuclei lie on two fold rotation axes of symmetry of the crystal, and from a study

of the symmetry centres shown in fig. 6.3. it can be predicted that the four lithium nuclei in the unit cell have identical electrical environments and the four aluminium nuclei also are identical in this sense (Volkoff, Petch and Smellie 1952). Hence only one centre line and satellite system is to be expected for each nucleus, three lines from the Li^7 and five from the Al^{27}. This was indeed the spectrum found by Volkoff, Petch and Smellie 1952 for Li^7 and Petch, Cranna and Volkoff 1953 for Al^{27}. They were able to fit these spectra to a much more complicated form of equation 6(1) derived by Volkoff for the general case of non-axially symmetric electric field gradients

The spectra of Li^7 and Al^{27} in spodumene are thus well known and were used to identify the lines found in the present experiments.

6.3.b. Mounting the Crystals.

Spodumene is very hard and wherever possible crystals were mounted in close fitting perspex cylinders in their natural shape. The MAIN cleavage plane is 110 and by measuring the angles between cleavage faces by reflected light on a spectrometer turntable it was possible to identify the c axis (fig. 6.3) of the crystal. All the specimens were mounted so that they were rotated about the c axis.

Specimens were obtained from various geological specimen dealers in this country and in the U.S.A., and from the Museum d'Histoire Naturelle Paris through the agency of Dr. N.F.M. Henry of the Mineralogy Department of the University of Cambridge who also supplied us with some of his own specimens.

In selecting crystals for study the choice was made of those which were optically clear and free from colour as it was hoped that these would be the more perfectly uniform crystals and would contain the least amount of paramagnetic impurity.

Some of these crystals had to be cut into sizes small enough to fit inside a reasonable r.f. coil in the specimen tube. Early attempts to cut them with a rotating steel disc on which carborundum powder in water was allowed to drip were successful but slow, with cutting times of the order of a centimetre per hour. Later samples were kindly cut for us by the Geology Department of Liverpool University using a diamond saw.

6.3.c. Results for Crystal Number 119.248 from the Museum Nationale d'Histoire Naturelle.

This crystal, which was clear, was in the shape of a flat rectangular slab.

(i) The Li^7 spectrum of three lines was located and the orientation of the crystal relative to the field was found by checking the spectrum against the results of Volkoff, Petch and Smellie 1952. For rotation about the c axis the splitting of the satellite lines varies from a maximum of 70 kc/s through zero to a subsidiary maximum of 40 kc/s, this pattern being repeated symmetrically every 90° of rotation. Saturation runs were done on the superposed lines, the separate lines near the superposition angle, the separate lines at maximum splitting and on the separate lines at the sub-maximum splitting. The second order terms in the quadrupole splitting are so small that all three lines are effectively superposed at one orientation. The

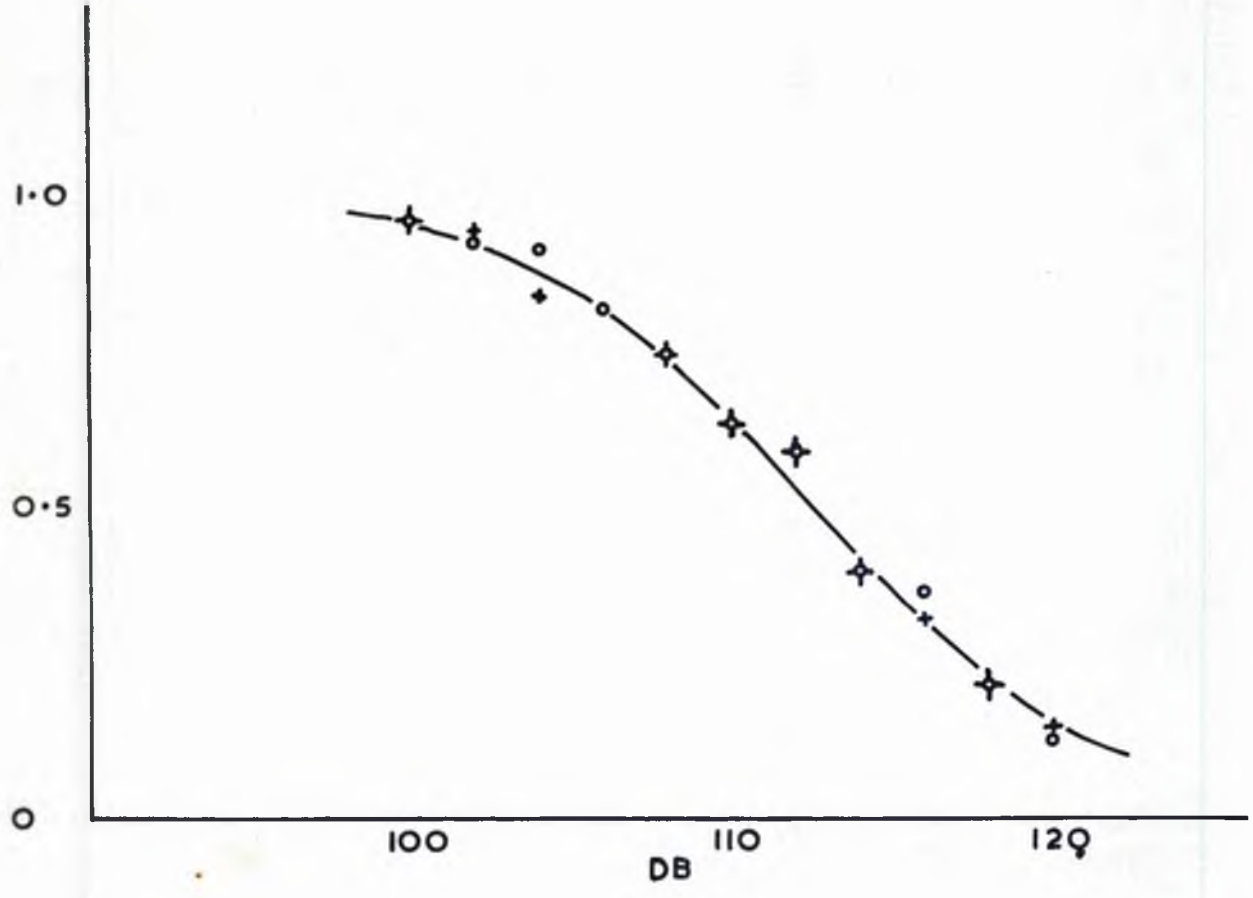

Figure 6.4.

Saturation of Li^7 in Spodumene

O - centre line

\+ - satellite

The curve is $(1 + P)^{-1}$

superposition is not perfect as the superposed line is 20% broader than the single lines. The results are plotted in table 6.3 and figure 6.4.

The results indicate a magnetic relaxation with a satellite line and centre line giving the same saturation curve at each angle. There is however a change of relaxation time with angle, the relaxation time at the maximum splitting angle being twice that at zero splitting, while T_1 at the sub maximum splitting angle is 1.75 times that at zero splitting. T_1 for the single lines near superposition was found where the lines were just separated at an angle 11.6° from the cross over angle, and it is 1.2 times T_1 for zero splitting which is consistent with a cyclic variation of T_1 in phase with the satellite splitting. The linewidths also varied with angle the narrowest lines corresponding to the shortest times T_1 near superposition and the widest lines occurring with the largest times T_1 at maximum splitting. The saturation curves are corrected for linewidth in table 6.3.a.

Table 6.3.

R.F. Input Power	Relative Signal Strength		
100 db ≡ 100 m.v.	$\theta = 11.6°$ Centre Line	$\theta = 11.6°$ Satellite	$\theta = 0°$ Lines Superposed
100 db	0.955	0.94	0.94
102	0.92	0.94	0.93
104	0.91	0.835	0.89
106	0.815	0.82	0.86
108	0.735	0.75	0.82
110	0.63	0.635	0.73
112	0.60	0.58	0.635
114	0.39	0.395	0.53
116	0.36	0.32	0.40
118	0.215	0.21	0.29
120	0.145	0.125	0.20

Table 6·3 cont.

R.F. Input	Relative Signal Strength			
	Maximum Splitting		Sub-Maximum Splitting	
	θ = 45° Centre Line	Satellite	θ = 135° Centre Line	Satellite
96 db	0.951		0.955	0.98
100	0.915	0.93	0.91	0.93
102	0.895	0.90	0.87	0.87
104	0.89	0.85	0.80	0.84
106	0.80	0.80	0.75	0.75
108	0.73	0.77	0.69	0.70
110	0.645	0.65	0.58	0.58
112	0.545	0.50	0.525	0.51
114	0.44	0.47	0.455	0.455
116	0.26	0.25	0.37	0.37
118		0.16	0.33	0.26

Table 6.3.a.

θ	Line	Input Power (db) for ½ saturation	Line Width m.v. 1 m.v. = 2.36 gauss	Correction	Corrected db for ½ saturation
0°	3 Superposed	114.4 db	0.83 mv	-0.8 db	113.6 db
11.6°	Centre	112.5 db	0.69 mv	0 db	112.5 db
11.6°	Satellite	112.6 db	0.70 mv	-0.06 db	112.5 db
45°	Centre	112.8 db	1.33 mv	-2.85 db	109.95 db
45°	Satellite	112.3 db	1.25 mv	-2.6 db	109.7 db
135°	Centre	112.6 db	1.1 mv	-2.0 db	110.6 db
135°	Satellite	112.6 db	1.1 mv	-2.0 db	110.6 db

(ii) The Al^{27} spectrum in crystal 119.2A8 was looked for after orienting the crystal to an angle where the splitting of the satellite lines is small. This angle was found from the results of Petch, Cranna and Volkoff 1953. It is near the angle corresponding to maximum splitting of the Li^{7} spectrum. The centre line of the Al^{27} was found to be strong while the inner satellites were very broad and weak, and the outer satellites could not be seen.

The most probable reason for the very wide satellite lines is that imperfections and impurities in the crystal give rise to a spread in the local values of the field gradient to which the satellite lines are sensitive. The centre line has no first order dependence of the resonance frequency on the field gradient and hence would only be slightly broadened by the variations in local electric field gradient. The satellites do have such a first order dependence and may be so broadened as to be unobservable. This effect is much greater for the Al^{27} nuclei in spodumene for which the quadrupole coupling constant is 2,950 kc/s than it is for the Li^{7} nuclei for which the quadrupole coupling constant is only 76 kc/s (Pound 1953 has pointed out that such evidences of crystalline imperfections are to be found in resonance experiments).

Saturation runs were done on the weak inner satellites and the centre line. The satellites were seven gauss wide and it was necessary to use modulation of this amplitude H_m to make them measurable. The same modulation was used on the centre line to make comparison easier. The lines are broadened by this large modulation and the saturation

curves should then correspond to those of case 4 Bloembergen (1948). The degree of saturation is determined by the quantity $\gamma H_1^2 T_1/H_m$ rather than $\gamma^2 H_1^2 T_1 T_2$. No correction is then necessary for linewidth to make the two saturation curves comparable when the lines are broadened by the same large modulation. The saturation curves are plotted in table 6.4. The power input for half saturation is the same for the centre and the satellite line which indicates that the relaxation is magnetic. The slope of the saturation curve of the artificially broadened centre line is considerably flatter than the slope of the theoretical $(1 + P)^{-1}$ curve.

Table 6.4

Al^{27}

R.F. Input	Relative Signal Strength	
100 db ≡ 100 mv.	Satellite Line	Centre Line
98 db		
100	0.95	0.96
102		0.95
104	0.895	
106		
108	0.82	0.73
110	0.78	0.695
112	0.695	
114	0.61	0.56
116	0.50	0.50
118	0.44	0.40
120	0.36	
122		0.22
126		0.125

6.3.d. Al^{27} Spectra in Spodumene Crystals.

After the limited success gained in observing the Al^{27} lines in the French spodumene crystal of catalogue number 119.248 a search for the Al^{27} lines was carried out in four other spodumene crystals selected for their clearness and lack of colouration. These were crystals 47, 48, 64, 65 in the Bangor Physics Department crystal catalogue. In each of these crystals a strong centre line was found. This line shifts in frequency cyclically over 60 kc/s as the orientation about the c axis is changed. The position of maximum frequency of the centre line corresponds to the position of minimum splitting of the outer and inner satellite lines (Petch, Cranna and Volkoff 1953) and this condition was used to find an orientation at which the satellites should appear on the sweep of the bridge spectrometer.

In Crystal 47 which had a faint purple colour relatively weak inner satellites of line width 7 gauss from peak to peak of the differential curve were observed and no outer satellites were visible. The Al^{27} spectrum of crystal 48, which was clear apart from irregular and apparently external slight brown colouration, was almost identical to that of crystal 47. In both cases the intensity of the inner satellites grew with approach to the centre line until at minimum splitting their amplitude was a quarter of the centre line amplitude, but the line shape of the satellite was much broader and flatter than the line shape of the centre line. The breadth of the satellites grew with separation from the centre line and they rapidly became unobservable. When the splitting is near zero any variation in electric field gradient

due to crystal imperfections is not so effective in smearing out the satellite lines as their frequencies change only to a second order with field gradient when splitting is zero. As the line shape of centre line and satellite differed in these crystals it was not considered that useful information would be gained from comparison of their saturation behaviour.

In crystals 64 and 65 the satellites were not observed. Saturation runs were done on the centre lines of these two crystals in turn in the same radiofrequency sample coil. They are tabulated in table 6.5.

The very large ratio of T_1 values in the same type of crystal is strong evidence for impurity relaxation, i.e. paramagnetic relaxation on the Bloembergen scheme, for the impurity concentration can vary widely from crystal to crystal. Quadrupole relaxation on the other hand depends on inherent properties of the nucleus and the crystal concerned and should give reasonably constant values of T_1 for different specimens of the same crystal. Any change of the electric field gradient brought about by crystal imperfections could not conceivably shorten T_1 by a factor of 200 on the quadrupole relaxation scheme. This does not of course rule out quadrupolar relaxation for crystal 65.

Table 6.5.

R.F. Input db 100 db = 100 mv	Relative Signal Strength Al^{27} Centre Line Crystal 65	 Crystal 64
94	0.94	
98	0.765	
100	0.65	
102	0.56	
104	0.52	
106	0.40	
108	0.365	
110	0.280	1
112		
114	0.15	0.95
116		
118		0.82
120		
122		0.76
124		
126		0.58
128		0.38
130		0.29
132		0.26

Crystal	Db for Half Saturation	Line Width	Relative Value of T_1
64	127 db	3.3 gauss	1
65	104 db	3.3 gauss	200

6.3.e. Results for Li^7 in Crystals 48 and 65.

Although these spodumene crystals did not give satisfactory Al^{27} satellite lines they both gave satisfactory Li^7 spectra and the saturation behaviour of these lines was studied in detail. The results are given in tables 6.6 and 6.7. These are selected from thirty saturation runs done on these two crystals

The Li^7 saturation runs on crystal 65 were not satisfactory as the slope of the saturation curves were in general less than those of a $(1 + P)^{-1}$ curve. The centre line and satellite reached half saturation at nearly the same input power which would suggest that the relaxation mechanism is magnetic, but the tendency was for the centre line to require slightly more power than the satellite for half saturation, a situation which does not agree with either of the proposed relaxation mechanisms. It is possible that the paramagnetic impurities are not distributed evenly through the crystal so that different segments have different concentrations of impurity and different relaxation times. If these segments were large enough ($> (100)^3$ atomic spacings in volume) so that the spin-spin collision process was relatively ineffective in causing the spins in different segments to have a common spin temperature, then we have a range of T_1 values in the crystal and the slope of the saturation curve for the crystal would be flattened as the low impurity regions saturated before the high impurity regions.

Crystal 48 gave satisfactory curves which indicated that the relaxation was magnetic. There was also a change of T_1 with angle, the

Table 6.6.

Spodumene Crystal 48 Li^7 Resonance.

R.F. Input Power	Relative Signal Strength				
100 db = 100 mv	θ = 295.4°		θ = 0	θ = 19.2°	
	Centre Line	Satellite	Superposed Lines	Centre Line	Satellite
100 db	0.93	0.92	0.93	0.94	0.94
102	0.905	0.89	0.90		
104	0.86	0.87	0.87	0.85	0.86
106	0.80	0.78	0.81		
108	0.75	0.70	0.73	0.73	0.71
110	0.57	0.58	0.65	0.605	0.65
112	0.465	0.45	0.56	0.51	0.51
114	0.37	0.36	0.44	0.42	0.405
116	0.24	0.27	0.33	0.33	0.33
118	0.19	0.20	0.26	0.27	0.24
120	0.155	0.16	0.19		
122			0.13	0.14	0.10
124	0.07	0.10	0.08		
126			0.05		
128					

θ	Line	Input (db) for Half Saturation	Line Width	Correction for Width	Corrected db for Half Saturation
0	Superposed lines	113 db	0.85 mv	0 db	113.0 db
295.4°	Centre	111.4 db	1.4 mv	-2.2 db	109.2 db
295.4°	Satellite	111.0 db	1.3 mv	-1.8 db	109.2 db
19. 2°	Centre	112.0 db	0.88 mv	-0.15 db	111.85 db
19. 2°	Satellite	112.4 db	0.97 mv	-0.6 db	111.80 db

Table 6.7.

Spodumene Crystal 65 Li^7 Resonance.

R.F. Input Power 100 mv = 100 db	Relative Signal Strength Centre Line	Satellite
86 db	0.93	0.96
88	0.90	0.95
90	0.87	0.93
92	0.83	0.92
94	0.82	0.87
96	0.72	0.74
98	0.68	0.69
100	0.57	0.58
102	0.485	0.51
104	0.41	0.44
106	0.33	0.39
108	0.30	0.34
110	0.26	0.27

Line	Input for Half Saturation	Line Width	Correction for Line Width	Corrected Input for Half Saturation
Centre	102.0 db	0.80 mv	0	102.0 db
Satellite	102.1 db	0.83 mv	-0.16	101.84 db

shortest relaxation time being when the satellites were superposed on the centre line where the lines are also at their narrowest. At an angle 65° from the superposition angle the relaxation time T_1 was over twice as long and the lines were 1.7 times as broad. Comparison of the relaxation times T_1 between the different crystals will be made at the end of this chapter.

6.4. Euclase.

A set of saturation runs were done on the Al^{27} spectrum in a crystal of euclase H Be Al SiO_5. This crystal was chosen because its spectrum was known from the work of Eades 1955, and as the same single crystal which was used by Dr. Eades in his investigation of the spectrum was kindly made available by Professor Volkoff, it was known that the satellite lines would be observable.

Euclase is a monoclinic crystal and its structure is given by Biscoe and Warren 1933. The aluminium nuclei do not lie on symmetry axes of the crystal as they do in spodumene. The main cleavage plane is (010) and the crystal was mounted so that it was rotated about its long axis parallel to the intersection of cleavage planes. In this orientation there are ten lines in the spectrum, five for each of two non-equivalent Al^{27} sites. The maximum splitting of the outer satellites is over 2 Mc/s while the second order perturbation on the centre lines moves them over 130 Kc/s about their central position as the crystal is rotated.

The movement of the centre lines was used to find the position $\theta = 0$ where the centre lines coincide which is also the position where

the inner and outer satellites are superposed. This setting was made to an accuracy of ± 0.1° by plotting the spectrum at angles near θ = 0. The rotation was then moved to θ = 1.6° where the centre lines were just separated and two of the inner satellites were on the same field sweep.

Table 6.8.

R.F. Input	Relative Signal Strength			
100 mv = 100 db	Centre Line (a)	Centre Line (b)	Satellite (a)	Satellite (b)
96	0.95	0.90	0.92	0.95
100	0.93	0.75	0.83	0.80
104	0.68	0.60	0.71	0.60
108	0.55	0.44	0.50	0.45
112	0.39	0.35	0.42	0.35
116	0.24	0.27	0.33	0.25
120			0.23	0.125
124			0.14	0.10

Line	Power for Half Saturation	Line Width	Correction for Line Width	Corrected Power for Half Saturation
Centre (a)	108.6 db	2.2 mv	0 db	108.6 db
Satellite (a)	109.5 db	2.7 mv	-0.9 db	108.6 db
Centre (b)	106.4 db	2.2 mv	0 db	106.4 db
Satellite (b)	107.1 db	2.7 mv	-0.9 db	106.2 db

Saturation runs were done on each of these four lines in turn. They are tabulated in table 6.8. From the data of Eades 1955 the lines were identified as a centre line (a) and satellite (a) belonging to one Al^{27} site while the other centre Line (b) and satellite (b) belonged to the other Al site.

It is seen that the centre line (a) and satellite line (a) have the same saturation curve. Also centre line (b) and satellite line (b) have identical saturation curves which differ from the saturation curve of the (a) lines by a factor of 2.4 db. Magnetic relaxation is indicated with a relaxation time difference of 40% between the two different Al^{27} sites in the crystal.

The saturation curves for Al^{27} in Euclase were again of lower slope than $(1 + P)^{-1}$ curves. An increase of saturation from 0.8 to 0.2 of the maximum signal strength required $\sim$16 db increase in power input, whereas for a $(1 + P)^{-1}$ saturation curve only $\sim$13 db increase is required for the same increase in saturation.

6.5. Sodium Thiosulphate $Na_2S_2O_3\ 5H_2O$ (Hypo.)

As it appeared that the quadrupole relaxation process is swamped by the impurity relaxation in the natural crystals examined, it was decided to grow pure crystals in the laboratory. Crystals of hypo, borax and sodium chlorate were grown from solution. The analysis of the paramagnetic impurity in these crystals will be given in the general discussion at the end of the chapter.

The sodium thiosulphate crystal was $\sim$2 cc. which volume it attained in ten days growth. It was mounted with a coil wound on the crystal.

The crystal grew to fill the specimen tube in which it was grown, so the orientation of the crystal in the coil, which could only be guessed from the free faces of the top growing surface, was not known precisely.

6.5.a. The Na^{23} Spectrum.

The spectrum of Na^{23} in a sodium thiosulphate crystal has been studied by Itoh, Kusaka and Yamagata 1954. Its crystal structure has been determined by Taylor and Beevers 1952. There are in general two non-identical molecular positions in the crystal, and each molecule contains two non-identical sodium sites. The Na^{23} spectrum then consists of four centre lines each with two satellite lines. For orientation about one axis, the crystal b axis, this spectrum degenerates into two centre lines and four satellites, but this orientation was not achieved in the present experiment.

As the precise orientation of the crystal axes in the r.f. coil was not known, the data of Itoh, Kusaka and Yamagata could not be used directly to identify the lines observed at various angles. Instead note was made of the fact that the satellite lines corresponding to one sodium nucleus in the molecule had a maximum splitting more than double that of the satellites corresponding to the other sodium site in the molecule. The quadrupole coupling constants are 2.26 Mc/s and 0.83 Mc/s respectively. (The splittings for the sodium sites in the other non-identical molecule were of the same size and varied in sympathy, differing only in phase angle as the crystal was rotated). These satellites were named the 'fast moving' and 'slow moving' satellites respectively and could be identified by their rate of shift with angle near angles at

which they crossed the centre lines. The centre lines, because of their different second order perturbation shifts, could also be identified as fast moving and slow moving with rotation.

Near cross-over the 'fast moving satellite' moved 21 gauss along the sweep for every degree of rotation. As the total sweep available was 55 gauss this line moved completely over the sweep range for less than a 3° rotation. Comparable figures for the 'slow moving satellite' were 7.5 gauss/degree and for the 'fast moving centre line' 2.5 gauss/degree. The slow moving centre line was virtually stationary and was plotted by using as reference the Cu^{63} resonance from the copper of the r.f. coil which gave a strong line independent of crystal rotation and near the Na^{23} unperturbed frequency.

As the search for a fast moving satellite entailed traversing at slow speed the maximum obtainable field sweep for every 1° change of rotation angle, the identification of lines was a slow process. By plotting the value of field sweep current at the line centre against angle for any line found, the lines were identified quite unambiguously by the slopes of the plots.

6.5.b. Results for Sodium Thiosulphate.

Saturation runs were done on the fast and slow sets of lines. They are tabulated in Table 6.9. The saturation runs agree with the theoretical plots for quadrupole relaxation, the satellites requiring 3.0 db and 2.7 db more power than their corresponding centre lines for half saturation as compared with a theoretical difference of 2.5 db for quadrupole relaxation. The fast moving lines have the shorter relaxation times requiring~2.5 db more power for half saturation than

Table 6.9

R.F. Input	Relative Signal Amplitude			
100 mv = 100 db	Slow Centre Line	Slow Satellite	Fast Centre Line	Fast Satellite
90 db	0.93	0.95	0.96	0.98
92	0.89	0.90	0.94	0.99
94	0.82	0.89	0.90	0.94
96	0.75	0.85	0.89	0.92
98	0.66	0.78	0.80	0.90
100	0.525	0.70	0.70	0.85
102	0.44	0.57	0.63	0.74
104	0.36	0.55	0.55	0.68
106	0.30	0.40	0.41	0.56
108	0.19	0.30	0.34	0.47
110	0.14	0.22	0.26	0.36
112	0.09	0.18	0.18	0.26
114				0.20
116				

Line	Power for Half Saturation	Line Width	Correction for Line Width	Corrected Power for Half Saturation
Slow Centre	101.0 db	1.7 mv	0 db	101.0 db
Slow Satellite	104.0 db	1.7 mv	0 db	104.0 db
Fast Centre	104.8 db	1.7 mv	0 db	104.8 db
Fast Satellite	107.5 db	1.7 mv	0 db	107.5 db
Fast Centre and Satellite Superposed	110.7 db	1.9 mv	-0.5 db	110.2 db

their slow counterparts.

Due to the fact that the spectrum from the crystal is split into twelve lines the signals have only fair signal to noise ratio and there is some scatter of the points on the saturation plots, leading to an uncertainty in the half saturation values of ~ 0.7 db. The agreement with theory of the best lines through these points is reasonable both as regards slope and separation of lines, and the conclusion can be drawn that the relaxation mechanism is quadrupolar in origin for the Na^{23} nuclei in this crystal. It would also seem a reasonable result that the nuclei with the larger quadrupole coupling factor giving the fast moving lines, should also have the shorter relaxation time. The ratio of relaxation times is 2.5 and of coupling constants is 2.7.

The slow moving centre line is too noisy at the low power required for no saturation to make saturation runs on it easy. However it is the easiest line to follow as the angle of rotation is changed. So to get an indication of whether T_1 changes with orientation in this crystal the input power was set at 102 db, which is near half saturation for the slow centre line, and runs were made over the slow centre line at a range of orientations. It seems from these runs that T_1 does vary to some extent, the period of the variation being 90° from maximum to minimum.

6.6 Borax $Na_2B_4O_7\ 10H_2O$.

A single crystal of Borax was grown by slow evaporation to a size of $\frac{1}{2} \times 1 \times 2$ cm^3. Borax was chosen because it contains Na^{23} and B^{11} nuclei both of spin $\frac{3}{2}$.

No results have previously been reported for nuclear magnetic resonance in this crystal. Crystallographic data for it is also meagre. Wyckoff gives the space group only and no other reference to its structure was found.

The crystal is a flat slab with bevelled edges. It was mounted with a coil wound directly on the crystal, and so that it could be oriented with its large flat sides perpendicular to the field.

The Na^{23} spectrum was looked for by setting the signal generator at the unperturbed Na^{23} resonance frequency with the field at half maximum sweep. Then the field was swept with the crystal at several chosen angles, for example with its large flat faces parallel, perpendicular, and at 45° to the magnet field. No Na^{23} lines were seen. This could mean that the second order perturbation on the centre lines is large and that the angles chosen were unlucky so that no lines appeared on the sixty gauss sweep range available or alternatively there may be a large number of non-equivalent sites for Na in the crystal so that the absorption is spread over a large number of lines which would make the lines very weak and possibly unobservable. In any case further search with the bridge was considered to be unprofitable and the frequency was changed to look for the B^{11} spectrum.

6.6.a <u>The B^{11} Spectrum in Borax.</u>

B^{11} lines were found immediately and they were located at 5° intervals over a 90° rotation in so far as they remained on the sweep range. Six different lines were observed of which two showed the symmetry of behaviour to be expected of a satellite pair, while one was almost stationary, behaving like a centre line with very small second

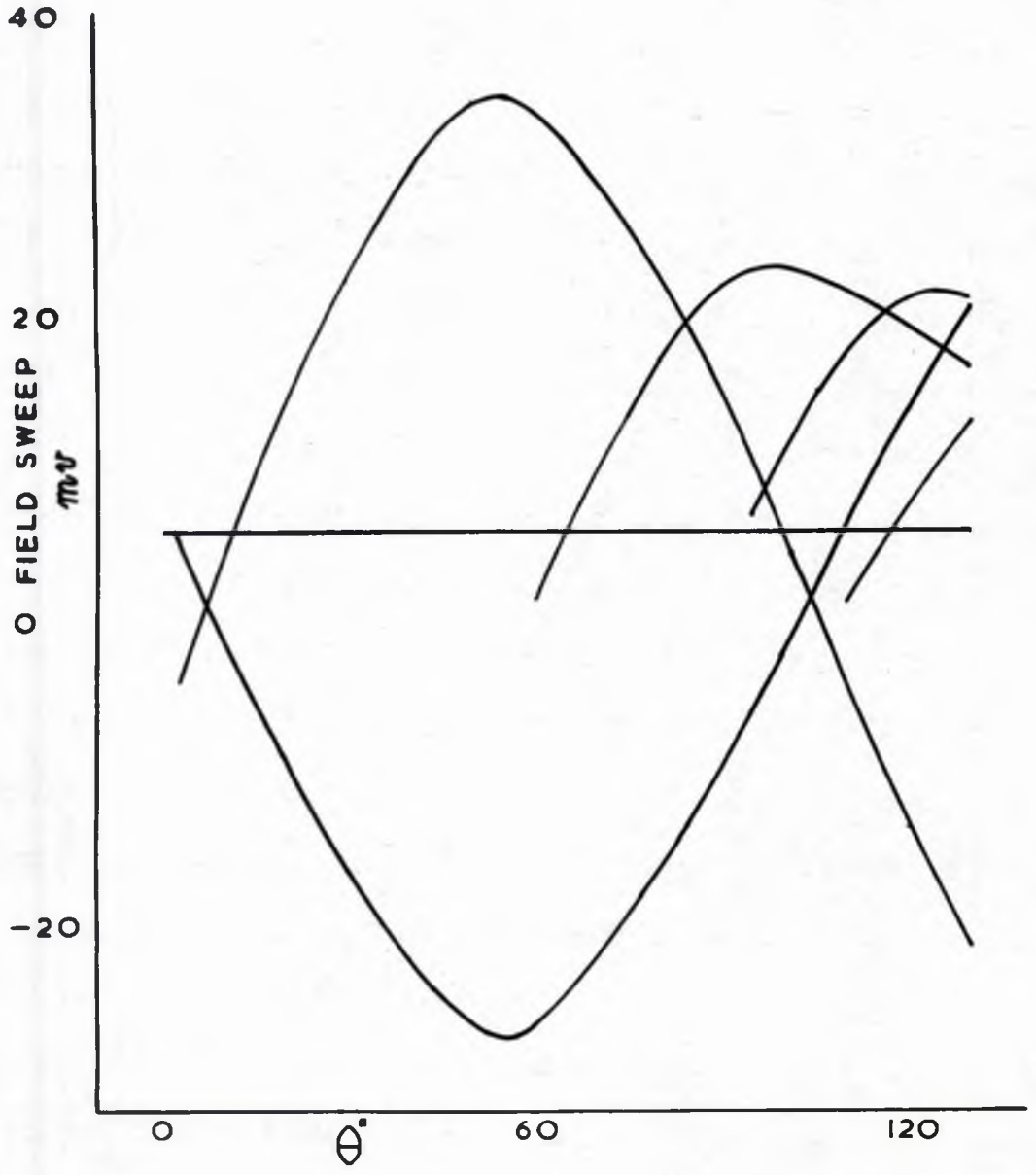

Figure 6.5.

The B^{11} spectrum in Borax. 1 m.v. = 2.36 gauss. The more fully plotted symmetrical lines and the near stationary line are taken to be a pair of satellites and a centre line. The other three loci are thought to correspond to centre lines of different B^{11} sites.

order perturbation. The other three lines were thought to be centre lines with fairly large second order perturbation. The satellites belonging to these centre lines would move very rapidly through the sweep range and no attempt was made to observe them, as the bridge apparatus is not suited to wide range search. The symmetrically disposed lines were plotted over a range of 130° by changing frequency when they moved out of the sweep range. The plot is given in fig. 6.5. It seems reasonable to assume that the two symmetrically moving lines and the stationary line form a centre line - satellite trio belonging to one B^{11} site in the crystal. In all probability the other three lines are centre lines belonging to three other independent boron sites in the crystal. It would seem then that there are four non-identical boron sites in Borax, where as usual, by non-identical we mean that the sites have different electrical environments and so give rise to different quadrupole split spectra. It is tempting to assign these four sites to the four boron atoms in the molecule, but in the absence of knowledge of the crystal structure such a proposal has no great weight. For the allied, naturally occurring crystal Kernite, $Na_2B_4O_7\ 4H_2O$, the boron spectrum has been studied by Waterman and Volkoff 1955, and they explain its spectrum in terms of four non-identical sites in the crystal filled by the four boron atoms in the basic B_4O_7 unit.

6.6.b. Results of the Saturation Runs on Borax.

Progressive saturation runs were done on the stationary centre line and the two lines assumed to be its associated satellites and also on the centre line with a satellite superposed. There was no significant

difference in the saturation curves for any of these cases so that magnetic relaxation is indicated. The results are tabulated in table 6.10. The slope of the saturation curves agreed, within the experimental scatter, with that of a $(1 + P)^{-1}$ curve.

It would be interesting to have the complete spectrum of this crystal plotted with a spectrometer suited to wide range sweeping. The widely varying satellite lines and their centre lines could then be investigated to see if they also were relaxed magnetically. Similarities in the spectrum to that found for Kernite by Waterman 1955 would also be of interest as regards assigning a structure to this crystal.

Table 6.10.

B^{11} Lines in Borax.

Input Power	Relative Signal Amplitude		
100 db = 100 mv	Centre Line	Satellite	Superposed Centre and Satellite
84 db	0.94	0.94	0.95
86	0.905	0.90	0.93
88	0.85	0.87	0.89
90	0.80	0.76	0.83
92	0.86	0.65	0.64
94	0.64	0.59	0.59
96	0.555	0.52	0.57
98	0.515	0.47	0.425
100	0.37	0.315	0.36
102	0.21	0.23	0.295
104	0.17		
106	0.05	0.12	0.16

Angle θ	Line	Power for Half Saturation	Line Width 1 mv = 2.36 gauss	Correction for Line Width	Corrected Power for Half Saturation
8°	Centre	96.6 db	2.9 mv	-0.15 db	96.45 db
0°	Satellite	96.2 db	2.8 mv	0	96.2 db
0°	Superposed Centre and Satellite lines	96.8 db	3.3 mv	0.7 db	96.1 db

6.7. Sodium Chlorate.

The Na^{23} spectrum in a sodium chlorate crystal has been investigated by Gutowsky and Williams 1956.

The crystal structure of sodium chlorate (R. Wyckoff, Crystal Structures Vol. II Chapter VII) is cubic. The unit cell contains four molecules. The sodium ions occupy positions near alternate corners of the cube and the chlorate ion centres occur near the other corners. The chlorate ion is a flat trigonal pyramid having the three oxygen atoms as its base. The electric field gradient at the chlorine nucleus is mainly due to the covalent bonding within the ion and is large; the splitting of the Cl^{35} nuclear levels is such that the pure quadrupole resonance f frequency is near 30 Mc/s. (Wang, Townes, Schwalow and Holden 1952). At the sodium sites the electric field gradient is due principally to the crystalline fields of the Na^{+} and ClO_3^{-} ions, and the quadrupole splitting of the zeeman levels is such as to form a relatively small perturbation of the unperturbed levels giving a splitting of the N.M.R. spectrum of the order of 800 Kc/s in 7 Mc/s.

The principal axis of the electric field gradient tensors at the sodium sites are parallel to the body diagonals of the unit cell and hence to the body diagonals of the cubic crystal. These fields are axially symmetric so equations 6(1) apply. As there are four sodium ions in the unit cell a maximum of twelve lines, four centre lines each with two satellites, is to be expected.

The crystal grown was rectangular rather than cubic, due probably to the confined space in which it was grown, and to the fact that it rested on the flat bottom of the container during growth.

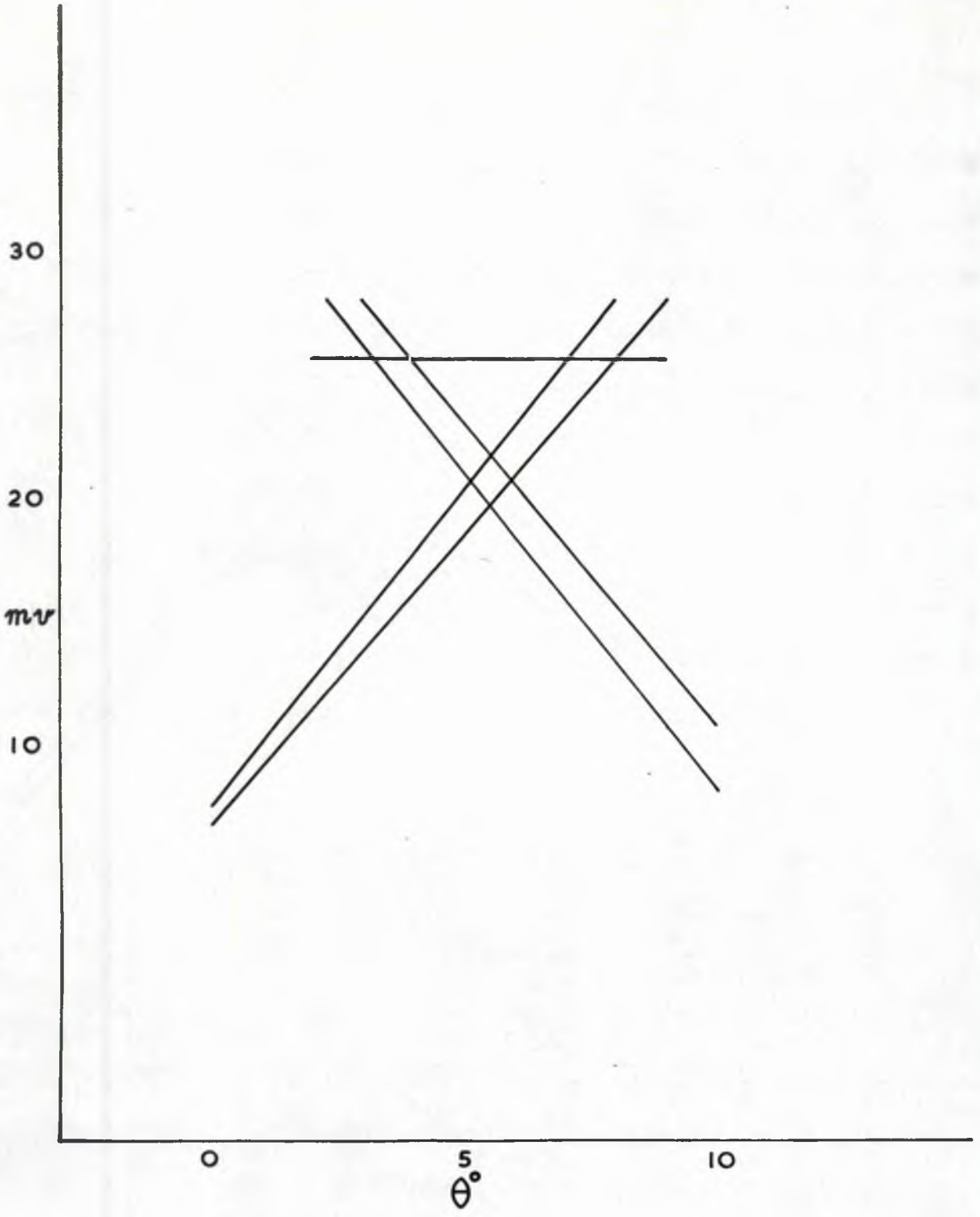

Figure 6.6.

The spectrum of Na^{23} in $NaClO_3$ near cross-over angle.

θ is arbitrary. 1 m.v. = 2.36 gauss.

The crystal was mounted in the down tube so that one face was perpendicular to the axis of rotation. In this configuration it was possible to turn the crystal until a face was perpendicular to the external field. At this point all the body diagonals make the same angle $\theta = \cos^{-1}\frac{1}{\sqrt{3}}$ with the external field, and it can be seen from equation 6(1) that the first order splitting is zero. At this orientation we would expect the centre lines and the satellites nearly to coalesce.

The spectrum was investigated over a small range of settings near this orientation and the results are plotted in fig. 6.6. Due to the fact that the setting of the crystal face perpendicular to the axis of rotation was not perfect two sets of satellites are resolved which cross over at angles 0.8° apart.

6.7.a. Measurement of the Quadrupole Coupling Constant.

Equation 6(1) gives the quadrupole splitting of the nuclear magnetic energy levels for $I = \frac{3}{2}$ in the axially symmetric case. The fact that when $\theta = 0°$ the satellite separation is $\frac{e^2qQ}{h}$ in frequency is often used to determine the value of the nuclear quadrupole coupling constant $\frac{e^2qQ}{h}$, where eQ is the nuclear electric quadrupole moment in e.s.u. cm^2 and eq is the electric field gradient at the nucleus in e.s.u. cm^{-3}. A value of e^2qQ is also obtainable from a study of the spectra near $\theta = \cos^{-1}\frac{1}{\sqrt{3}} = \sin^{-1}\frac{\sqrt{2}}{\sqrt{3}}$, for at this value of θ the satellites are superposed at a frequency given by equations 6(1)

$$\frac{1}{h}\left(E_{\frac{1}{2}} - E_{-\frac{3}{2}}\right) = \frac{1}{h}\left(E_{\frac{3}{2}} - E_{\frac{1}{2}}\right) = \nu_o\left(1 + \frac{1}{12}\eta^2\right)$$

while the centre line is at a frequency

$$\frac{1}{h}\left(E_{\frac{1}{2}} - E_{-\frac{1}{2}}\right) = \nu_o\left(1 - \frac{1}{16}\zeta^2\right)$$

The difference in these frequencies is $\frac{7}{48}\zeta^2\nu_o = \frac{7}{48}\frac{(e^2qQ)^2}{h^2\nu_o}$

This frequency difference in terms of field shift can be read from fig. 6.6.

Field shift = 4.95 mv units = 11.68 gauss

Equivalent frequency shift for Na^{23} = 11.68 x 11.267 x 10^2 c/s

= 13.12 Kc/s

Frequency of the signal generator = 6.816 Mc/s.

Assuming initially that this is frequency ν_o we have

$$\frac{7}{48}\zeta^2 \times 6.816 \times 10^6 = 13.12 \times 10^3$$

$$\therefore \zeta \doteq 0.115$$

With this approximate value for ζ and using the fact that the centre line frequency 6.816 Mc/s is displaced $-\frac{1}{16}\zeta^2\nu_o$ at this angle we get a true value of ν_o = 6.820 Mc/s.

Then we have

$$\left(\frac{e^2qQ}{h}\right)^2 = \frac{48}{7} \times 6820 \times 10^3 \times 13120 \text{ c/s}$$

$$= 615.464 \times 10^6$$

$$\therefore \frac{e^2qQ}{h} = 784.5 \text{ Kc/s} \pm 8 \text{ Kc/s}.$$

The greatest error in this measurement is in determining the field sweep difference between the lines at the cross-over point. For this determination an accuracy of only 2% has been assumed for this measurement

giving an error of 1% in $\frac{e^2qQ}{h}$. With care the accuracy of this measurement could be increased to give a value of $\frac{e^2qQ}{h}$ with a probable error of less than 0.3%. The value found above compares with a value of 779.2 ± 4 Kc/s obtained by Gutowsky and Williams 1957 and 801 ± 8 Kc/s reported by Itoh and Kusaka 1954.

This measurement of the quadrupole coupling factor by measuring a small field shift at cross-over has accuracy comparable to that obtained by measuring the large field shift at maximum splitting because in the first case the quantity measured is the square of the coupling factor. For a bridge spectrometer, which is better adapted to making small accurate field sweeps than large ones, the cross-over measurement is probably superior.

6.7.b. Progressive Saturation Runs on Sodium Chlorate.

For all runs on the sodium chlorate crystal the modulation frequency was raised from 25 c/s to 212 c/s with a considerable increase of signal to noise ratio. The signal to noise ratio does rise with modulation frequency, as thermionic valve noise due to the flicker effect tends to be greater at the lower audio frequencies. The upper limit on the modulation frequency which can be used is imposed by the fact that the line is artificially widened by an amount of the order of the modulation frequency. Thus the modulation frequency must be small compared to the line-width in cycles per second, just as the modulation amplitude must be small compared to the line-width in gauss to avoid artificial broadening. A higher modulation frequency was used at this point because only then did a variable frequency source of modulation become available. High

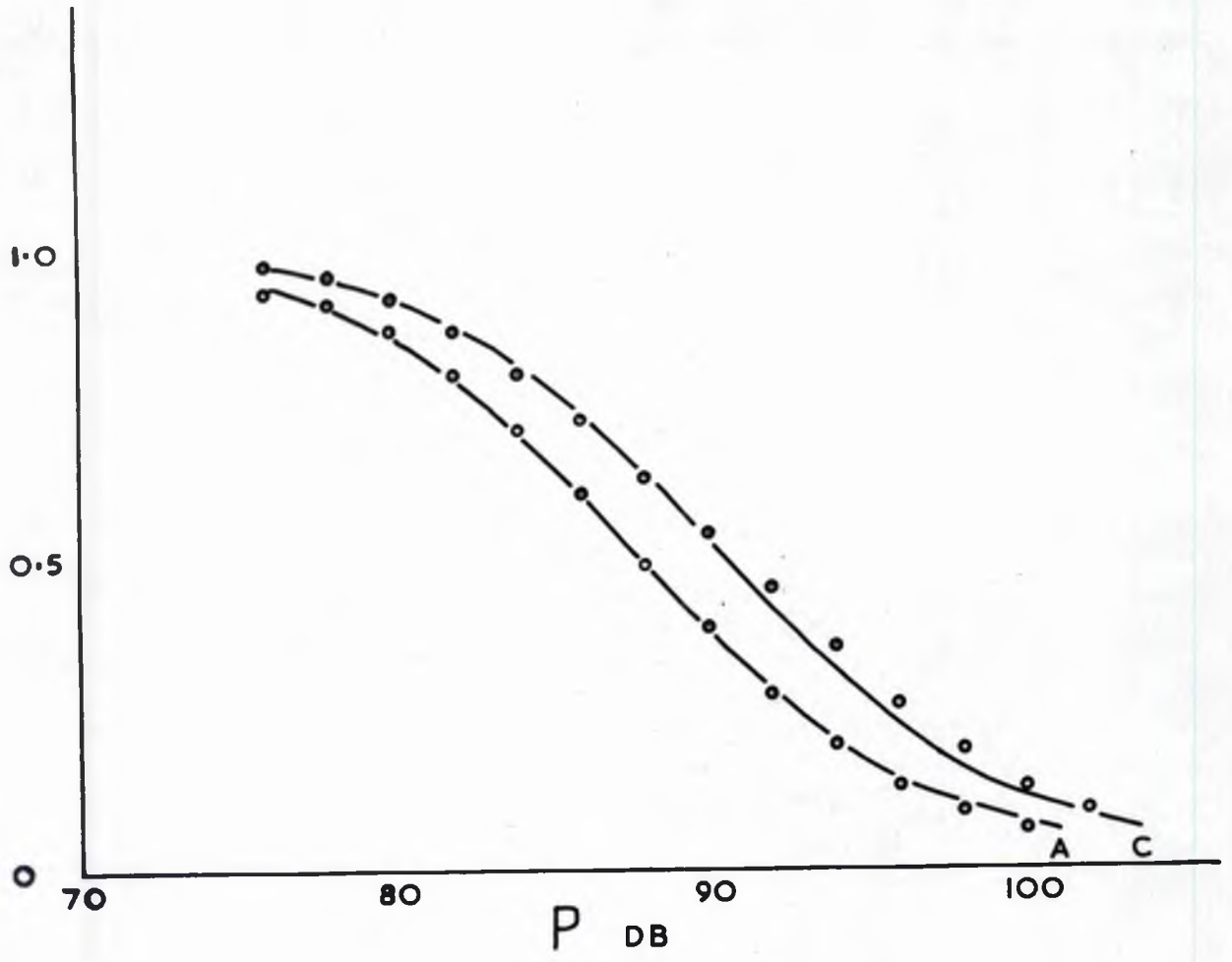

Figure 6.7.

Saturation of Na^{23} in $NaClO_3$

The experimental points are for centre line and satellite line. Curve A of fig. 4.1. is fitted to the centre line points. Curve C of fig. 4.1. is then a near fit for the satellite points.

impedance modulation coils were used, designed to be driven from the output of an audio frequency signal generator without an intermediate stage of power amplification. Most a.f. signal generators deliver ~ 0.1 watts output and it is possible to design modulation coils to give the maximum modulation of a few gauss required at this power level. The frequency of modulation can then be easily varied. The frequency of the narrow band amplifier preceding the lock-in amplifier must also be varied by changing the twin-T feedback network to suit the new frequency. In our apparatus the twin-T network was mounted on a valve base and could be unplugged and interchanged easily. For these runs the audio unit built by B.R. Williams and designed to work at 212 c/s was used.

With the crystal near the cross-over orientation all the sodium nuclei are in near identical environments and no difference in relaxation time is to be expected between different satellites. In fact no significant difference in saturation behaviour was found between the various satellites and the results of the various runs are averaged and presented in table 6.11 and those for the centre line and satellite line are plotted in figure 6.7. The satellites observed are each due to nuclei at two different sites while the centre line is due to nuclei at four different sites for which the electric environment happens to become identical near the cross-over angle. In fact the centre line could be split into two separated lines corresponding to the two sets of satellites by turning the rotation head 15° from the cross-over angle, and saturation runs on the two centre lines separated were done at this angle. The results did not vary significantly from those of the saturation runs on the superposed centre lines near the cross-over point. The variation of

T_1 with angular setting in this crystal will be investigated by B.R. Williams as part of a study of the anisotropy of T_1 in crystals.

The results of the saturation runs are in qualitative agreement with a quadrupole relaxation mechanism, and in the case of the centre line and satellite lines the quantitative agreement with the predicted separation of the saturation curves is good. However the saturation curve for two satellites superposed lies to the right of that for a single satellite, while our theory would predict that it should lie between the centre line and lone satellite saturation curves. Lack of time prevented the checking of whether the saturation curve for superposed satellite lines retained this position at an orientation where the separated satellites were single rather than double lines.

Our theory does not cover the case of a double satellite line superposed on a quadruple centre line as is the case where the recorded satellites cross the centre line. The saturation curves found for this case, which are not plotted in table 6.11 lie very close to those for the satellite line.

Table 6.11.

R.F. Level	Mean Relative Signal Strengths (corrected to a common linewidth of 1.39 gauss)		
100 db = 100 mv	Centre Line	Satellite	Superposed Satellites
76 db	0.93	0.97	0.98
78	0.91	0.95	0.96
80	0.865	0.915	0.935
82	0.795	0.862	0.90
84	0.705	0.795	0.86
86	0.60	0.72	0.77
88	0.485	0.625	0.68
90	0.385	0.535	0.58
92	0.275	0.445	0.48
94	0.195	0.35	0.385
96	0.125	0.26	0.285
98	0.085	0.185	0.215
100	0.055	0.125	0.14
102		0.085	0.105
104			0.08

Unsaturated Line Width

Centre Line	1.6 gauss
Satellite	1.39 gauss
Superposed Satellites	1.45 gauss

6.8. Calibration of the Saturation Curves Using Lithium Fluoride.

A crystal of lithium fluoride which had been obtained from the Harshaw Chemical Company was known to have a very long relaxation time from measurements made by B.R. Williams. These measurements were made using a Pound-Watkins spectrometer and he found that at the lowest possible power of operation the Li^7 and F^{19} resonances were still partially saturated, which made the measurement of T_1 difficult. A novel method was developed of measuring T_1 under these conditions. The half period of the decay from the unsaturated state to partial saturation where the saturation factor is Z is $T_1 Z$ rather than T_1. Accordingly a series of such decays was measured with Z varied by known ratios, which enabled T_1 to be measured.

To check the values found by this novel method the LiF crystal was placed in the bridge spectrometer which can operate at levels at which the crystal is unsaturated. The input power was then raised until the Li^7 resonance was completely saturated. With the frequency fixed on top of the line the radiofrequency power level was then reduced suddenly to a low level (1 mv) and the recovery of the signal recorded. The time for the signal to rise to e^{-1} of its maximum value is T_1, and this value was found to be 6 minutes in agreement with B.R. Williams' measurements using the other method.

The input power was then progressively increased by small steps, the signal meter of the receiver being held at a constant reading and a period longer that fifteen minutes being allowed for the spin system to come to equilibrium at each setting. In this way the input power for half saturation was found.

At half saturation the factor $\gamma^2 H_1^2 T_1 T_2 = P = 1$ for all saturation curves of the form $(1 + P)^{-1}$. If then all the saturation curves had been found using the bridge with the same setting of its components and using the same sample coil as was used for the LiF crystal, so that relative values of H_1 would be proportional to relative values of input voltage, then the actual value of T_1 for each crystal would be found by comparison with the known value of T_1 for the Li^7 in LiF.

To enable the best filling factor to be attained different coils were wound for each crystal in general, but these coils were all similar in inductance and Q factor. Thus the comparison of T_1 values has been made in table 6.12, on the assumption that a constant relation between input power and H_1 existed throughout the experiments. It is unlikely that different coils differed enough to make the power input for half saturation change by 7 db so that the T_1 values quoted can be considered good to better than a factor of 5. In cases where the same coil was used, as for instance for the two different sites in Euclase and for the Al^{27} resonance in crystals 64 and 65 the relative values of T_1 are good to 0.6 db or 15%.

The procedure used in compiling the T_1 values of table 6.12 was to take $P_{\frac{1}{2}}$, the value of input power (αH_1^2) for half saturation, and in quadrupole relaxed cases where the saturation curve is $(1 + xP)^{-1}$ the $P_{\frac{1}{2}}$ value was shifted to what it would be on a $(1 + P)^{-1}$ curve by using the factor x from the theory developed in Chapter 4. For example if the value for half saturation is y db on a quadrupole relaxed centre line for which $x = 4$ then the value on a $(1 + P)^{-1}$ curve is $(y + 6)$ db. Similar shifts are applied for gyromagnetic ratio γ and inverse line width T_2

so that the final corrected column gives the ratio of T_1 values in decibels. The Li^7 in LiF is in a spherically symmetric environment so the lines are not quadrupole-split. For superposed lines the saturation follows a $(1 + P)^{-1}$ curve whether the relaxation is magnetic or quadrupolar. So $x = 1$ in LiF.

It is to be noted that for the range of T_1 values shown the condition $W_m T_1 > 1$ does not hold throughout and that some of the saturation curves correspond to case 1, Bloembergen, Purcell and Pound 1948 in which the maximum meter deflection is $\alpha \frac{a}{dv} g(v)x(v)$ and the saturation varies during a modulation cycle. The correction factor to make the T_1 values comparable when we change from case 2 to case 1 can be calculated if the line shape function is known. For the damped oscillator line shape the correction factor is 0.5 which is small enough not to alter the values quoted to within a factor of 5 in table 6.12.

6.9. Paramagnetic Impurities.

The spodumene crystal which gave the longest relaxation time T_1 and hence would be expected to have the lowest degree of paramagnetic impurity on the Bloembergen relaxation theory, was crystal 65. It was analysed for paramagnetic content by two different methods.

Dr. Ingram looked at the paramagnetic resonance lines from a chip of this crystal in an x-band spectrometer at Southampton University. From the spectrum he estimated a density of 10^{18} unpaired electrons per gm with manganese as the dominant paramagnetic element present.

Part of the crystal was later analysed spectroscopically by members of the Agricultural Chemistry Department at Bangor. The detailed analysis is given as follows:

Table 6.12

Crystal	Reference Number	Nucleus	$P_{\frac{1}{2}}$ db	Y Correction db	Line Width mv	Line Width Correction db	Corrected $P_{\frac{1}{2}}$ db	T_1 Seconds	Relaxation Mechanism
LiF	-	Li^7	74.0	0	5.1	-10.8	62.2	360	-
$NaClO_3$	-	Na^{23}	93.6	-3.35	0.59	-1.4	88.9	0.8	Quadrupolar
$Na_2B_4O_7\ 10H_2O$	-	B^{11}	96.45	-1.7	2.8	-8.2	86.55	1.3	Magnetic
$NaNO_3$	-	Na^{23}	107.0	-3.35	0.85	-3.0	101.65	4.1×10^{-2}	Quadrupolar
$Na_2S_2O_3\ 5H_2O$	-	Na^{23}(1)	107.0	-3.35	1.7	-6.0	97.65	0.1	Quadrupolar
		Na^{23}(2)	110.8	-3.35	1.7	-6.0	101.45	4.2×10^{-2}	Quadrupolar
$LiAl(SiO_3)_2$	65	Li^7	101.8	0	0.80	-2.8	99.0	9.5×10^{-2}	Magnetic
		Al^{27}	105	-3.45	1.4	-5.1	96.45	0.13	Magnetic
$HBeAlSiO_5$	-	Al^{27}(1)	106.3	-3.45	2.2	-7.1	95.75	0.15	Magnetic
		Al^{27}(2)	108.6	-3.45	2.2	-7.1	98.05	9.0×10^{-2}	Magnetic
$LiAl(SiO_3)_2$	48	Li^7	113	0	0.85	-3	110.0	6.0×10^{-3}	Magnetic
$LiAl(SiO_3)_2$	119.248	Li^7	113.9	0	0.69	-2.1	111.8	4.1×10^{-3}	Magnetic
		Al^{27}	116	-3.45	2.3	-7.3	105.25	1.8×10^{-2}	Magnetic
$LiAl(SiO_3)_2$	64	Al^{27}	127	-3.45	1.4	-5.1	118.45	8.5×10^{-4}	Magnetic

$P_{\frac{1}{2}}$ is the input power for half saturation on a $(1 + P)^{-1}$ curve. 100 db = 100 mv r.f. input. 1 mv line width = 2.36 gauss. The line-width correction shifts the $P_{\frac{1}{2}}$ value of each line to the value it would have if the line width were 1 gauss. The Y correction shifts the $P_{\frac{1}{2}}$ value of each line to the value it would have if the gyromagnetic ratio of the nucleus were that of lithium^7.

Mn	50	parts per million
Cu	1	" " "
Ti	< 50	" " "
Ni	< 2	" " "
Co	< 2	" " "
Cr	~ 30	" " "
La	nil	" " "
Ga	40	" " "

Thus we have ~ 100 p.p.m. of paramagnetic impurity in the purest natural crystal examined.

The artificial single crystals were analysed by the Chemistry Department at Bangor using a Spectrophotometric method. The predominant paramagnetic impurity to be expected in these specimens is iron and the analysis on a Spekker was specifically for iron. The results are accurate to ± 0.1 p.p.m.

Crystal	Fe Impurity
$NaNO_3$ (Hilger)	0.8 p.p.m.
$Na_2S_2O_3\ 5H_2O$	0.4 p.p.m.
$Na_2B_4O_7\ 10H_2O$	0.5 p.p.m.
$NaClO_3$	0.3 p.p.m.

In the case of the home-grown crystals the analysis was done on the recrystallized salt used for growing the final large crystal specimens. The Fe impurity of these crystals is low as compared with the pure $NaNO_3$ crystal obtained commercially.

6.10. Nuclear Quadrupole Moments and Polarization Factors.

Polarization factors for some ions have recently been calculated from Hartree and Hartree-Fock wave functions. The values for the nuclei in which we are interested are taken from Bersohn 1958. The polarization factor γ_∞ is defined in the following way.

$$Q_{total} = Q_{nucleus} + Q_{electron}$$

$$= Q - \gamma_\infty Q$$

Ion	Q (barns)	γ_∞
Li^{7+}	0.042	0.256
B^{11+++}	0.0355	0.1455
Na^{23+}	0.10	-4.53
Al^{27+++}	0.149	-2.59

The greater the $Q_{total\ value}$, the greater is the interaction between the quadrupole moment of the nucleus and the time varying electric field gradient at the nucleus, and consequently the more likely it is that T_1 should be controlled by quadrupole relaxation rather than impurity magnetic relaxation.

6.11. Discussion of Results.

(i) B^{11}

In the light of the table in section 6.10 B^{11} is not a nucleus which is likely to have a short T_1 due to quadrupole relaxation. Its quadrupole moment is low and is further reduced by 15% due to the shielding effect of its electrons. It is not then surprising that the

relaxation mechanism in B^{11} is magnetic. It only remains to see if a T_1 near 1 second is reasonable in a crystal containing < 1 p.p.m. of paramagnetic iron impurity.

$$1 \text{ p.p.m. by wt.} \quad \doteq \quad 10^{16} \text{ impurity atoms/gm.}$$
$$\sim \quad 1 \times 10^{16} \text{ impurity atoms/cc.}$$

The magnetic relaxation time will be determined by the number of spin-spin collisions required on average to move the excess spin energy to the neighbourhood of an impurity atom. When energy is exchanged with the impurity atom the energy is passed on to the lattice in a time of the order of the paramagnetic relaxation time $\sim 10^{-8}$ sec. so that T_1 is governed only by the time taken in spin-spin collisions.

$T_1 \sim n^2 T_2$ where the energy has to be transported n lattice spacings by means of n^2 random collisions. In fact Bloembergen 1949 suggests the relation

$$T_1 = 10\, n^2 T_2$$

Suppose the crystal is divided into N cubes per cm^3 each cube containing one impurity ion on average so that there are N impurity ions per c.c. Then the average distance of a nucleus in the cube from the impurity ion is $\sim \frac{1}{3}$ x length of cube side

$$= \frac{1}{3N^{\frac{1}{3}}} = na \text{ where a is the nearest distance between}$$

the nuclei absorbing the r.f. energy.

$$\therefore N = \frac{1}{27n^3a^3} = \frac{1}{27a^3}\left(\frac{10T_2}{T_1}\right)^{\frac{3}{2}}$$

$$\therefore T_1 = \frac{10T_2}{9a^2N^{\frac{2}{3}}} \doteq \frac{T_2}{a^2N^{\frac{2}{3}}} \qquad 6(2)$$

For B^{11} $N \doteq 10^{16}$ Line-Width $\doteq$ 10 Kc/s $\therefore T_2 = 10^{-4}$ sec.

a is unkown but will be a few Angstrom units.

$a \sim 3 \times 10^{-8}$

$$\therefore T_1 \doteq \frac{10^{-4}}{9 \times 10^{-16} \times 10^{16} \times \frac{2}{5}} \doteq 2.0 \text{ sec.}$$

The recorded T_1 of 1.3 seconds could then be attributable to the paramagnetic impurity, though the near coincidence of the figure found by the rough model is fortuitous.

(ii) $\underline{Na^{23}}$

Putting the values $a \sim 3 \times 10^{-8}$ cm, $T_2 \sim 0.5 \times 10^{-3}$ sec, $N \sim 10^{16}$/cc. in equation 6(2) we again get $T_1 \sim 1$ sec which would be the relaxation time for sodium in $NaNO_3$ of the purity of our specimen if the relaxation were due to paramagnetic impurity. It appears that sodium, with a larger quadrupole moment than B^{11} and a much more favourable antishielding polarisation factor, has enough quadrupole coupling to the lattice to provide a quadrupole relaxation giving a T_1 over ten times shorter than the magnetic relaxation time in our $NaNo_3$ crystal. It also follows that at concentrations of paramagnetic impurity greater that fifty times the concentration in our crystal the magnetic relaxation would begin to dominate the quadrupolar relaxation process.

The same argument applies to Na^{23} in sodium thiosulphate where the two relaxation processes will be of comparable strength near impurity values of 10 p.p.m.

(iii) Li^7

The spectroscopic and paramagnetic resonance analysis of crystal 65 of spodumene both give an estimate of 10^{18} impurity ions per gram. Substituting in equation 6(2): $N = 3 \times 10^{18}/cm^3$, $T_2 = \frac{1}{3 \times 10^5} = 3 \times 10^{-4}$ sec and $a = 5 \times 10^{-8}$ cm which are the values for Li^7 in spodumene 65, we get $T_1 \doteq 0.01$ sec in good agreement with the time found. With the low nuclear Q value and γ_∞ factor in lithium and the high impurity content in the crystal this result is to be expected. As far as geological samples are concerned the crystal is of course relatively pure. The shorter relaxation time of the other crystals is explained by assuming a higher paramagnetic impurity content.

(iv) Al^{27}

T_1 for Al^{27} in spodumene 65 is found to be very similar to that of the Li^7 nucleus, and as T_2 and 'a' have similar values for both nuclei there is no doubt that the relaxation process is magnetic. As Q and γ_∞ are not unfavourable in Al^{27}, quadrupole relaxation may dominate the paramagnetic relaxation process in unusually pure crystals, and it might well be possible to find a spodumene crystal in which the Al^{27} nuclei are relaxed by a quadrupolar mechanism while the Li^7 nuclei are relaxed by paramagnetic impurities.

7. Summary.

An analysis of the behaviour of the nuclear magnetic resonance lines in a quadrupole split spectrum under saturation conditions shows that the dominant relaxation process for nuclear spins can be ascertained by a study of the saturation curves of the different lines.

A nuclear magnetic resonance spectrometer using a twin T bridge has been constructed and used to study the saturation behaviour of the quadrupole split spectra of four different nuclei in nine different crystals. It has been found that the spectrometer is well suited to the study of such crystals at the wide range of input power required.

Three of the single crystal specimens have been grown and the spectrum of one of them (borax) is given for a limited range for the first time. The quadrupole coupling constant in another (sodium chlorate) has been measured.

It has been found that within the limits of measurement the qualitative predictions of the analysis are well supported by the experiments. The relaxation mechanism in three of the crystals is through the electric quadrupole moment of the nuclei, while in the other six it is through the magnetic dipole moment of the nuclei.

A calibration of the spectrometer using the spectrum of lithium in a lithium fluoride crystal in which the relaxation time is long enough to be measured directly, enables values of spin-lattice relaxation time to be given for all the crystals examined. The relaxation times found are shown to be in reasonable agreement with the predictions of theory using in each case the appropriate relaxation mechanism found for the crystal.

Appendix I.

Nucleus	Crystal	Reference
Li^7	$Li_2SO_4H_2O$	Murahami and Hirahara, J. Phys. Soc. Japan 11 607 1956.
	$LiAl(SiO_3)_2$	Petch, Cranna and Volkoff, Can. J. Phys. 31 837 1953.
Be^9	$Be_3Al_2(SiO_3)_6$	Brown and Williams, J. Chem. Phys. 24 751 1956.
	$BeAl_2O_4$	Schuster and Pake, Phys. Rev. 84 886 1951.
Na^{23}	$NaNO_3$	Pound, Phys. Rev. 79 685 1950.
	$NaClO_3$	Itoh and Kusaka, J. Phys. Soc. Japan 9 434 1954.
	$NaBrO_3$	Itoh and Kusaka, J. Phys. Soc. Japan 9 434 1954.
	$Na_2S_2O_3 \cdot 5H_2O$	Itoh, Kusaka and Yamagata, J. Phys. Soc. Japan 9 209 1954.
	$NaH_2PO_4 \cdot 2H_2O$	Hoby and Petch, Can. J. Phys. 34 1169 1956.
Al^{27}	Al_2O_3	Pound, Phys. Rev. 79 685 1950.
	$LiAl(SiO_3)_2$	Petch, Cranna and Volkoff, Can. J. Phys. 31 837 1953.
	$HBeAlSiO_5$	Eades, Can. J. Phys. 33 286 1955.
	$BeAl_2O_4$	Hockenberry, Brown and Williams, Bull. Am. Phys. Soc. 2 225 1957.
	$Be_3Al_2(SiO_3)$	Brown and Williams, J. Chem. Phys. 24 751 1956.

Appendix I. (Cont.)

Nucleus	Crystal	Reference
K^{39}	$KClO_3$	Kaplan and Hahn, Bull. Am. Phys. Soc. 2 384 1957.
Cs^{133}	$Cs_2Mg(SO_4)_2 6H_2O$	Kiddle and Proctor, Phys. Rev. 104 932 1956.
Rb^{87}	$Rb_2Mg(SO_4)_2 6H_2O$	Kiddle and Proctor, Phys. Rev. 104 932 1956.
Cu^{63}	Cu_2O	Kushida, Benedek and Bloembergen, Phys. Rev. 104 1364 1956.
Nb^{93}	$KNbO_3$	Cotts and Knight, Phys. Rev. 96 1285 1954.

Appendix II

Plotting of Saturation Curves.

As the output of the Signal Generator comes from an attenuator calibrated in decibels it is convenient to plot the saturation curve against relative input power P in decibels rather than against log P.

Any saturation curve $(1 + xP)^{-1}$ is derived from the $(1 + P)^{-1}$ curve by displacing it $-10 \log x$ decibels along the p axis.

P	10 log P db	$\frac{1}{1 + P}$
0	-	1
0.01	-20	0.990
0.02	-16.99	0.980
0.03	-15.23	0.971
0.05	-13.01	0.953
0.07	-11.55	0.935
0.1	-10.0	0.909
0.2	-6.99	0.833
0.3	-5.23	0.769
0.5	-3.01	0.667
0.7	-1.55	0.588
1.0	0	0.500
2.0	+3.01	0.333
3.0	4.77	0.250
5.0	6.99	0.167
7.0	8.45	0.125
10.0	10.0	0.091
20.0	13.01	0.048

Saturation Curve	Displacement from $(1 + P)^{-1}$
$(1 + \frac{14}{11} P)^{-1}$	-1.05 db
$(1 + \frac{9}{4} P)^{-1}$	-3.52 db
$(1 + 3 P)^{-1}$	-4.77 db
$(1 + 4 P)^{-1}$	-6.02 db
$(1 + \frac{837}{539} P)^{-1}$	-1.91 db
$(1 + \frac{18}{11} P)^{-1}$	-2.14 db
$(1 + \frac{1794}{539} P)^{-1}$	-5.00 db
$(1 + \frac{48}{11} P)^{-1}$	-6.4 db
$(1 + \frac{49}{11} P)^{-1}$	-6.5 db

References.

Anderson, H.L., 1949, Phys. Rev. 76, 1460.

Andrew, E.R., 1955, Nuclear Magnetic Resonance. Cambridge Univ. Press.

Andrew, E.R. and Swanson, K.M., 1957, Proc. Phys. Soc. 70, 436.

Bersohn, R., 1958. To be published.

Bisco[illegible], J. and Warren, B.E., 1933, Z. Krist., 86, 292.

Bloch, F., 1946, Phys. Rev. 70, 460.

Bloembergen, N., 1948, Nuclear Magnetic Relaxation. The Hague: Nijhoff.

Bloembergen, N., Purcell, E.M. and Pound, R.V., 1948, Phys. Rev. 73, 679.

Bloembergen, N., 1949, Physica 15, 386.

Eades, R.G., 1955, Can. J. Phys. 33, 286.

Eades, R.G., Hughes, D.G. and Andrew, E.R., 1958, Proc. Phys. Soc. 71, 1019.

Grivet, P., 1955, La Resonance Paramagnetique Nucleaire, C.N.R.S. Paris.

Gutowsky, H.S., Meyer, L.H. and McClure, R.E., 1953, Rev. Sci. Instr. 24, 8, 644.

Gutowsky, H.S. and Williams, 1957, Phys. Rev. 105, 464.

Itoh, J., Kusaka, R., and Yamagata, Y., 1954, J. Phys. Soc. Japan 9, 209.

Itoh, J. and Kusaka, R., 1954, J. Phys. Soc. Japan 9, 434.

Kopfermann, 1958, Nuclear Moments (Translated by E.E. Schneider), Academic Press Inc., New York.

Pake, G.E., 1950, Am. J. Phys. 18, 438.

Pake, G.E., 1956, Solid State Physics, Vol. 2, Academic Press Inc., New York

Petch, H.E., Gnellis, D.W.L and Volkoff, G.M., 1951, Phys. Rev. 84, 602.

Petch, H.E., Cranna, N.G. and Volkoff, G.M., 1953, Can. J. Phys. 31, 837.

Pound, R.V., 1948, Proc. Phys. Soc. 61, 576.

References (Cont.)

Pound, R.V., 1950, Phys. Rev. 79, 4, 685.

Pound, R.V., 1953, J. Phys. Chem. 57, 743.

Purcell, E.M., Torrey, H.C. and Pound, R.V., 1946, Phys. Rev. 69, 37.

Schuster, N.A., 1951, Rev. Sci. Insts. 22, 254.

Taylor, P.G. and Beavers, C.A., 1952, Acta.Cryst. 5, 3, 341.

Van Kranendonk, 1954, Physica 20, 781.

Volkoff, G.M., 1953, Can. J. Phys. 31, 820.

Volkoff, G.M., Petch, H.E. and Smellie, D.W.L., 1952, Can. J. Phys. 30, 270.

Waller, 1932, Z. Phys. 79, 370.

Wang, Townes, Shawlow and Holden, 1952, Phys. Rev. 86, 809.

Warren, B.E. and Biscoe, J., 1931, Z. Krist 80, 391.

Waterman, H.H. and Volkoff, G.M., 1955, Can. J. Phys. 33, 156.

Watkins, Thesis, 1951, Harvard (microfilm).

Werts, J.E., 1955, Chem. Reviews 55, 829.

I am indebted to the Carn
Universities of Scotland for
Scholarship which enabled me
years of this work.